2016-01-01

Geochemical Signatures As A Chemostratigraphic Tool To Correlate Stacked Carbonates Of The Glorieta, Victorio Peak, Cutoff, And Upper San Andres Formations West Dog Canyon, Guadalupe Mountains, New Mexico

Eric Bergersen
University of Texas at El Paso, bergersen828@gmail.com

GEOCHEMICAL SIGNATURES AS A CHEMOSTRATIGRAPHIC TOOL TO CORRELATE STACKED CARBONATES OF THE GLORIETA, VICTORIO PEAK, CUTOFF, AND UPPER SAN ANDRES FORMATIONS WEST DOG CANYON, GUADALUPE MOUNTAINS, NEW MEXICO

ERIC BERGERSEN

Master's Program in Geology

APPROVED:

Benjamin Brunner, Ph.D., Chair

Katherine Giles, Ph.D.

Terence Garner, Ph.D.

Charles Ambler, Ph.D.
Dean of the Graduate School

DEDICATION

This thesis is dedicated to my wife, Abby, and to my parents, Barbara and Steve. Anything good that has come to my life has been because of your example, guidance, and love.

GEOCHEMICAL SIGNATURES AS A CHEMOSTRATIGRAPHIC TOOL TO CORRELATE STACKED CARBONATES OF THE GLORIETA, VICTORIO PEAK, CUTOFF, AND UPPER SAN ANDRES FORMATIONS WEST DOG CANYON, GUADALUPE MOUNTAINS, NEW MEXICO

by

ERIC BERGERSEN, B.S.

THESIS

Presented to the Faculty of the Graduate School of

The University of Texas at El Paso

in Partial Fulfillment

of the Requirements

for the Degree of

MASTER OF SCIENCE

Department of Geological Sciences

THE UNIVERSITY OF TEXAS AT EL PASO

December 2016

ACKNOWLEDGEMENTS

I would like to express my sincerest appreciation to my wife, whom without her selfless support, this adventure would not have been possible. I would like to thank my parents for listening to my most "optimistic" of rants and providing the needed motivation and mentorship.

In the Fall of 2014, Dr. Benjamin Brunner agreed to take a chance on a stubborn geologist from Houston. You have worn numerous hats throughout the voyage but have been unwavering in your support and guidance throughout. I'm thankful our paths crossed, I could never have imagined a better partnership between student and thesis advisor. Additional thanks to Dr. Gail Arnold for providing the necessary open door, caffeine, and keeping Dr. Brunner and I on track. I thank Dr. Katherine Giles for serving as committee member and Dr. Garner for his time, support, and suggestion of the study area.

Finally, my shadow, Ossa, our German Shepherd. Thank you for bringing joy and entertainment to my and Abby's life.

ABSTRACT

For oil exploration, stratigraphic correlation of formations over distance and across structural complications is essential. I tested if an established method – carbon and oxygen isotope composition of carbonates ($\delta^{18}O_{carbonate}$, $\delta^{13}C_{carbonate}$) and a new chemostratigraphic tool – sulfur isotope composition of Carbonate Associated Sulfate ($\delta^{34}S_{CAS}$) can aid in the correlation of rock packages belonging to multiple stacked carbonate horizons from a carbonate platform.

In my study area, located in the Brokeoff Mountains, north of the Guadalupe Mountains National Park, the $\delta^{18}O_{carbonate}$, $\delta^{13}C_{carbonate}$ and $\delta^{34}S_{CAS}$ scatter strongly within single beds of the Leonardian-aged Victorio Peak Formation. In stratigraphic order, the $\delta^{18}O_{carbonate}$, $\delta^{13}C_{carbonate}$ and $\delta^{34}S_{CAS}$ also strongly scatter, making it difficult to identify distinct isotope trends. The scatter in $\delta^{18}O_{carbonate}$ and $\delta^{13}C_{carbonate}$ is predominantly caused by meteoric diagenesis and dolomitization, processes that change the original $\delta^{18}O_{carbonate}$ and $\delta^{13}C_{carbonate}$ to lighter or heavier values. The scatter in $\delta^{34}S_{CAS}$ is mainly caused by the addition of isotopically light sulfate from pyrite oxidation. Importantly, the $\delta^{34}S_{CAS}$ for the samples from the Victorio Peak Formation are heavier than what is expected for the $\delta^{34}S$ of sulfate from Permian seawater, indicating that during the Leonardian, the sulfur cycle within a part of the Permian basin was partly decoupled from the global ocean.

The findings of this pilot study lead to the conclusion that $\delta^{34}S_{CAS}$ is not a suitable chemostratigraphic tool in an industry setting, where rapid assessment/analysis and low costs are essential. However, for the reconstruction of the paleoceanographic evolution of Permian basin, $\delta^{34}S_{CAS}$ has the potential to yield unprecedented insight into intrabasinal sulfur cycling, which is tied to basin restriction, water column stratification, and paleoproductivity.

TABLE OF CONTENTS

LIST OF FIGURES

1. INTRODUCTION

When targeting rock units that are potential oil and reservoirs stratigraphic correlation of formations over distance and across structural complications is essential. Chemostratigraphy is complimentary to sequence stratigraphy, and essential in cases where the latter is not applicable. The geochemistry of sediments is highly sensitive to changes in sediment provenance, facies, weathering, palaeoenvironment, and climate. Each formation, and each subunit within a formation, can have its own distinct geochemical fingerprint that can be used to differentiate between rock packages. Unfortunately, carbon and oxygen isotope fingerprints of carbonate rocks can sometimes be overprinted to a degree where they can no longer be used as identifiers of the original lithologies. An alternative chemostratigraphic tool that is less prone to alteration is needed. Carbonate Associated Sulfate (CAS) – i.e. dissolved sulfate that is trapped in carbonate rocks at the time the rocks form – can be partially lost from the carbonate rocks during diagenesis and weathering. However, the sulfur signature of the remaining CAS is much less affected than the carbon and oxygen isotope composition of carbonates, mainly because little sulfate is added to the CAS pool during such processes. Thus, while the concentration of CAS may be lowered after its incorporation into the carbonates, the sulfur isotope composition of CAS is expected to reflect the isotope composition of sulfate from the water bodies in which the carbonate rocks formed.

I hypothesize that fluctuations in the sulfur isotope signature of sulfate were recorded in the form of CAS, and can now be used as a chemostratigraphic tool to correlate carbonate formations and sequences in the Permian Basin. In the Permian Basin, many of the formations are made of a similar carbonate rock type, but each formation possesses different reservoir qualities, so accurate correlation across the basin is important for creating reservoir and

production models. Due to glacioeustatic sea level fluctuations, the connection between the Permian Basin and the global ocean was restricted to various degrees during the deposition of the reservoir facies that today constitute the important oil and gas plays in this area. Restrictions in water exchange likely heavily impacted biogeochemical sulfur cycling within the Permian Basin, resulting in rapid excursions in the sulfur isotope signature of sulfate in the water body.

The Guadalupe Mountains of southeast New Mexico and West Texas hosts one of the world's finest ancient fossil reefs (Scholle, 2003). The region also provides excellent opportunities to study the relationships of depositional facies, diagenetic alteration, and hydrocarbon-rich carbonate reservoirs (Scholle, 2003). Much of the depositional spectrum of the reef complex and its associative carbonate platform can be seen in outcrops found in a series of deep canyons running approximately perpendicular to the regional facies strike. With limited vegetation cover, these outcrops provide an excellent lateral and vertical cross sectional view through geologic time and the associated depositional environments of a carbonate platform. This holds true for the study area (Figs. 1, 2, 3). Located in the Brokeoff Mountains just west of the Guadalupe Mountains National Park on the Texas/New Mexico border, the study area is composed of well-exposed outcrops amongst an intricate series of northwest-trending Quaternary fault packages (Fitchen, 1993). The outcrops from the Brokeoff and Guadalupe Mountains represent analogs to some of the most important carbonate platform oil reservoirs in the Permian Basin. Recent regional extension and block faulting creates the present physiography of the Guadalupe and Brokeoff mountains. Paleogeographically the sediments outcropping in the Brokeoff mountains were located on the shelf-crest and outer shelf of the reef's carbonate platform (Fig. 4; Fitchen, 1992). Thanks to their paleogeographic location, these outcrops helped in defining the sequence stratigraphic framework of the Permian Basin, and in resolving the

difficult interfingering platform-to-basin correlations (Fitchen, 1992; Fitchen, 1993; Kerans and Fitchen, 1995). In the study area, well-exposed outcrops of carbonate dominate packages which belong to the Leonardian-aged Glorieta and Victorio Peak formations, and the Guadalupian-aged Cutoff, and Upper San Andres formations (Figs. 5, 6; Fitchen, 1993; Kerans and Tinker, 1999). This is an ideal setting to test my hypothesis that the sulfur isotope signature of CAS can be used as a chemostratigraphic tool. In the framework of this project, the formations were studied, with primary focus on elucidating if the isotope signature of CAS entrapped within sedimentary carbonates is a faithful recorder of the sulfur isotope composition of seawater sulfate at the time of deposition and to learn if these signatures can be used as a tool for regional correlation.

1.1 DEPOSITIONAL HISTORY OF THE PERMIAN BASIN

The Permian Basin structure was generated from an asymmetrical depression formed during Ouachita-Marathon orogeny the Precambrian basement along the southern margin of the North American plate (Ward et al., 1986). The Permian Basin encompasses three sub-basins, the Delaware, the Midland, and Val Verde Basins. In the Permian, these sub-basins were interconnected by the Sheffield Channel (Fig. 1), and connected to the global ocean by the Hovey Channel (Fig. 1; Ward et al., 1986). In the West, the Delaware Basin was bounded by the Diablo Platform, in the north by the Northwestern Shelf and the Capitan Reef, in the east by the Central Basin Platform and in the south by the Southern Shelf.

1.1.1 Three Depositional Stages During the Paleozoic

The thickness of Paleozoic sediments is in the Delaware Basin over 10,668 m (35,000 feet) and more than 4572 m (15,000 feet) in the Midland Basin. The depositional history of the Permian Basin can be divided into three distinct stages; the Upper Cambrian to Mississippian,

Upper Mississippian to Early Permian, and mid to late Permian (Adams, 1965; Ward et al., 1986; Sarg et al., 1999).

Stage 1. Upper Cambrian to Mississippian: The first depositional stage was the Paleozoic post-rift phase of Laurentia during the Upper Cambrian to Mississippian, which followed the dismantlement of the late Precambrian Rodinian supercontinent. During this time, shallow-marine passive margin deposition dominated (Sarg et al., 1999).

Stage 2. Upper Mississippian to early Permian: The second depositional stage corresponds to the development of the SE-NW trending Marathon thrust belt located in present southwest Texas, caused by the collision of the North American and South American cratons. The development of the Marathon thrust belt caused the formation of two syn-orogenic foreland basins in the Upper Mississippian to early Permian, namely the Delaware and Midland basins, which are separated by the topographically higher Central Basin Platform. The tectonic uplift combined with the formation of foreland basins initiated the deposition of siliciclastic sediments into the deeper portions of the basins during early Pennsylvanian and was ensued by the development of Wolfcampian (early Permian) carbonate shelves and margins along the foreland basins (Ward et al., 1986).

Stage 3. Mid to late Permian: The third and final stage of the depositional history of Paleozoic sediments is characterized by the post-orogenic basin fill beginning during the late Permian period. More than 4 km of sediments were deposited in succession filling the newly conceived foreland basins (Ward et al., 1986). By the Guadalupian epoch of the Permian Period, the Permian Basin region was sitting along the western margin of Pangaea and roughly at 10° north of the paleo-equator of that time (Scholle, 2003). In the late Guadalupian, a shift of sedimentation occurred where less carbonates were deposited and an

increase in sandstone and evaporites began accumulating along the platform (Sarg et al., 1999). Near the end of the Permian, rapid deposition of Ochoan evaporites filled the remaining remnants of the foreland basins. These evaporites, such as gypsum/anhydrite, halite, sylvite, and other salts, preserved much of the original Permian facies from erosional modification during late Tertiary uplift and are the reason why remarkably well preserved outcrops of Paleozoic strata can be found today in the Guadalupe Mountain National Park (Scholle, 2003).

1.1.2 Differences in Paleogeographic Settings Between Subprovinces

Each sub-province of the greater Permian Basin chronicles different amounts of subsidence, which creates different basin-fill patterns. For example, the paleogeographic settings of both the Delaware and Midland basins in the early Leonardian were characterized by the presence of a platform shelf and the development of barriers along the seaward edge creating a distinct rimmed margin. The establishment of this rimmed margin influenced the depositional environments on the shelf, forming the complicated facies changes found located behind the shelf edge in the Leonardian and Guadalupian rocks (Ward et al., 1986). Along the northern shelf of the Delaware basin large-scale retrogradational and progradational sedimentary cycles formed during the Leonardian caused by glacio-eustatic sea level changes. These cycles correspond to the deposition of the Glorieta Formation – and during the Early-Mid Guadalupian to deposition of the San Andres Formation (Atchley et al., 1999). By late Guadalupian, the Delaware basin had achieved maximum shelf-to-basin relief. Its counterpart, the Midland basin, had already been filled by this time and become a part of a sizable, largely evaporitic shelf (Atchley et al., 1999).

1.2 GLORIETA, VICTORIO PEAK, CUTOFF, AND UPPER SAN ANDRES FORMATIONS

The Glorieta, Victorio Peak, Cutoff, and Upper San Andres Formations, deposited during the late Leonardian and into the early Guadalupian epochs, were part of the second (syn-orogenic) and third (post-orogenic) stages of basin filling. In the second stage, the pre-Wolfcampian faulting associated with the Marathon thrust belt created abundant secondary uplifts and depressions across the Central Basin Platform. The generated topography affected the facies distribution and sedimentary thicknesses of the marine carbonates and non-marine clastic sediments in the adjacent Midland and Delaware basins (Atchley et al., 1999). Drape anticlines that formed above of the uplifts created numerous traps that account for major hydrocarbon accumulations (Atchley et al., 1999).

Previous mapping of West Dog Canyon and the Brokeoff Mountains (Fitchen, 1992; Fitchen, 1993; Kerans and Fitchen, 1995) provided key insight into platform-to-basin transitions along the carbonate platform (Fig. 4). These studies found that the final outbuilding of the Leonardian-aged carbonate platform is evidenced by the silty dolomitized tidal flats belonging the Glorieta Formation. The outcropping upper segments of the upward shallowing sequences of dolomitic mudstone to grainstone of the Leonardian-aged Victorio Peak Formation were paleogeographically located along the platform margin to slope facies (King et al., 1965) and equivalent to the platformal Lower San Andres Formation (Kerans and Tinker, 1999). In the field area, the Guadalupian-aged Cutoff Formation, represents another mappable platform-to-basin transition, serving as the distal, deeper ramp toes of the shelf equivalent Lower San Andres Formation (Fitchen, 1993). Previous studies in the area identified an interfingering tongue of the siliciclastic Cherry Canyon Formation in the Upper San Andres Formation (Fig. 7; Fitchen, 1992; Kerans and Tinker, 1999).

1.2.1 Glorieta Formation

The Glorieta Formation is of late Leonardian age and represents an oil-producing formation in the Permian Basin while also functioning as an important reservoir seal in some areas for the underlying Clear Fork Formation (Ruppel and Harrington, 2012). Much of the Glorieta Formation's production comes from enhanced recovery techniques such as waterflooding and CO_2 flooding along the Central Basin Platform. Along the Central Basin Platform, it is the lowermost portion of the Glorieta Formation that is commonly targeted including its underlying Clear Fork Formation (Montgomery, 1998). Typically, the stratigraphic distinction of the Glorieta Formation from other formations is challenging. This is evident from the fact that many reservoirs along the Northwest Shelf in New Mexico are commonly attributed to the Glorieta Formation, but in truth belong to the underlying Paddock member of the Yeso Formation (Dutton et al., 2005). Some studies include the Glorieta Formation as a member of the Yeso and/or Lower Victorio Peak Formations (Sarg and Lehmann, 1986).

The Glorieta Formation is often referred to as a silty carbonate (Dutton et al., 2005). These sediments are interpreted to form from dominantly sandy siliciclastic-rich tidal flat deposits (Kerans and Fitchen, 1995; Ruppel, 2002) along the Northwest Shelf of both Texas and New Mexico and the Central Basin platform. The most detailed subsurface studies of the Glorieta Formation are from the Robertson Field Area (Atchley et al., 1999; Stoudt and Raines, 2004), an oil and gas play along the Central Basin Platform ~200 km to the east of West Dog Canyon where the Glorieta Formation can be found in the subsurface to be ~150 m thick at a depth of ~1,750 m (Southwell and Stoudt, 2001). Along the Central Platform and the Northwest Shelf of Texas, the Glorieta Formation is underlain by the Clear Fork Formation (Fig. 5). The contact between the Clear Fork Formation and the Glorieta Formation is characterized by

dolomitic shale and siltstone with abundant desiccation cracks (Montgomery, 1998). The Glorieta Formation is capped by the dolopackstones and dolograinstones of the San Andres Formation. This contact is marked by a karst surface between the units (Stoudt and Raines, 2004). In some locals the sediments of the Glorieta Formation intertongue with sediments that belong to the Lower San Andres composite sequence (in the literature sometimes referred to as Lower San Andres Formation) (Milner, 1978).

The use of high-frequency sequences (HFSs, defined in detail in the section 1.3), plays a critical role in understanding reservoir, source, and sealing rock distribution at the play and prospect scale (Mitchum and Wagoner, 1991). A HFS is composed of cycle sets, arranged in distinctive retrogradational, aggradational, and progradational patterns that are bound at the top and base by unconformities or their correlative conformities (Kerans and Tinker, 1999). A HFS is considered a fourth-order sequence, forming at 0.1-0.2 million year cyclicity (Kerans et al., 1994). These cycles can be observed in well logs, cores, and outcrops of areas with very rapid deposition.

Previous studies have identified that the Glorieta Formation is composed of one HFS, the HFS L6 – Leonardian 6, the sixth HFS of the Leonardian epoch (Fitchen, 1993; Kerans and Fitchen, 1995; Kerans and Kempter, 2002; Stoudt and Raines, 2004) and is considered to be the thickest of the Leonardian HFS's due to depositional loading (Hunt and Fitchen, 1999). Composed of 1) basal, mud-rich, subtidal rocks 2) overlying, grain-dominated, subtidal rocks, and 3) cycle-capping, tidal flat rocks (Ruppel, 2002), the HFS L6 represents a lowstand systems tract (LST) in a series of regressive phases with a distally steepened ramp profile and the contact with the overlying HFS of L7-L8 marked by subaerial unconformity with sparse karstification (Kerans and Fitchen, 1995).

Within my study area the uppermost beds of the Glorieta Formation – previously considered a member of the Yeso Formation (Sarg and Lehmann, 1986) are exposed in a horst block, flanked by the fallen fault blocks belonging to the Upper San Andres Formation. These upper beds of the Glorieta Formation are composed of alternating, inner and middle shelf facies of peritidal cycles and shallow restricted subtidal dolomite and siltstones with carbonate cement (Fig. 8). Each alternating bed is between 0.3 to 2.5 meters thick and found to be laterally continuous. Immediately above the Glorieta Formation lies the Victorio Peak Formation made of open marine skeletal packstones.

1.2.2 Victorio Peak Formation

The Victorio Peak Formation is composed of lithologies that belong to a ramp margin to slope facies (King et al., 1965), composed of large scale upward shallowing sequences of dolomitic mudstone to grainstone with minor siliciclastic pulses. The upper section of the Victorio Peak Formation is the only portion that outcrops within the Guadalupe and Brokeoff Mountains (Fitchen, 1992) and is ~550 m thick. This upper section is equivalent to the L7-L8 sequences of the platformal Lower San Andres Formation (Kerans and Tinker, 1999). In outcrop, the lithologies belonging to the Victorio Peak Formation form a package that is situated along a ramp margin and that is unconformably to paraconformably overlain by the Cutoff Formation as it extends basinward (Fitchen, 1992).

The Victorio Peak Formation has two HFSs, Leonardian 7 (L7) and Leonardian 8 (L8), which are both transgressive sequence sets. The top of the first HFS, L7, is marked by an unconformity that occurred prior to the deposition of the overlying Cutoff Formation. This unconformity resulted in a low angle (<1°) truncation of the Victorio Peak ramp top and a high angle truncation (<15°) of the ramp margin and slope, where 300 m of section was eroded

(Kirkby, 1982). The L8 HFS that marks the top of the Victorio Peak Formation, is truncated by another unconformity that separates it from the overlying Cutoff Formation. This uppermost unconformity was formed during subaerial exposure of the platform top during a relative fall in sea level (Sarg and Lehmann, 1986). The carbonates of Victorio Peak Formation are interpreted to be deposited in a shallow water environment, whereas the overlying Cutoff Formation consist of deep marine carbonates representing a major flooding event in the Delaware Basin (Fitchen, 1992).

1.2.3 Cutoff Formation

The Guadalupian-aged Cutoff Formation is a relic of the Lower Permian platform that was drowned during a craton-wide sea level transgression (Hurd et al., 2016) and serves as a basinal drape that buried the carbonate margin of the Victorio Peak Formation (Amerman et al., 2011). The Cutoff Formation consists of a series of deep-water carbonates, shales, and sandstones found along the northwest shelf of the Delaware Basin. These sediments were deposited after the subsidence rates for the basin had substantially decreased (Kerans and Fitchen, 1995).

The outcrops of the Cutoff Formation found in the area correspond to the high stand HFS's of G1-G4 and represent the distal, deeper ramp toes of the shelf equivalent Lower San Andres Formation (Fitchen, 1993; Hurd et al., 2016). Going up-dip towards the shelf, the Cutoff Formation grades into the lower ~120 m of the Lower San Andres Formation (Boyd, 1958). The separation between the HFS G1 to G4 is caused by several unconformities, which leave certain areas with no preserved Cutoff Formation (Kirkby, 1982). The packstones and wackestones of G1-G3 are separated by unconformities and are thought to have formed in a submarine environment. These unconformities become more prominent basinward (Kirkby, 1982). The

spiculite rich carbonate muds of G4 are marked by another unconformity at the top, which is interpreted as a subaerial exposure surface. This exposed surface served as a bypass for the younger siliciclastics belonging to the Brushy Canyon Formation (G5-G7), which were deposited along the slope and basin floor. In the basin, the Brushy Canyon Formation is overlain by the Upper San Andres Formation (G8-G9).

1.2.4 Upper San Andres Formation

On the platform, the San Andres Formation (Permian, upper Leonardian-lower Guadalupian) is composed of two separate formations, the Lower San Andres and Upper San Andres formations. As of the early 2000's, the combined San Andres formations had been the most prolific hydrocarbon producer in the Permian Basin with a cumulative production of over 8.5 billion bbl (Stoudt and Raines, 2004) since its first oil discovery in 1921. Most of the reservoir facies are in the Upper San Andres Formation (Stoudt and Raines, 2004). The Upper San Andres Formation represents one of the several shallow water carbonate platforms and mixed siliciclastic-carbonate units that were created along the shelf of the Permian Basin (Kerans et al., 1994). This formation can be found on the Central Basin Platform, Northwest Shelf, and along the gently dipping to distally steepened ramps of the Delaware Basin to the west and Midland Basin to the east of the Central Basin Platform.

The San Andres Formation lithofacies include deep water limestones to shallow water oolite bar deposits, shallow shelf or lagoonal carbonates containing siliciclastics, anhydrite and even sabkha, brine-pan, and mudflat deposits (Todd, 1976; Ramondetta et al., 1982). Due to this wide range of lithofacies, four facies tracts were established based on their associated energy, water depth, and sediment supply along the ramp profile (Stoudt & Raines, 2004). The four facies tracts and characteristics are as follows (Fig. 4; Kerans et al., 1994):

Facies Track 1. Inner ramp: This facies consists of mudstones, wackestones, and packstones, with peloids, dasycladacean grains. Mollusk fragments are dominant.

Facies Track 2. Ramp crest: This facies consists of mudstones, peloid wackestones with lesser amounts of fusulinids, peloid and ooid grainstones, and grain-dominated packstones.

Facies Track 3. Outer ramp: This facies is dominated by mudstones and fusulinid wackestones-packstones with minor pelmatozoan grains.

Facies Track 4. Distal outer ramp/basin: This facies shows a gradual change from burrowed to platybedded laminated mudstones.

Previous studies along the Algerita Escarpment, located near the western margin of the Guadalupe Mountains and only ~12 km away from West Dog Canyon, indicate that the average thickness of the Upper San Andres Formation is 80-120 meters (Fitchen, 1992). On the Northwest Shelf, moving basinward, the Upper San Andres Formation is separated from its underlying unit, the Cutoff Formation. At the base of the Upper San Andres Formation's overlying unit, the Grayburg Formation (G10), is an unconformable karst surface, located at the boundary between G9 and G10. The Grayburg Formation is considered much more quartz rich than the basinal portions of the Upper San Andres and consists of white sandstones and dolomitized mudstones (Stoudt and Raines, 2004).

Within the Upper San Andres Formation, Kerans and Kempter, (2002) identified two HFSs, Guadalupian 8 (G8) and Guadalupian 9 (G9), that correspond to intermediate-order transgressive to regressive cycles that locally are bound by unconformities. The HFS G8 is a transgressive sequence set with aggradational shelf accumulation along a well-developed shelf-margin buildup complex that includes a narrow ramp crest of 0.4 miles and the shelf-crest to toe-of-slope of 450 feet (Kerans and Kempter, 2002). The base of G8 is marked by the lower energy

carbonates on top of G4 grainstones. The reason for the large jump in the number sequencing of the Guadalupian-aged HFSs is a 1 to 3 million year unconformity (Kerans et al., 1994). During this time sediment accumulation on the San Andres carbonate platform was interrupted by a sea level fall of at least 100 meters, leaving the Lower San Andres and Victorio Peak formations equivalents exposed for nearly 0.5 to 1 million years. This created a large-scale unconformity (Ruppel, 1998), and shifted the facies tracts 3-5 km in the basinward direction (Kerans et al., 1994). The exposed platform became a zone of siliciclastic sediment bypass. These siliciclastics were deposited in the adjacent Delaware Basin (King, 1948) resulting in the accumulation of approximately 460 m of basinal sandstone (G5-G7) of the Brushy Canyon Formation (Sarg and Lehmann, 1986; Kerans et al., 1994; Gardner and Sonnenfeld, 1996). The top of the G8 sequence is marked by the G9 Cherry Canyon sandstone, whose basinal equivalent is the Lovington Sandstone (Kerans and Fitchen, 1995). The remainder of the Upper San Andres G9 sequence is composed of ramp margin buildups containing deeper water spongebryozoans-pelmatozoan faunas with a muddy matrix above the Cherry Canyon Sandstone (Kerans and Kempter, 2002).

The HFSs are further suddivided into high-order cycles or simply “cycles” (see section 1.3), which by their definition are comparable to parasequences (Kerans et al., 1992). The HFSs of the Upper San Andres Formation are up to 75 m thick, whereas high-order cycles are up to 12 m thick and typically bounded by marine flooding surfaces at their bases (Kerans et al., 1994). Cycles often show an upward-shallowing succession of facies with grain size coarsening upward and may or may not be capped by a subaerial exposure surface. In total, 108 high-order cycles were recognized in the San Andres Formation (Kerans et al., 1994). The HFSs and their respective high-order cycles are illustrated for the Glorieta, Victorio Peak, Cutoff and Upper San Andres Formation in Figure 6.

1.3 SEQUENCE STRATIGRAPHY OF THE PERMIAN BASIN

Sequence stratigraphy is a powerful tool in the interpretation of complex depositional systems and their geometric architecture. To great extent, the stratigraphic relationships of sediments in the Delaware Basin have been reconstructed from the well-preserved outcrops of the Guadalupe Mountains region. This is especially true for the nearly continuous outcrop exposures of reservoir equivalent strata in the study area of West Dog Canyon that belongs to a section of the Brokeoff Mountains located between the Algerita Escarpment and the Western Escarpment (Kerans et al., 1994). Data from continuous outcrops such as these are vital because they supply the detailed description and measurements needed to complete reservoir models and define the petrophysical properties of a formation (Kerans et al., 1994). Within the lower reaches of West Dog Canyon, key exposures of individual fault blocks of the regional northwest trending Pleistocene to recent fault packages can be observed (Fitchen, 1993). Boyd (1958) was the original mapper of the Brokeoff Mountains. Subsequent work by Fitchen (1992,1 993) and Kerans and Fitchen, (1995) contributed a large portion of the framework for the depositional sequence model that is currently used throughout the Permian Basin. Much of this sequence stratigraphic framework was developed from the very same outcrop exposures used in this study.

The sequence stratigraphic approaches described in this study are based on the regional cyclostratigraphic model developed for the greater Permian Basin system by Kerans and Kempter (2002). Using cyclostratigraphy, which deals with the identification, characterization, correlation, and interpretation of cyclic or periodic variations by forming a hierarchy using a numbered ordered system (1st = longest term, 5th = shortest term) allows for a robust stratigraphic framework to be developed. Knowledge of the stratigraphic terminology and concepts and their application to field observations is essential. The terminology and inner-

relations of this stratigraphic hierarchy approach of cycles, HFSs, and composite sequences are described below:

- *Cycles*: (5th order) refer to the smallest set of genetically related facies deposited during a single sea level fluctuation from a position of a highstand through a lowstand to the return of a highstand (Mitchum and Wagoner, 1991). Comparable to parasequences (Kerans and Tinker, 1997), cycles constitute the fundamental building block of the stratigraphic analysis of carbonates. Often forming on the scale of 1-5 m in thicknesses, cycles are indicative of water depth and water energy fluctuations (Kerans and Tinker, 1997). Cycles group together in packages of 2 to 5, these groups form cycle sets that can be interpreted across multiple facies tracts.
- *Cycle sets*: an assemblage of cycles that illustrate a consistent trend, either progradational, aggradational, or retrogradational transgressive. In many reservoirs located in the Permian Basin the understanding of cycle set construction is crucial to reservoir framework construction as many of the individual cycles are too thin to be recognized on petrophysical logs (Kerans and Tinker, 1997). Cycle sets are a component of high frequency sequences.
- *HFS (High Frequency Sequence)*: (4th order) bounded at its top and base by unconformities or their correlative conformities (Mitchum and Wagoner, 1991). HFSs are composed of cycle sets, arranged in distinctive retrogradational, aggradational, and progradational patterns. Forming at 0.1-0.2 m.y. cyclicity, HFSs can be identified in well logs, cores, and outcrops of areas with highly rapid deposition (Kerans et al., 1994). HFSs play a critical role in understanding reservoir, source, and sealing rock distribution at the play and prospect scale (Mitchum and Wagoner, 1991). Bounding surfaces of HFSs

are identified based on the following criteria: subaerial unconformities and karstification, a change from progradational to retrogradational cycles, major basinward shifts or offsets in the location of lithofacies tracts across a single surface, and analysis of stacking trends with their associated thicknesses and proportion of cycles (Kerans and Tinker, 1997). The HFS designation is utilized for higher-frequency unconformity-bound sequences within the larger composite sequences.

    - The 9 HFSs of the study area as, defined by Kerans and Tinker (1997), are shown in their hierarchy in Figure 6;
        - Leonardian 6: Glorieta Formation
        - Leonardian 7-8: Victorio Peak Formation and its platform equivalent the lowest sequences of the Lower San Andres Formation
        - Guadalupian 1-4: represent the Cutoff Formation and is equivalent to the high stand sequences of the Lower San Andres on the platform
        - Guadalupian 8-9: Upper San Andres composite sequences, with the G4-G8 contact serving as a hiatal surface where most of the Brushy Canyon sandstones were bypassed to the basin (Fitchen, 1993).

- *Composite Sequence*: (3rd order) also known as a depositional sequence, is composed of multiple unconformity bound sequences (HFSs). Similar to HFS, composite sequences are made of a relatively conformable succession of genetically related strata, bound at its top and base by unconformities or their correlative conformities (Kerans and Tinker, 1997). While HFSs are divided based on retrogradational and progradational cycle sets, composite sequences use system tracts made of comparable sets of HFSs to form sequence sets of lowstand system tracts (LST), transgressive system tracts (TST), and

highstand system tracts (HST). Key characteristics of these system tracts in carbonate systems are described below:

- TST: Bound at the top by a maximum flooding surface and below by an underlying sequence boundary and transgressive surface. HFSs show upward thickening and upward deepening facies trends with mounded geometry. Lithologically, TSTs have more diverse skeletal assemblages and are less prone to have grainstones (Kerans and Tinker, 1997).
- HST: bound at the top by an overlying sequence boundary and below by a maximum flooding surface. HFSs show upward thinning and upward shallowing facies trends with shingled or offlapping stratal geometries. Lithologically, HSTs have less diverse skeletal assemblages compared to TST, and are more grainstone prone (Kerans and Tinker, 1997).
- LST: under-studied in carbonate systems (Kerans and Tinker, 1997).

The use and understanding of this sequence stratigraphic terminology is vital to maintain coherence when comparing results to earlier studies of the Permian Basin. Figure 9 illustrates the continuous development of the numbering system of HFSs of past regional studies and how they compare to present day interpretations of the stratigraphic composition of the Permian Basin.

2. THE CHALLENGE: IDENTIFICATION AND CORRELATION OF STACKED CARBONATE UNITS

The distinction of different carbonate units can be challenging in well logs. In the Leonardian-Guadalupian age formations, there are multiple large genetically-related groupings of shallow shelf carbonate and siliciclastic reservoirs that dominate hydrocarbon production in the Permian basin, those being the San Andres, Glorieta, Clear Fork Group, Grayburg, Queen, Seven Rivers, and Yates formations (Kerans et al., 1994). Distinction of each unit is further complicated by the fault network of the Permian Basin, as Pleistocene to recent northwest trending faults associated with regional uplift are abundant (Fitchen, 1993). Within the lower reaches of West Dog Canyon, key exposures of individual fault blocks of the regional northwest trending Pleistocene to recent fault packages can be observed (Fitchen, 1993).

Correlation of these stacked carbonates has been left to complex reservoir models, which combine practices of petrophysical logs, geostatistical relationships, along with outcrop and core sample observations (Kerans et al., 1994). Each of these methods individually has limitations, leaving a level of uncertainty within each reservoir model. For example, in much of the Vacuum Glorieta field located on the Central Basin Platform, the Glorieta Formation is often erroneously correlated with the underlying Paddock Formation (Dutton et al., 2005). Luckily both formations are productive reservoirs, however misinterpretations like this can lead to disappointing exploration outcomes and dry holes. A key component for the reservoir models is information gathered from outcrop and core samples. The stratigraphic correlation of these samples is often achieved by paleostratigraphy or the identification of trace fossils and macrofossils. The dependence on such fossils can limit the resolution of a model if these fossils are not present or present at multiple stratigraphic levels throughout the formations, as is the case with the

formations investigated in this study. Consequently, chemostratigraphic approaches become an attractive alternative or complementary tool when interpretation of core, outcrop, and well logs leads to inadequate or inconclusive results.

Chemostratigraphy or chemical stratigraphy is the identification and correlation of rock units using variations in elemental composition of sediments. These variations in apparently homogenous sediment reflect key minor changes in variables like sediment source, facies, paleoenvironment, climate, and diagenesis. These signals stored within rocks provide a distinct geochemical fingerprint, which can be a powerful correlation tool. Especially in oil and gas exploration, where each formation possesses different reservoir qualities, it is of the utmost importance to know which formation one is drilling in. Earlier attempts to use the carbon and oxygen isotope composition of carbonate rocks as geochemical identifiers turned out to be ineffective, because the original carbon and oxygen isotope fingerprints of the different carbonate rock packages were altered during fluid migration, diagenesis, and weathering of the rocks (Katz et al., 2005). An alternative chemostratigraphic tool, which is less prone to be affected by isotopic alteration, is needed.

3. HYPOTHESIS

I hypothesize that sulfur and oxygen isotope signatures of carbonate associated sulfate (CAS) provides a promising chemostratigraphic tool for correlating carbonate formations and sequences in the Permian Basin. In the following, I present reasons why sulfur and oxygen isotope signatures of CAS are more robust than carbon and oxygen isotope signatures of carbonates, and provide an argument why it is likely that the sulfur and oxygen isotope signatures of sulfate in the water bodies of the Permian Basin fluctuated.

3.1 ROBUSTNESS OF SULFUR AND OXYGEN ISOTOPE SIGNATURES OF CAS

During their formation, carbonates entrap sulfate ions from the solution they form in, archiving the primary sulfate isotope composition ($\delta^{18}O_{sulfate}$ and $\delta^{34}S_{sulfate}$) of paleo-seawater at the time of precipitation (Wotte et al., 2012). There is only a minor sulfur and oxygen isotope fractionation associated with the incorporation of sulfate into the carbonates, meaning that ancient CAS can be used as a proxy for the $\delta^{18}O_{sulfate}$ and $\delta^{34}S_{sulfate}$ of the ocean at the time the minerals formed (Paytan and Gray, 2012).

Processes such as fluid migration, diagenesis, and weathering that alter the carbonate minerals (e.g. inducing re-crystallization, dolomitization, transformation of aragonite to calcite, or high Mg calcite into low Mg calcite) and thereby also affect their carbon and oxygen isotope composition ($\delta^{13}C_{carbonate}$ and $\delta^{18}O_{carbonate}$), will also impact CAS. Namely, it can be expected that CAS can be partially lost from the carbonate rocks during such alterations. However, the sulfur and oxygen isotope composition of the CAS ($\delta^{18}O_{CAS}$ and $\delta^{34}S_{CAS}$) that remains in the rock is much less affected by such alterations and will not give false readings from overprinting such as the carbon and oxygen isotope composition of carbonates, mainly because little sulfate is added

to the CAS pool during such processes. Moreover, unlike carbonates, sulfate does not readily exchange oxygen isotope with water (Rennie and Turchyn, 2014). Thus, while the concentration of CAS may be lowered during carbonate transformations, the $\delta^{18}O_{CAS}$ and $\delta^{34}S_{CAS}$ continues to reflect the isotope composition of sulfate that was dissolved in the water bodies that once covered the Permian Basin.

3.2 Reasons Why it is Likely that the $\delta^{18}O_{sulfate}$ and $\delta^{34}S_{sulfate}$ of Water Bodies of the Permian Basin Strongly Fluctuated During the Permian

Sulfur as sulfate (SO_4^{2-}) is the second most abundant anion in modern seawater and third most abundant ion after chloride and sodium (Staudt and Schoonen, 1995; Paytan and Gray, 2012). The residence time of sulfate in the ocean today is approximately 10 million years (Berner and Berner, 1987), whereas the residence time of carbon in the ocean is on the order of 100,000 years (Walker, 1986). The approximately 100 times longer residence of sulfur compared to carbon in the ocean is owed to a much larger inventory of sulfate (approximately 28mmol/l) in the ocean, and much smaller fluxes of sulfur in and out of the ocean. Due to this discrepancy, the sulfur isotope signature of sulfate in the ocean is expected to change much more gradually than the carbon isotopes, making sulfur isotopes a less sensitive tracer of disturbances in the global biogeochemical carbon and sulfur cycle. The correspondingly small expected signal in the rate of change for concentration or isotopic composition of sulfate reduces the viability of sulfur as a tool for stratigraphic correlation (Paytan and Gray, 2012).

I believe that because of two key reasons, both of which pertain to marine basins that become decoupled from the global ocean, my study will reveal significant variability in the isotopic composition of sulfate in the Permian Basin. First, a decoupling removes the dampening influence that the immensely large sulfate pool of the global ocean exerts on changes in the

$\delta^{18}O_{sulfate}$ and $\delta^{34}S_{sulfate}$ of the detached basin (Fig. 10). Basins with restricted water exchange with the ocean, such the exchange of water through the Hovey Channel in the Permain mid-Guadalupian epoch (Hill, 1999), may have lower sulfate concentrations than the global ocean. This is exemplified by sulfate concentrations of approximately 17mmol/l in the Black Sea relative to approximately 28 mmol/l in the global ocean, which reduces the residence time of sulfate in the basin relative to the ocean (Treude et al., 2007). Second, restricted basins tend to become stratified, with a denser, saline and cold water body at the bottom and a less dense, brackish warm water body at the top. Due to lack of mixing with freshwater, the bottom water portion of the basin is prone to become anoxic, with the consequence that sulfate reduction instead of oxygen respiration drives organic matter mineralization, as observed for the Black Sea (Treude et al., 2007). This intensified sulfur cycling leads to the sequestration of isotopically light sulfur into marine sediments, leaving residual sulfate that is enriched in ^{34}S and ^{18}O. Thus, the $\delta^{18}O_{sulfate}$ and $\delta^{34}S_{sulfate}$ in a marine basin can change from steady global marine sulfate isotope signatures during periods of relative sea level highstands, to rapidly changing signatures during basin detachment corresponding to relative sea level lowstands (Fig. 10 and Fig. 11). In such cases, the $\delta^{18}O_{CAS}$ and $\delta^{34}S_{CAS}$ in carbonates formed in the basin become tracers for the restrictedness of the basin and extent of anoxia within.

3.3 CAUSE FOR OPTIMISM

While many challenges are associated with the here proposed novel approach, there are reasons for optimism. For my chemostratigraphic tool to work, a change in restriction/openness of the basin with respect to the global sea is needed. Previous studies suggest that the water exchange between the Permian Basin and the global ocean through the Hovey Channel may have been restricted to various degrees during the Guadalupian epoch of the Permian (Fig. 1; Hill,

1999). This matches the sequence stratigraphic model postulating that the platform was flooded throughout the Leonardian HFSs with a sea level maximum achieved at G1, followed by progressive drops to G4, which coincides with the deposition of the Cutoff Formation (Garcia-Fresca et al., 2012). This progressive fall in sea level increases the chance for basin restriction to occur. Moreover, a progressive fall in sea level may not be a prerequisite for basin restriction. A previous study (Milner, 1976) proposed that the first 25 m of the the Lower San Andres composite sequence, an equivalent to the Victorio Peak Formation, was deposited in a restricted marine environment. This may correspond to a time slice with limited exchange of water masses through the Hovey Channel during the early Guadalupian. The notion of a restricted water exchange during the deposition of the sediments belonging to the Victorio Peak Formation is corroborated through facies analyses, that observed an impoverished fauna dominated by dasycladaceans along the inner ramp and fusulinids on the outer ramp, indicating mesohaline or restricted conditions (Kerans et al., 1994).

Having found arguments that basin restriction during the deposition of the late Leonardian to early Guadalupian formations in the Permian Basin is encouraging, however, there also needs to be an argument for how one will be able to distinguish local isotope excursions from global isotope trends for the Permian oceans. Luckily, the sulfur isotope composition of global marine sulfate during the time slice of interest, the Permian, was almost steady and at a Phanerozoic all-time low (Paytan and Gray, 2012). Such curves are depicted in Figures 12 and 13. This means that excursions $\delta^{18}O_{CAS}$ and $\delta^{34}S_{CAS}$ from carbonates that belong to the Glorieta, Victorio Peak, Cutoff, and Upper San Andres formations can be interpreted as local or basin-wide events, such as the decoupling from the global ocean and development of anoxic conditions in the water body.

Based on these reasons I hypothesize that:

- **Sea level changes during the deposition of the Glorieta, Victorio Peak, Cutoff, and Upper San Andres formations led to fluctuations in the openness/restrictedness of the Permian Basin with respect to the global ocean.**
- **Basin restriction during relative sea level lowstands lead to stratification of the water masses in the basin, inducing anaerobic conditions in the sediments and bottom water. These conditions enhance microbial sulfate reduction, leading to shifts in the $\delta^{18}O_{sulfate}$ and $\delta^{34}S_{sulfate}$. Because each of these events is unique, I expect that the corresponding isotopes signatures are also unique (different patterns and magnitudes of excursions).**
- **The shifts in $\delta^{18}O_{sulfate}$ and $\delta^{34}S_{sulfate}$ will be recorded as excursions in $\delta^{18}O_{CAS}$ and $\delta^{34}S_{CAS}$, and – with an offset that corresponds to the sulfur isotope fractionation during microbial sulfate reduction - as shifts in $\delta^{34}S_{pyrite}$.**
- **The CAS and pyrite isotope fingerprints will be preserved in the rock record because they are not overprinted by fluids, diagenesis or weathering.**

In summary: It is my belief that I have a chemostratigraphic tool that may be powerful for correlating carbonate units in stacked carbonate plays. Ideally, I will find isotope fingerprints that are specific for individual units.

4. OBJECTIVES

4.1 QUESTIONS ARISING FROM HYPOTHESIS

The stated hypotheses raise a suite of questions:

- Is it true that $\delta^{13}C_{carbonate}$ and $\delta^{18}O_{carbonate}$ are unsuitable as chemostratigraphic tool in the studied area?
- Are $\delta^{18}O_{CAS}$, $\delta^{34}S_{CAS}$ and $\delta^{34}S_{pyrite}$ robust geochemical tracers that resist overprinting? Are these tracers more robust than $\delta^{13}C_{carbonate}$ and $\delta^{18}O_{carbonate}$?
- What is the chemostratigraphic resolution of $\delta^{18}O_{CAS}$, $\delta^{34}S_{CAS}$ and $\delta^{34}S_{pyrite}$? Can this tool be used for correlations on the outcrop scale?
- Is there a connection between excursions in $\delta^{18}O_{CAS}$, $\delta^{34}S_{CAS}$ and $\delta^{34}S_{pyrite}$ and relative sea level fluctuations?

Due to the complexity of the various geochemical analyses, within the framework of this Masters' thesis, the above questions could not be addressed for all listed geochemical signatures. I decided to focus my efforts on $\delta^{13}C_{carbonate}$, $\delta^{18}O_{carbonate}$ and $\delta^{34}S_{CAS}$ instead of $\delta^{18}O_{CAS}$ and $\delta^{34}S_{pyrite}$ because the former are more commonly used as proxies for stratigraphic correlations and isotope inventory (carbon and sulfur) of large scale water bodies than the latter. Based on these considerations, I formulated the following four objectives for my project.

1. Identification of previously described formations and sections in the field area.

   Rationale: A prerequisite to address the above questions is a detailed knowledge of the stratigraphy of my research area, which is essential for choosing sampling locations and chemostratigraphic profiles.

   Action: Using the previously defined sequence stratigraphy of the Glorieta, Victorio Peak, Cutoff, and Upper San Andres formations (Kerans and Fitchen, 1995; Kerans and

Tinker, 1997), existing geological maps (Fitchen, 1993), and detailed geo-referenced aerial photography of the West Dog Canyon field expeditions were conducted.

2. Assessing robustness of $\delta^{13}C_{carbonate}$, $\delta^{18}O_{carbonate}$, and $\delta^{34}S_{CAS}$ as chemostratigraphic tracers.

   Rationale: There is a need to demonstrate that $\delta^{34}S_{CAS}$ is indeed more reliable than $\delta^{13}C_{carbonate}$ and $\delta^{18}O_{carbonate}$ when exposed to overprinting.

   Action: Different rock types (alteration patterns) along bedding that show variable degree of overprinting (cements, replacements, oxidation, karstification, dolomitization) were sampled and analyzed for their isotope composition.

3. Assessment of chemostratigraphic resolution of $\delta^{34}S_{CAS}$.

   Rationale: What is the resolution that can be achieved with this novel approach to chemostratigraphy? Will it provide a tool that can define high-order cycles, which are at most 12 meters thick, i.e. an identifier at cyclostratigraphic resolution? If such resolution is attainable, this tool would be able to represent the scale at which rock fabric variability occurs (Kerans et al., 1994). Such a resolution would be the equivalent of well log values deviating along a curve. However, if this sort of extremely fine resolution is unattainable, will I be able to successfully correlate HFSs that are up to 75 m in thickness? Or will I be left with a chemostratigraphic tool that can only identify different formations?

   Action: The severe faulting observed at West Dog Canyon is ideal to test the usefulness of this chemostratigraphic tool. I located fault blocks in the field that have distinct facies or unit changes and collected samples along transects from each side of the fault block. Analysis of $\delta^{34}S_{CAS}$ allowed me to test if the obtained signatures can be used for

chemostratigraphic correlations across the fault, and what chemostratigraphic resolution can be achieved.

4. Test if there is a connection between excursions in isotope composition of CAS and relative sea level changes.

   Rationale: I postulate that there should be a connection between relative sea level changes and excursions in the isotope composition of CAS due to basin restriction. To establish or refute such a connection, the geochemical fingerprints of the rocks from the Glorieta, Victorio Peak, Cutoff, and San Andres formations must be compared to indicators of basin restriction, such as lowstands.

   Action: I analyzed $\delta^{13}C_{carbonate}$, $\delta^{18}O_{carbonate}$, and $\delta^{34}S_{CAS}$ of samples collected from the stratigraphically most complete section in West Dog Canyon. The isotope trends were then compared to relative sea level changes that can be inferred from the sequence stratigraphical interpretation of the rock record.

5. METHODS

To reach my objectives, I employed the following methods: i) field work including identification of formations and sections as well as sample collection, ii) petrographic thin section analyses, and iii) light stable isotope analyses of samples from the Glorieta, Victorio Peak, Cutoff, and Upper San Andres Formations ($\delta^{13}C_{carbonate}$, $\delta^{18}O_{carbonate}$, $\delta^{34}S_{CAS}$).

5.1 FIELD SURVEY, PROFILES, AND SAMPLE COLLECTION

5.1.1 Field Area

The field area for this study is in the southwestern portion of the Brokeoff Mountains along West Dog Canyon (Otero County, New Mexico; Fig. 2 and Fig. 3). The area, located just northwest of the Guadalupe Mountains National Park on the Texas/New Mexico border is comprised of well-exposed outcrops ranging from 4,500 to 5,000 feet in elevation. West Dog Canyon serves as the main drainage for the Southern Brokeoff Mountains. This drainage consists of winding canyon walls that are consistently steep and typically several hundred feet in height, and empties just north of the Salt Flats located east of Dell City.

The study area is on public land under the jurisdiction of the Bureau of Land Management (BLM). A high clearance vehicle is needed to gain access to the field area, which can be reached by a dirt road maintained by the BLM. It is important to note that this road crosses land owned or leased by local ranchers and that all gates should be left as they were found (opened or closed). These ranchers also communicated that it was likely unsafe to partake in fieldwork during deer season as the land is available to hunters during the fall and early winter months.

5.1.2 Field Survey, Profiles, and Sample Collection

Field work for this study was accomplished in five expeditions, two trips during September 2015 and three trips during April and May of 2016. The two trips during September 2015 served primarily as reconnaissance expeditions, to gain familiarity with the study area. The final last three trips provided many of the key observations needed for this study, including time spent in the field with thesis advisor Dr. Benjamin Brunner for the collection of samples for geochemical analyses and Dr. William Fitchen, an expert on the sedimentology and sequence stratigraphy in the area (Fitchen, 1992; Fitchen, 1993).

Detailed geological maps of the region were available (Fitchen, 1992; Fitchen, 1993; Kerans and Fitchen, 1995). This work provided detailed formational descriptions, which were used for the identification of the boundaries between the Glorieta, Victorio Peak, Cutoff, and Upper San Andres formations. These boundaries were mapped throughout West Dog Canyon using a georeferenced ArcGIS program. A total of 80 hand samples (typically heavier than 350 g) were collected across all four primary formations of focus in this study. Of the 79 samples collected 15 samples belonged to the Glorieta, 33 to the Victorio Peak, 8 to the Cutoff, 20 to the Upper San Andres (4 of which were from the interfingering Cherry Canyon Formation), and 3 to the Grayburg Formation.

Overall there were four primary sample collection points, described below:

1. The Bench: Faulting was abundant throughout the field area, where north by northwest-trending Quaternary normal faults (Fitchen, 1993) where encountered frequently. With displacement of up to 300 m, smaller faults of 20 m or more were prevalent every 300 to 500 m (Fitchen, 1992). One of these faults smaller scale normal faults served as one of the primary testing methods used assess the isotopic continuity of CAS as a

chemostratigraphic tool known in this study. A total of 8 samples (Fig. 14) were taken across two different depositional cycle sets belonging to the Victorio Peak Formation, with an offset of 1.2 m across the fault plane. This sample set is referred as, The Bench, throughout this thesis, as it serves to test how consistent/robust the isotope signatures of carbon, oxygen, and sulfur are within one bed. I chose this sampling location because I consider this sample set as the most challenging test for the geochemical proxies of interest. The proximity of the sample locations to faults is expected to allow for ample, and spatially heterogeneous alteration by fluids. Moreover, when hit with a hammer, the samples smelled of sulfur dioxide, which is a good indicator for the presence of ample reduced sulfur in the rock, Sulfur that can be oxidized can alter the CAS isotope signature.

2. Cutoff to Upper San Andres transect: Another set of samples was collected using the ramp margin and slope transect of Plate 3A from Kerans et al., (1992) (Fig. 7). This transect consists of identifiable carbonate cycles of the deepwater Cutoff Formation's cherty sponge-brachiopod mudstone/wackestone and fusulinid-peloid wackestone that grades upward into packstone. Also encountered were the dolomite-dolomite sand cycles of the Upper San Andres Formation, which are microcosms of larger-scale (3rd-or 4th-order) depositional sequences. Here one finds the Upper San Andres Formation containing a basal sandstone wedge of the Cherry Canyon Formation (lowstand systems tract) that fines upward and becomes more carbonate-rich (transgressive systems tract) and that is downlapped by relatively pure carbonates (highstand systems tract) (Fitchen, 1992). The goal of this sample collection was to test if there was large scale isotopic variability across an entire formation. Samples were collected at a 2 m spacing with 15

samples collected across the highstand systems tract of the Upper San Andres. Additionally, 1 sample was collected in the lowstand systems tract corresponding to a dolomitic sandstone wedge (Cherry Canyon Formation) found in the Upper San Andres Formation, and another 8 samples were collected in the highstand system tract of the Cutoff Formation.

3. Glorieta Samples: Collection of samples from the Glorieta Formation was done in an exposed horst block (Fig. 8). This horst block resides next to down-dropped fault blocks consisting of sedimentary rocks that belong to the Upper San Andres Formation. The sedimentary rocks that belong to the Glorieta Formation are exposed as a steep cliff face that displays thick bedded dark brown dolomites at the base that thin into whitish and tannish brown dolomite and siltstone. These white to light brown beds consist of peritidal to shallow restricted subtidal dolomite and sandstone corresponding to the upper portion of the Glorieta Formation. The overlying massive dark brown beds were identified as members of the Victorio Peak Formation, consisting of open marine subtidal dolomite and skeletal packstones. Overall, 15 samples from the Glorieta Formation were collected at this location.
4. High Frequency Cycle Testing: To test the carbon and oxygen isotopic variability of carbonates within a cycle sequence 9 samples were collected every 20 cm cross two separate 5th order cycle sequences of the Victorio Peak Formation. Both cycles are 80 cm thick and are referred to as Cycle A & Cycle B in this thesis (Fig. 15).

5.2 SAMPLING FOR THIN SECTIONS AND GEOCHEMISTRY

Each sample needed to be at least 70 g to perform analysis of $\delta^{13}C_{carbonate}$, $\delta^{18}O_{carbonate}$, and $\delta^{34}S_{CAS}$. A larger sample size was needed for the 47 samples from which thin sections were

made. Samples selected to be made into thin sections, were slabbed and trimmed to a uniform size and further cut into billets (approximately 50x40x8 mm) prior to being sent out to a third party for thin section preparation and staining.

5.2.1 Thin Section Analysis

Background: Thin section analysis was used as a tool in aiding in the identification of sedimentary rocks, the correlation of studied sequences, and in recognizing overprinting by fluid migration, diagenesis (e.g. cementation, recrystallization, dolomitization, dedolomitization), and weathering.

Employed Approach: Oriented hand specimens were slabbed and cut into billets at UTEP, the orientation of the samples was marked on the billets during the cutting process. The specimens were then sent out to a third party for thin section creation, which included alizarin red and potassium ferricyanide staining for carbonate identification. The alizarin red stain allows to clearly distinguish between dolomite (does not stain) and limestone (stains red), while potassium ferricyanide indicates presence of carbonate phases that contain ferrous (reduced, i.e. Fe^{2+}) iron (stains blue). Further microscopic analyses were focused on the identification of grains (e.g. siliciclastics, fossils, ooids), assessment of grain size and relative abundance of grains and identification of the mineralogy such as dolomite or calcium carbonate, authigenic silicates, cement types, and diagenetic features as indicators for mineral dissolution.

5.2.2 Geochemical Analyses

Background: Three isotope systems were tested for their potential as chemostratigraphic tools: $\delta^{13}C_{carbonate}$, $\delta^{18}O_{carbonate}$ and $\delta^{34}S_{CAS}$. The isotope analysis of carbonates (i.e. $\delta^{13}C_{carbonate}$, $\delta^{18}O_{carbonate}$) is a well-established chemostratigraphic tool, the approach based on the sulfur

isotope analysis of CAS is not commonly used for chemostratigraphic work. However, sulfur isotope analysis of CAS is well established for the reconstruction of paleo-environmental applications, such as the assessment of redox conditions in sediments and the water column.

Employed approach: The sampling strategy was based on my objectives, discussed in section 5.1.2, and subsequent sample selection relied on field and thin section observations. For geochemical analyses, I avoided weathered surfaces, veins, and areas that displayed obvious alteration (e.g. rusty stains and pitting that indicated pyrite oxidation). If necessary, such areas were removed by cutting or with a rock hammer. The geochemical methodology for the extraction of sulfur phases such as CAS is outlined in Figure 16. In the first step the rock sample is crushed and powdered (24-51 g) by a hand mortar. To ensure consistent grain size, the crushed samples were sieved through a 150 micron USA Standard Test Sieve.

An aliquot (approximately 2 mg) of the crushed samples was sent out to the University of Washington's IsoLab for carbon and oxygen isotope measurements of carbonates. This laboratory uses the standard phosphoric acid digestion method for isotope analysis. The carbon and oxygen isotope composition of carbonate is reported by the laboratory in the standard delta notation relative to the Vienna Pee Dee Belemnite (VPDB) standard, assuming the carbonate in the samples is calcite. Consequently, the oxygen isotope composition of dolomite had to be corrected accordingly using published correction procedures (Kim et al., 2015), which in the case of the samples in this study resulted in a subtraction of 1.2‰ from the calculated value for calcite.

My CAS extraction protocol follows the methodology employed by (Ziegenbalg et al., 2010; Wotte et al., 2012). The powdered samples were submerged in a 2M NaCl solution and mixed using test tube rotators for 24 hours, with the goal to remove easily soluble sulfate (ESS)

phases such as sulfate derived from pyrite oxidation on the outcrop and minor evaporite inclusions (Kampschulte and Strauss, 2004). Using a centrifuge the sample was separated from the fluid (supernatant). The supernatant was decanted into a syringe fitted with a 0.45 µm membrane filter, and filtered. Subsequently, 200 µl of 10% HCl (drives dissolved carbonate off as CO_2) and 500µl of 1M $BaCl_2$ (induces precipitation of $BaSO_4$) were added to the supernatant. If the solution turned cloudy/milky after this addition, which indicates substantial sulfate content and the potential that the treatment did not remove all ESS from the sample, the ESS extraction was repeated until no further immediate precipitation of $BaSO_4$ could be observed (analogous to Wotte et al. (2012), but in a less rigorous fashion).

After completion of the ESS extraction procedure, the remaining sample was washed three times with warm deionized water to remove NaCl. The sample was then placed into beakers where 12M HCl was slowly added until all carbonate was dissolved and degassed as CO_2. Once the reaction was completed, the sample and acid mixture were placed into tubes and immediately centrifuged. At this stage, it was important that the samples were centrifuged within no more than 15 minutes of the carbonate leaching process. Keeping the time between carbonate dissolution and centrifugation as short as possible is critical because hydrochloric acid activates ferric iron, which can oxidize sulfur bearing compounds such as pyrite or organically bound sulfur. After centrifuging the sample, the remaining solid residue was collected and frozen. This residue contains residual sulfur after the HCl leach ($\delta^{34}S_{residual\ sulfur}$). Typically, the dominant sulfur species in such residues is pyrite-bound sulfur, whereas other refractory sulfur phases (native sulfur, organic-bound sulfur, barite) tend to be rare. Thus, in most cases, bulk sulfur isotope analysis of the residue is sufficient to determine $\delta^{34}S_{pyrite}$. This analysis was not done in

the framework of this thesis, but as the samples are kept frozen, such analyses, or further sequential extraction of separate sulfur phases, can be performed at a later stage.

Similar to the ESS step, the supernatant of the residual sulfur was collected after filtration through a 0.45 μm membrane filter, removing insoluble particulate matter. To induce precipitation of barium sulfate ($BaSO_4$), 1 ml of 1M $BaCl_2$ solution was added. The sulfate in the precipitated $BaSO_4$, corresponds to CAS (no acidification to expel CO_2 is needed in this step, as the sample was dissolved with HCl). To remove hydrochloric acid from the $BaSO_4$-ESS and $BaSO_4$-CAS precipitates, the $BaSO_4$ was separated via decanting the major portion of the supernatant, followed by several centrifugation steps, in which the sample is transferred from large centrifuge tubes (50 ml) into small tubes (2.5 ml), and at each step covered with deionized (18 MΩ) water. These washing steps not only remove the HCl from the sample, but also make the sample accessible for subsequent transfer into tin capsules. In a final centrifugation step, the samples were covered with acetone, which displaces water. After this, the purified $BaSO_4$ was dried in a drying oven at 60º C overnight.

Throughout this procedure, sample weights were determined at the beginning of the procedure (total sample weight), after the leaching with NaCl (weight after ESS extraction), and after leaching with HCl (weight after HCl extraction/weight of residue). The dry weight of the sample needed to be determined for the sample after the ESS extraction and after leaching with HCl. A 0.12 to 0.2 g aliquot was taken from the well stirred wet residue, weighed, allowed to dry, and then weighed again. Based on these two measurements, the total dry weight of the wet sample could be determined without drying the entire sample. Having to dry the entire sample would be detrimental for CAS analysis, as it would induce oxidation of sulfur bearing phases such as pyrite or organically bound sulfur. Due to an oversight in the sampling protocol, only a

small number of ESS weights was recorded. Fortunately, my samples did not lose a lot of weight during the extraction of ESS, and the amount of sulfate lost (presumably gypsum) can be accounted for from the weight of the $BaSO_4$ fraction. For consistency, in this study, the CAS content is reported with respect to the difference between total dry weight and calculated dry weight after the HCl leaching step, which approximates the ratio between CAS and carbonate that was dissolved during the extraction. The ESS content is reported as the ratio between ESS and the total sample weight.

It must be noted that the above extraction procedure cannot be blindly applied to all samples, and that one must carefully observe and protocol what happens in each of these steps. Depending on these observations, modifications of the protocol are required. For example, it is critical to record the color of the supernatant. If it turns intensely green it is likely that significant amounts of ferrous iron (Fe^{2+}) were released during the leaching. During the precipitation of sulfate as $BaSO_4$ with $BaCl_2$, such a solution can take up atmospheric oxygen, which oxidizes the ferrous iron to ferric iron (Fe^{3+}), which then precipitates as iron oxyhydroxides (FeOOH, 'rust'). Such a co-precipitation of $BaSO_4$ and FeOOH is problematic, as it jeopardizes oxygen isotope analysis of $BaSO_4$ by contamination with FeOOH. Identified at an early stage, this problem can be circumvented by the addition of an antioxidant (e.g. ascorbic acid; Hynes and Kelly 1988), or by oxidation of Fe^{2+} with bromine, and filtration of FeOOH prior to acidification and addition of $BaCl_2$ (Newton et al. 2004). With the samples in this study, I did not encounter this challenge. Another important qualitative observation includes the smell of the sample during crushing, and during treatment with HCl. Scents, such as that of burnt matches (SO_2) or petroleum during crushing indicates the presence of dead oil and native sulfur, and a smell of rotten eggs (H_2S) is indicative of liberation of sulfide from highly reactive monosulfide minerals.

If such smells are noted, they serve as warning that the to-be-extracted CAS is prone to contamination with those sulfur species during the extraction (or even on the outcrop). Hydrocarbon in the rock can also be detected by the presence of oily film on the fluids and beaker walls after extraction with HCl. This does not only provide important information about the investigated rocks, but also serves as an alert for the subsequent filtration of the supernatant. The apolar oil tends to clog filters quickly, and overpressuring of the filters can lead to broken filters, and contamination of the collected $BaSO_4$. Indeed, such filters failures from oil clogs caused the contamination of 7 samples, which belonged predominantly to the Victorio Peak Formation. These samples could not be analyzed. Potentially, these samples can be treated with additional extraction steps to eliminate the contaminants, however, those methods first need to be established, a task that could not be achieved in the framework of this thesis.

Another issue that had to be dealt with was that in some cases $BaCl_2$ precipitated after the addition of the 1ml of 1M $BaCl_2$ solution instead of $BaSO_4$. The reason for this unexpected result is that I used concentrated hydrochloric acid (corresponds to 12M HCl), and that the chloride ion can become so abundant that it spontaneously precipitates with the added barium. Once this happens, the barium is no longer reactive towards sulfate ions in solution, i.e. CAS does not precipitate as barium sulfate any longer. The solution for this challenge is simple. Addition of deionized water causes the newly formed $BaCl_2$ to dissolve, allowing barium to then react with sulfate in solution. Still, this is a critical step: one might lose all extracted sulfate if the $BaCl_2$ is mistaken as $BaSO_4$ precipitate. A final challenge concerns the washing steps of the $BaSO_4$ when sample amounts turn out to be extremely small (as in this study). In these cases, excessive washing and centrifugation can lead to total sample loss. This can be counteracted by using fewer centrifugation and washing steps, following the argument that a small sample is washed

more easily than a large sample. However, this comes at the risk that not all salts are removed from the samples, rendering the final CAS sample (captured as $BaSO_4$) a mixture of sticky, hygroscopic salt and barium sulfate. This complicates the weighing procedure, as it is extremely difficult to weigh in a sticky sample and one does not truly know the actual amount of added $BaSO_4$. Moreover, such samples would not be useful for oxygen isotope analysis (contain oxygen-bearing water taken up from air moisture), and they can also harm the equipment, as chloride salts release corrosive chlorine gas during combustion. To deal with this challenge, 17 of the already dried CAS samples were again mixed with water, centrifuged, covered with acetone, again centrifuged, decanted and dried once more to remove the salts.

Once prepared, the sulfur isotope composition of CAS was measured in-house in the light stable isotope facility of CEEIR using continuous-flow isotope ratio mass spectrometry (CF-IRMS). Approximately 0.4 mg of sample was weighed into a tin cup. An equal amount of vanadium pentoxide, a catalyst that aids in the conversion of sulfate into sulfur dioxide, was added. Using tweezers, the tin cup was then carefully crimped at the top, and vigorously shaken to thoroughly mix the catalyst with the sample. The tin cup was then folded into a small ball. Samples were then combusted for conversion of sample sulfur into sulfur dioxide using an Elementar Pyrocube, followed by isotope analysis of the evolved gas with an IsoPrime GeoVisION CF-IRMS. Isotope compositions are reported in delta notation relative to the Vienna Canyon Diablo Troilite (VCDT) standard, as follows:

$$\delta^{34}S = \left\{ \frac{(^{34}S/^{32}S)_{sample} - (^{34}S/^{32}S)_{standard}}{(^{34}S/^{32}S)_{standard}} * 1000‰ \right\}$$

International standards, NBS-127, IAEA SO-5, IAEA SO-6 as well as in-house standards were used for calibration. The reproducibility of the sulfur isotope compositions is +/- 0.3‰. The measurements not only yield the sulfur isotope composition of the sample, but also quantify the amount of sulfur that the samples contain. I used this measurement to calculate the actual weight of CAS and ESS obtained during extraction, as the exact weights could not be directly determined due to the contamination with salts caused by insufficient washing.

While I feel confident in my CAS extraction method, it is important to point out that there are significant differences to the some of the extraction procedures employed in other studies. The powdered sample weight I chose to use for extraction of CAS from dolomites was nearly 5 times less than other studies, e.g. Marenco et al. (2008); Baldermann et al. (2015) also used 5 to 10 times more carbonate powder, collecting 150 to 300 grams of carbonate powder prior to extraction. The same study then used 2 liters of distilled water at a 16-hour wash to remove any ESS, which is far more water than I used but their sample size was also significantly larger. The samples were then washed for 8 hours in a solution consisting of 105 ml of 6% NaOCl (bleach) added to 1895 ml of DDI water. The bleach step was designed to oxidize organic matter and remove any organic sulfur present in the sample. I did not use bleach in my CAS extraction protocol. Marenco et al. (2008) used 3M HCl to dissolve the carbonate, and performed this treatment over a duration of 8 hours. I also did not rigorously follow the procedure of Wotte et al. (2012), which calls for ESS leaching to be repeated until absolutely no further sulfate is liberated, whereas I did only repeat the ESS leaching step if after the addition of the $BaCl_2$ solution immediately $BaSO_4$ precipitated, which is indicative for high sulfate content.

The differences between the above studies and my approach is a difference in philosophy. All CAS extraction procedures have in common that they attempt to minimize potential

contamination with sulfate from other sources, such as gypsum or sulfate from sulfur oxidation taking place during the extraction. Each procedure also faces the same challenge: the trade-off between speed and rigorousness. A rapid extraction procedure minimizes the time during which contaminants can form, such as oxidation of reduced sulfur compounds to sulfate, and minimizes the time in which this sulfate could take a form (e.g. adsorbed to clay or associated with a newly formed carbonate mineral) that could be carried over into the CAS extraction step. A rigorous extraction procedure minimizes the amount of contaminant that could be carried into the CAS extraction step, at the cost that the extra time allowed for this step could exactly lead to the opposite result. For the latter approach, also the uncertainty remains if the used measure was rigorous enough, exemplified by the fact that it was recently shown that bleach is not potent enough to oxidize pyrite during the steps preceding CAS extraction (Theiling and Coleman, 2015). If reduced sulfur, such as pyrite, cannot be removed prior to the treatment with HCl, an excessive amount of leaching time is probably detrimental. Liberated ferrous iron becomes rapidly oxidized to ferric iron in presence of oxygen, and can in turn rapidly oxidize pyrite, a process that is well known from acid mine drainage systems. Because of this challenge, some researchers used nitrogen flushed systems for the HCl step (e.g. Ohkouchi et al., 1999) while others employed the addition of reducing agents (e.g. a 5% $SnCl_2$ solution; (Planavsky et al., 2012). Moreover, the excessive application of pre-HCl steps could lead to adverse results. Using high ion-strength bleach and NaCl solutions always induce dissolution of carbonate. At extended duration, an equilibrium between dissolved carbonate and mineral is established, which means that continuously, carbonate is dissolved, and new carbonate is formed. If the latter is formed in a solution that contains large amounts of sulfate, it is likely that during the ESS or bleach extraction, new CAS is formed – the opposite of what is intended. Finally, it is curious to note

that the aforementioned, more rigorous protocols often do not specify to what size the samples are crushed. The grain size is probably one of the most critical aspects when it comes to the question if sulfate ends up in the ESS or CAS fraction, and if rapid and complete dissolution of gypsum during the ESS step and carbonate during CAS extraction step can be achieved. Accepting that to date there is no perfect CAS extraction protocol, I feel that my rapid extraction technique is advantageous, with the additional benefit that it allows for a higher sample throughput.

6. RESULTS AND DISCUSSION

6.1 THIN SECTIONS ANALYSIS

Petrographic analysis of the stained thin sections was conducted on samples from all four formations of this study. Thin sections were examined to aid in the interpretation of the geochemical data, such as to identify processes such as dolomitization that may lead to the alteration of $\delta^{13}C_{carbonate}$, $\delta^{18}O_{carbonate}$, and $\delta^{34}S_{CAS}$ as well as to characterize the heterogeneity or uniformity of the samples that belong to The Bench. Dolomite was found in some degree in all formations, also dead oil and pyrite were found throughout the entire study area (Fig. 17).

6.1.1 Characteristics of the Different Formations in Thin Section

The samples from the Glorieta Formation contain varying amounts of dolomite, a feature common in most modern carbonate tidal flats. This may be a setting to which the depositional system of the Glorieta Formation can be compared to. The samples are rich in peloids, particularly fecal pellets, which are abundant in both modern and ancient shelf settings (Milner, 1978). At times, the peloids appear blurred and can lack the typical high density grouping of fecal pellets. This may be caused by compaction of very poorly cemented or non-cemented peloids and the effects related to authigenesis of dolomite (Fig. 18A; Beales, 1965). Sporadic calcitic cementation took place within poorly compacted pore space during deeper burial cementation in the form of coarsely crystalline mosaic calcite, also known as blocky calcite (Fig. 18B).

The samples belonging to the Victorio Peak Formation are highly petroliferous. This was suggested early on by qualitative observations. In outcrop, the Victorio Peak Formation appears to be darker than the other carbonates, the rocks emit a fetid odor upon being struck by a

hammer, and oil films were found after the dissolution of the samples with HCl. Thin sections analysis confirmed the presence of dead oil within all four of the formations, however dead oil is most abundant in the samples from the Victorio Peak Formation. Unlike the Guadalupian Cutoff and Upper San Andres formations, dolomitization is not as pervasive in the Victorio Peak Formation. The predominance of mud-supported fabrics suggests that the dolomite crystals, classified as dolomicrite, are an early diagenetic replacement products of a calcium carbonate mud precursor (Milner, 1976). The presence of dolomitic stylolites indicates that either calcite was removed during stylolitization leaving dolomitic seams, or that at a later stage, Mg-rich fluids may have used stylolites as a conduit for horizontal fluid migration promoting the spread of dolomitization (Fig. 19A; Vandeginste and John, 2013). The presence of stylolites has shown to influence later diagenetic fluid flow or hydrocarbon migration as documented in the Lower Triassic Virgin Member of the Moenkopi Formation in Southern Nevada (Bissell, 1972). Also dead oil can be found along stylolites, which supports the hypothesis that stylolites played an important role in fluid migration through the Victorio Peak Formation (Fig. 19B). Most samples from the Victorio Peak Formation are non-fossiliferous mudstones, however, also wackestones with fusulinids (~4-6 mm long, ~2mm wide, Fig. 19C), fragments of brachiopods and bivalves, ooids, and rare pisolites can be found. These fusulinids lack evidence of significant transport and abrasion. Microscopic occurrence of hematite pseudomorphs after iron sulfides have been described as abundant through the Victorio Peak Formation (Milner, 1976), which is consistent with the observation of dark pyrite rhombohedrals in thin sections of the samples obtained in this study.

The Cutoff Formation has similar dolomitic muds (17C) as that of the Victorio Peak Formation but displays an increase in pellets, ooids, and fossil fragments that are difficult to

interpret due to significant dolomitization (Fig. 20A). It is well known that the Cutoff Formation was once used as a basinal bypass for the lowstand system of the Brushy Canyon siliciclastics and it is no surprise that the Cutoff Formation has a higher quartz content than the Victorio Peak Formation. This bypass surface likely also provided the Cutoff Formation with meteoric waters, increasing dolomitization within the formations and lessened the effects of burial diagenesis as can be seen with the poorly compacted pellets.

The Upper San Andres Formation has been pervasively dolomitized throughout the study area, which has historically made facies interpretations difficult (Fitchen, 1992). This dolomitization includes the siliciclastic wedge (Cherry Canyon Formation) found within the Upper San Andres Formation. Unlike the dolomicrospar that is found in the Victorio Peak Formation and that dominates the Cutoff Formation, the dolomite crystals in the Upper San Andres Formation are idiotopic dolomite, characterized by rhombic shaped euhedral to subhedral crystals that display a porphyrotopic texture with dolomite crystals floating in a dolomicrite matrix, making samples belonging to the Upper San Andres Formation uniquely identifiable in thin section (Fig. 20B). The very fine-crystalline sizes of the dolomites, 30 to 75 μm, indicate that the water from which they precipitated was lower in water saturation of dolomitizing fluids than that of the Victorio Peak and Cutoff formations (James and Jones, 2015). In addition to the dolomite rhombohedrals, also opaque pyrite rhombohedrals are present within the Upper San Andres Formation. Noting that pyrite is present in all four formations is important because it implies that there is a risk for contamination of CAS with sulfate derived from pyrite oxidation.

6.1.2 Analysis of Thin Sections of 'The Bench' Samples

Within the Victorio Peak Formation, one of the major tests for this study was conducted, referred to as The Bench. With abundant faulting throughout the area, a fault block was selected

to test continuity/fidelity of my chemostratigraphic tools along two correlative beds offset by 1.2 m by a normal fault (Fig. 14). Eight samples were collected, four for the lower correlative bed, referred to as Bed I and four for the upper bed, referred to as Bed II. The fault with the minor offset within The Bench is only one of several nearby faults. A major fault runs approximately east-west, forming West Dog Canyon and to the immediate east of one sampling location (samples 20 and 21) another NNW normal fault is present. This entanglement of faults might explain why two of the samples belonging to Bed I (samples 16 and 20), both resting in the footwalls of the normal faults, are dolomitized. The remaining samples, two in Bed I and four in Bed II are calcitic.

Within Bed I of The Bench, samples 16, 20, and 30 contain dead oil, located in small calcite pockets in the dolomitized samples 16 and 20 (Figs. 17B, 21B, 21C). The calcitic samples 18 and 30 consist predominantly of micritic mud, are rich in pyrite rhombs, and sporadically contain ooids and brachiopod fragments (Fig 21A and Fig. 21B). The fully calcitic Bed II is identical to the calcitic samples from Bed I, a micritic limestone with occasional ooids and brachiopod fragments. Dead oil is present in all four samples of Bed II. Sample 21 from Bed II, appears to be much more fossil rich and contains much coarser calcite crystals than samples 17, 19, and 31 (Fig. 21D).

6.1 Carbon and Oxygen Isotope Composition of Carbonates

The $\delta^{18}O$ and $\delta^{13}C$ of carbonates ($\delta^{18}O_{carbonate}$ and $\delta^{13}C_{carbonate}$) reflects the processes involved in the making of the carbonate sediments, such as photosynthesis, oxidation of organic matter, and vital effects such as the precipitation of a carbonate skeleton, and the processes that affect the water masses the carbonate was formed in, such as mixing between freshwater and seawater, or evaporation as well as temperature. Moreover, $\delta^{18}O_{carbonate}$ and $\delta^{13}C_{carbonate}$ also

record the conditions during diagenesis of the sediment, such as the formation of cements, and processes such as dolomitization. As such, $\delta^{18}O_{carbonate}$ and $\delta^{13}C_{carbonate}$ can be used as a tracer for these processes (Allan and Wiggins, 1993; Scholle and Ulmer-Scholle, 2003).

Negative $\delta^{18}O_{carbonate}$ and $\delta^{13}C_{carbonate}$ values indicate the sample is depleted in the heavier isotope (^{18}O or ^{13}C) relative to the VPDB standard. Conversely, a positive $\delta^{18}O_{carbonate}$ and $\delta^{13}C_{carbonate}$ means that the sample is enriched in ^{18}O or ^{13}C relative to VPDB.

The $\delta^{18}O_{carbonate}$ and $\delta^{13}C_{carbonate}$ can provide clues into environmental variations in carbonate formation. Assuming the isotopic composition of typical marine precipitates of a given age is known, meteoric precipitates typically have lighter $\delta^{18}O_{carbonate}$ and slightly-to-substantially lighter $\delta^{13}C_{carbonate}$. High water temperatures yield calcite and dolomite precipitates with lighter $\delta^{18}O_{carbonate}$ than carbonates formed at lower temperature. During burial diagenesis, the $\delta^{13}C_{carbonate}$ can be overprinted by variable isotope signatures that depending on the nature of the active organic decomposition during the time of carbonate precipitation, whereas the $\delta^{18}O_{carbonate}$ often become lighter to much lighter, due to the influence of isotopically light meteoric or basinal fluids, as well as due to the higher temperature at which these diagenetic processes occur.

6.1.1 Leonardian $\delta^{18}O$ and $\delta^{13}C$ of Carbonates

In total, 79 bulk rock samples were analyzed for $\delta^{18}O_{carbonate}$ and $\delta^{13}C_{carbonate}$ (Fig. 22), 15 of those samples were collected in the upper Leonardian (L6) Glorieta Formation with an additional 33 samples corresponding to the L7-L8 of the Victorio Peak Formation. Sample selection aimed to obtain material from the host calcite or dolomite of the rock and to avoid cements that reflect diagenesis instead of the conditions under which the carbonates formed (Given and Lohmann, 1985). The Leonardian data is plotted in Figure 23.

The isotope values for the Glorieta Formation carbonate and dolostone samples fall into the same range as previously published $\delta^{18}O_{carbonate}$ and $\delta^{13}C_{carbonate}$ for Leonardian carbonates (Ye and Mazzullo, 1993; Saller and Henderson, 1998; Ruppel, 2002; Ruppel and Harrington, 2012). This is especially true for the data from Ruppel (2002), who examined the isotope composition of samples from the formation immediately below the Glorieta Formation, the Clear Fork Formation. The samples from the Victorio Peak Formation show isotope trends that are typical for diagenesis (Fig. 23). The dolomitization that took place within the Glorieta Formation was likely syndepositional dolomite that forms just below the sediment surface during or shortly after sedimentation. Syndepositional dolomite is typically found in tidal flats, which likely is the environment in which the Glorieta Formation was deposited (Milner, 1978). These dolomites typically have heavy $\delta^{18}O$ reflecting the isotope composition of normal to highly evaporated seawater (James and Jones, 2015). Tidal flats are prone to restricted marine circulation and evaporation, sourcing the needed concentrated fluids capable of dolomitizing carbonate sediments (Deffeyes et al., 1965; Patterson and Kinsman, 1982).

The $\delta^{18}O_{carbonate}$ and $\delta^{13}C_{carbonate}$ for the Victorio Peak Formation are significantly lighter than the values previously reported for the Leonardian (Fig. 23). It is important to note that many of the other studies focused on early Leonardian to middle Leonardian formations (L1-L3), while the Victorio Peak Formation represents the last HFS's L7 and L8, which opens the possibility that the $\delta^{18}O$ of water and $\delta^{13}C$ of marine carbonate changed over time. During the late Leonardian, when the Victorio Peak Formation was being deposited, the platform was fully submerged. First exposure and hypersaline conditions did not occur until the late highstand of HFS G1 of the Cutoff Formation (Garcia-Fresca et al., 2012). This flooding of the platform is

corroborated by the fact that there is significantly less dolomitization found in the Victorio Peak Formation compared to any other formation in this study.

The $\delta^{18}O$ and $\delta^{13}C$ of the five dolomitic samples of the Victorio Peak Formation scatter strongly, a finding that matches the wide ranges observed for Leonardian dolostones in previous studies (Ye and Mazzullo, 1993; Saller and Henderson, 1998; Ruppel, 2002; Ruppel and Harrington, 2012). The $\delta^{13}C_{dolomite}$ for the dolomitic samples from the Victorio Peak Formation fall into the broad range of +3.4 to +6‰, whereas other Leonardian dolostones are primarily between +2 to +5‰ (Ruppel and Harrington, 2012). The same holds true for the $\delta^{18}O_{dolomite}$, which typically are between -1 to +3‰ in the Leonardian (Ruppel and Harrington, 2012) but are found in West Dog Canyon to be -2.3 to +2.4‰.

6.1.2 Test of Fidelity of $\delta^{18}O$ and $\delta^{13}C$: The Bench

Within the Victorio Peak Formation, one of the major tests performed for this study was conducted, referred to as The Bench. With abundant faulting throughout the area, a fault block was selected to test the continuity/fidelity of the $\delta^{18}O_{carbonate}$ and $\delta^{13}C_{carbonate}$ along two correlative beds offset by 1.2 m by a normal fault (Fig. 14). Eight samples were collected, four for the lower correlative bed, referred to as Bed I and four for the upper bed, referred to as Bed II. This entanglement of faults might explain why two of the samples belonging to Bed I (samples 16 and 20), both resting in the footwalls of the normal faults, are dolomitized while the remaining samples, two in Bed I and four in Bed II are calcitic (Fig. 24).

Examining the $\delta^{18}O$ and $\delta^{13}C$ for Bed I, the calcitic samples (samples 18 and 30) show nearly identical values, with $\delta^{18}O$ of -3.98‰ and -3.78‰ and $\delta^{13}C$ of +2.63‰ and +2.61‰. The dolomitized samples of Bed I ranges from -2.3‰ to -2.11‰ for $\delta^{18}O$ and +3.88‰ to +4.16‰ for $\delta^{13}C$. The heavier carbon and oxygen isotope values for the dolomitized samples are somewhat

counterintuitive, as one would expect that dolomitization is expected to drive the $\delta^{18}O$ and $\delta^{13}C$ values for the carbonates light.

The four calcitic samples (17, 19, 21, and 31) from Bed II are not as tightly grouped as observed in Bed I. The $\delta^{13}C$ range from +2.55‰ to +2.81‰ and a there is a fairly wide range of $\delta^{18}O$, from -4.47‰ to -3.04‰. The lightest $\delta^{18}O$ for Bed II was associated with sample 21, at -4.47‰, which is noteworthy because it contained the coarsest calcite crystals and was most grain rich compared to the other carbonate samples in Bed II (Fig. 21D). Overall, the $\delta^{18}O$ and $\delta^{13}C$ for both beds book end the $\delta^{18}O$ and $\delta^{13}C$ spectrum of all other Victorio Peak Formation samples. This finding lends support to the claim that $\delta^{18}O_{carbonate}$ and $\delta^{13}C_{carbonate}$ are an unreliable chemostratigraphic tool for the correlation of the stacked carbonates in the field area of this study.

6.1.3 Guadalupian $\delta^{18}O$ and $\delta^{13}C$ of Carbonates

In addition to the 48 Leonardian samples collected, 31 samples of Guadalupian age were also analyzed. From these samples 8 belong to the Cutoff (G1-G4), 4 to the Cherry Canyon (G8), 16 to the Upper San Andres, and 3 to the Grayburg Formation. To study the isotope trends, the Guadalupian data set was compiled in Figure 25.

The $\delta^{18}O$ and $\delta^{13}C$ for almost all Guadalupian samples collected in this study are significantly lighter than those from previous work in the Permian Basin (Vogt, 1986; Ruppel and Cander, 1988; Saller and Henderson, 1998). These studies found that typical $\delta^{18}O_{carbonate}$ values for the Guadalupian San Andres and Grayburg formations were in a range of +3‰ to +6‰. My results show a much lighter range for the Cutoff, Cherry Canyon, Upper San Andres, and Grayburg formations (Fig. 25). A possible explanation for the differing values compared to the existing regional Guadalupian studies, is that most of the previous studies were located on the

Central Basin Platform. Here the relatively heavy $\delta^{18}O$ signatures of Guadalupian dolomites have invariably been interpreted to have been produced during dolomitization by evaporatively concentrated seawater (Ruppel and Harrington, 2012). These brine waters may not have penetrated far enough downdip of the platform, leaving the shelfal Guadalupian samples with a lighter $\delta^{18}O$ signature. Alternatively, one could attribute the comparably light $\delta^{18}O$ and $\delta^{13}C$ found for the samples from the Cutoff, Upper San Andres, and Grayburg formations to meteoric diagenesis during the many lowstands associated with the Guadalupian.

6.1.4 Changes in $\delta^{18}O$ and $\delta^{13}C$ over a High Frequency Cycle

Obviously, it is difficult to correlate the shelf outcrops with platform sections with the help of $\delta^{18}O_{carbonate}$ and $\delta^{13}C_{carbonate}$. Both areas experienced significantly different environmental variations while primary carbonate formation and during subsequent diagenesis, resulting in large, and inconsistent isotope range for this study as well as previous work (Fig. 26). While this outcome highlights that $\delta^{18}O_{carbonate}$ and $\delta^{13}C_{carbonate}$ are not a suitable chemostratigraphic tool in my area of study, the question remains if $\delta^{18}O_{carbonate}$ and $\delta^{13}C_{carbonate}$ could reveal information on environmental or diagenetic conditions for small stratigraphic scales, namely throughout a single high frequency cycle.

To test the isotopic variability within a high frequency cycle, a total of 9 samples were collected across two separate 5th order carbonate cycle sequences of the Victorio Peak Formation, with a vertical distance between sampling points of 20 cm. These cycles are referred to as Cycle A (lower cycle) and Cycle B (upper cycle) and are approximately 80 cm thick (Fig. 15). Across these two cycles of less than 2 m total thickness, one observes a wide range of +2.4‰ to +4.6‰ for $\delta^{13}C$ and -4.2‰ to -1.9‰ for $\delta^{18}O$. Within Cycle A the isotopically light values are at the top and bottom. At the bottom of the cycle (sample 72) it appears that karsting

occurred, and the top of the cycle (sample 75) could also be the result of exposure to subaerial conditions. This would explain the light isotopic values found for sample 72 and 75. This implies that the top and bottom of the cycle may have been exposed to meteoric fluids driving the $\delta^{18}O_{carbonate}$ and $\delta^{13}C_{carbonate}$ to light values, while the samples in the core of the high frequency cycle (samples 73 and 74) preserved the heavy primary marine isotope signature. In Cycle B, light values are seen in both $\delta^{18}O_{carbonate}$ and $\delta^{13}C_{carbonate}$ as one gets closer to the exposed cycle top. Similar to Cycle A, samples likely have been exposed to meteoric waters causing the depleted isotopic values seen in samples 77 to 80. With sample 76 preserving the primary marine isotope signature.

These results underline that $\delta^{18}O_{carbonate}$ and $\delta^{13}C_{carbonate}$ may be powerful tools to decipher the diagenetic history of a sample or an entire sequence, but of limited applicability as a chemostratigraphic tool. Since CAS isotope signatures are expected to be more robust when it comes to diagenetic processes, they may be better suited as chemostratigraphic tool.

6.2 CONTENT AND SULFUR ISOTOPE COMPOSITION OF ESS AND CAS

The sulfur isotopic composition found in ancient rocks of seawater sulfate can provide insight into redox reactions in the ocean-atmosphere (Claypool et al., 1980). Traditionally the most commonly used tool for ancient sulfate analysis was through the study of evaporites but these are limited in time and space (Marenco et al., 2008). In contrast, the record of ancient carbonates is well understood, along with the understanding that trace amounts of sulfate are incorporated into carbonate minerals (Pingitore et al., 1995). This has led to the use of sulfur isotopic analysis of CAS as a geochemical proxy for the sulfur isotope composition of seawater sulfate over Earth's history (Kampschulte and Strauss, 2004). Along with the increased popularity of this approach comes the question of how reliable CAS isotope records truly are.

Marenco et al. (2008) stated, “Although CAS in recent sediments has been shown to agree with modern seawater sulfate, the fidelity of the CAS signals in rocks that have undergone variable degrees of alteration (including dolomitization) remains uncertain, and diagenetic studies are warranted.” I hope that the results of this study will contribute to a better understanding of the effects of diagenesis on the fidelity of isotope signatures from CAS.

In total, 36 samples were treated with my CAS extraction method. The ESS content was found to be between 10 and 3,525 ppm sulfate. The CAS content falls into a range of 0 to 742 ppm sulfate. In several instances, I was not able to extract CAS for isotope analysis, in some cases this was due to insufficient CAS content (seven in total), and in other cases due to failures in the CAS extraction procedure. Namely, seven samples were contaminated with insoluble particles due to defective 0.45 μm membrane filters and could not be analyzed for $\delta^{34}S_{CAS}$. Of the seven samples not producing adequate CAS, it should be noted that two of these samples were of the highly dolomitized siliciclastics of the Cherry Canyon and Grayburg formations. For a successful CAS extraction from these two samples, the sample size would have had to be significantly larger than the 28 and 40 grams collected. The loss of these 14 $\delta^{34}S_{CAS}$ values limited the stratigraphic extent of the study and did not provide enough with CAS data to perform a detailed analysis of the transect from the Cutoff through the Upper San Andres formations. The remaining 22 samples with $\delta^{34}S_{CAS}$ values represented the following formations: 5 samples from the Glorieta, 14 from the Victorio Peak, 2 from the Cutoff, and 1 from Upper San Andres Formation. While the sample distribution negatively impacted the proposed analysis of a transect, there is enough sample density within the Victorio Peak Formation to assess CAS as a chemostratigraphic tool in my study area.

6.2.1 Analysis of CAS Methodology

By examining the relationship between ESS and CAS content as well as sulfur isotope composition one can assess if the employed extraction procedure is sound. If, for example, the ESS extraction procedure was inefficient, one would expect that ESS from samples with high ESS content would be carried over into the CAS pool, leading to a correlation between ESS and CAS content, and to a convergence in the isotope composition of ESS and CAS (Fig. 27 and Fig. 28). The absence of such a trend, and the distinctly lighter $\delta^{34}S_{ESS}$ as compared to $\delta^{34}S_{CAS}$ corroborates that my method efficiently segregates ESS from CAS.

A major concern in the extraction of CAS is potential contamination with sulfate derived from the oxidation of ^{34}S-depleted iron sulfide (pyrite) that was previously formed via bacterial sulfate reduction (Chambers and Trudinger, 1979). This was particularly a concern because pyrite was abundantly found in thin sections investigated in this project. While no correlation was found between thin section characteristics and highest CAS content, samples with the highest ESS content all displayed varying degrees of pressure dissolution evidenced by stylolites. The sample with the highest ESS content of 3,526 ppm, sample 63 of the Glorieta Formation, had noticeable oxidation rims around one of its stylolites (Fig. 18C). Intense pyrite oxidation during the ESS extraction step can be discovered as a correlation between high ESS content and light $\delta^{34}S_{ESS}$, and for the CAS extraction step as a correlation between high CAS content and light $\delta^{34}S_{CAS}$. Several samples whose whole rock ESS was well above 1500 ppm coincide with low $\delta^{34}S_{ESS}$. Also a CAS sample with a content of higher than 500 ppm and a $\delta^{34}S_{CAS}$ below 11‰ can potentially be attributed to pyrite oxidation (Fig 29). However, it must be noted that there is also another case where pyrite oxidation can have a detrimental effect. If CAS contents are generally low, even a minute contribution of pyrite oxidation can drive $\delta^{34}S_{CAS}$ light, leaving

little evidence in form of elevated CAS contents. Such a scenario could be envisioned for a sample that contains abundant siliciclastics, and little carbonate. Indeed, my samples yielded comparably low contents of CAS for carbonates (0 to 742 ppm) and dolomites (0 to 521 ppm) when compared to compilations (Fig. 30). The question arises if my method under-extracted CAS due to difficulties in the precipitation of $BaSO_4$ linked to the precipitation of $BaCl_2$ in presence of high concentrations of HCl. Non-quantitative precipitation of CAS could potentially also lead to isotope fractionation between sulfate that remains in solution and the precipitate, with the precipitate potentially being enriched in ^{18}O and ^{34}S. Currently, there is no evidence that this scenario occurred, however, I cannot disprove this possibility either.

6.2.2 Test of Fidelity of $\delta^{34}S$: The Bench

The Bench consists of two separate horizons, referred to as Bed I and Bed II with beds that could be correlated across a fault plane. The sampling location is situated near two additional pronounced faults, potentially allowing for ample fluid flow and heterogeneous diagenesis. Moreover, the carbonates in this part of the Victorio Peak Formation contain dead oil and ample pyrite, which were detected in thin section, as residue of oil after acid dissolution of carbonate, and as sulfur smell during rock crushing (Figs. 17B, 19B, 21B, and 21C). These circumstances create conditions that are challenging for CAS extraction. If $\delta^{34}S_{CAS}$ in this setting turns out to be robust this proxy could indeed prove to be a powerful chemostratigraphic tool. Eight samples were collected across two beds, Bed I and Bed II. Bed I was the lower of the two beds and contains two dolomitized samples (samples 16 and 20). These samples were likely dolomitized by migrating fluids along one of the several fault planes (Fig. 14 and Fig. 28). Two samples did not provide enough CAS for $\delta^{34}S_{CAS}$ analysis, the dolomitized sample 16 and a sample from Bed II (sample 31). Moreover, another sample (sample 19) from Bed II was part of

the contaminated sample group with insoluble particles due to defective 0.45 μm membrane filters, and could not be run for analysis. This with 5 of the original 8 to assess the fidelity of $\delta^{34}S_{CAS}$.

Of the two remaining calcitic samples from Bed I, the $\delta^{34}S_{CAS}$ of sample 18 has a value of +18.5‰ and sample 30 has a value of +16.8‰, meaning that they are 1.7‰ apart. The dolomitic sample 20, of Bed I, has a $\delta^{34}S_{CAS}$ of +15.5‰, 1.3‰ lighter than sample 30. This finding is important because previous studies by Marenco et al. (2008) had reported dolomitization to create 6‰ to 8‰ depletion in $\delta^{34}S_{CAS}$. The $\delta^{34}S_{CAS}$ of Bed II's calcitic samples, sample 17, has a value of +14.9‰ and sample 21 has a value of +11.6‰, meaning that they are 3.3‰ apart. All together, these findings do not bode well for $\delta^{34}S_{CAS}$ as a new tool for chemostratigraphic applications. Considering that the entire data span for $\delta^{34}S$ of sulfate in seawater during the Permian was +12.5‰ to +19.5‰ (Claypool et al., 1980), a data difference of 3.3‰ for CAS from a single bed is detrimental. Curiously, if one plots Bed I and Bed II samples against the rest of the dataset, one can still identify The Bench samples out of the large data spread, which raises the question if there were drastic changes in the $\delta^{34}S$ of sulfate in the waters in which the samples formed.

6.2.3 CAS Trend Analysis

The reasons I chose this study area was because basin restriction could be detected with $\delta^{34}S_{CAS}$, which would be revealed as divergence from the $\delta^{34}S$ reported for seawater sulfate during this time interval. The $\delta^{34}S_{CAS}$ values found in this study range from +10.3‰ to +18.5‰ (Figs. 28 & 29). These values fall within a much wider range than the previously defined average of CAS during the Permian, +12.1 to +14.4‰, with increasing CAS values towards the end of the Permian (Kampschulte and Strauss, 2004).

To investigate the $\delta^{34}S_{CAS}$ over the Lower and Upper Permian in a marine basin with potentially changing restriction with regards to the open ocean, I took samples in a stratigraphic transect spanning four formations, from the Glorieta to the Upper San Andres formations, with greatest sample density in the Leonardian section of the profile, which corresponds to the Victorio Peak Formation (Fig. 31). A key observation is that $\delta^{34}S_{CAS}$ are generally heavier than the 12‰ to +14.4‰ value that characterizes the $\delta^{34}S$ of sulfate in seawater during the Permian (Kampschulte and Strauss, 2004; Paytan and Gray, 2012), and that the $\delta^{34}S_{CAS}$ range for the Victorio Peak Fromation (+11.6‰ to +18.5‰) is noticeably heavier than for the other formations (+10.3‰ to +15.8‰) (Fig. 31).

This observation is important because $\delta^{34}S_{CAS}$ that are heavier than expected cannot be easily attributed to artifacts, unlike $\delta^{34}S_{CAS}$ that are lighter than expected, where oxidation of reduced sulfur compounds is a valid explanation. Incorporation of isotopically heavy sulfate into carbonates can occur during carbonate precipitation associated with microbial sulfate reduction within marine sediments (Fig. 32). However, for a substantial increase in the $\delta^{34}S$ of dissolved sulfate to take place, the amount of sulfate must be limited – a condition that also limits the amount of sulfate that can be incorporated in the carbonates formed during diagenesis (Fig. 33). Based on this argument, one can consider isotopically heavy $\delta^{34}S_{CAS}$ as more reliable recorders of the $\delta^{34}S$ of seawater sulfate than light $\delta^{34}S_{CAS}$, especially if the heavy $\delta^{34}S_{CAS}$ display a consistent trend that is interrupted by isolated data points with much lighter values. Following this scenario, the trend to heavy $\delta^{34}S_{CAS}$ for the samples from the Victorio Peak Formation indicates that during the Leonardian a phase of enhanced basin restriction took place.

I expect that relative sea level lowstands lead to stratification of the water masses, which causes a reduction in the amount of oxygen that is available for the mineralization of organic

matter. Once oxygen is fully depleted (anoxia/anoxic conditions) sulfate reducing bacteria dominate the mineralization of organic matter, by coupling its oxidation to the reduction of sulfate to sulfide (H_2S). Microbial sulfate reduction drives the $\delta^{34}S_{sulfate}$ to heavier values, which is recorded in the form of heavier $\delta^{34}S_{CAS}$ like what is seen in the Victorio Peak Formation. This scenario is supported by the fact that the basinal equivalent of the Victorio Peak Formation is the Bone Springs Formation, which has been interpreted as an organic rich anoxic basin facies (Newell et al., 1953; Kirkby, 1982; Fitchen, 1992).

Conversely, trends to light $\delta^{34}S_{CAS}$ values close to the value of 12‰ that characterizes Permian seawater sulfate (Paytan and Gray, 2012), can be interpreted as enhanced connection of water masses between the Permian Basin and the global ocean. It is known that at some point in the Guadalupian, a large-scale transgression occurred, burying the Leonardian-aged platform beneath deepwater sediments (Meissner, 1972). This transgression can be correlated across the Delaware Basin into the Western Interior of the North American continent, indicating this was a craton-wide, if not global in scale event (Hurd et al., 2016) and that the Delaware Basin was no longer decoupled from the global ocean. The $\delta^{34}S_{CAS}$ from the Upper San Andres Formation with +10.7‰ it is nearly 5‰ lighter than the average $\delta^{34}S_{CAS}$ value from the Victorio Peak Formation and distinctly lighter than the $\delta^{34}S_{CAS}$ from the early-Guadalupian Cutoff Formation (+15.3‰ and +15.8‰). This indicates that this major transgression likely occurred Mid-Guadupian, during the deposition of the Upper San Andres Formation. The $\delta^{34}S_{CAS}$ data set does not reveal the transgression that must have occurred between the deposition of the Victorio Peak Formation (ramp margin to slope facies) and the Cutoff Formation (deep water facies). Either, this transgression did not alleviate basin restriction, or my sampling density was not high enough to pin down the transgression.

Another important observation can be made from the $\delta^{34}S_{CAS}$ from the five samples collected from the Glorieta Formation. The $\delta^{34}S_{CAS}$ of the only calcitic sample within this group falls in between the $\delta^{34}S_{CAS}$ of two dolomitic samples, constituting a trend to heavier $\delta^{34}S_{CAS}$ before a drop to the lightest $\delta^{34}S_{CAS}$ measured in the entire study. These changes could reflect a true change in $\delta^{34}S_{CAS}$ or be the result of diagenetic overprints. Marenco et al. (2008) demonstrated that the $\delta^{34}S_{CAS}$ of dolomitized samples can be 6‰ to 8‰ lighter than their calcitic counterparts. Out of the four dolomitic samples from the Glorieta Formation, three record lighter $\delta^{34}S_{CAS}$ than the calcitic sample, however, there is also a dolomitic sample that is strongly enriched in ^{34}S compared to the calcitic sample. Thus, my sample set shows that dolomitic samples may either be faithful recorders of $\delta^{34}S$ of seawater sulfate, or that dolomitization can arbitrarily lead to an enrichment or depletion in ^{34}S, and that it cannot be assumed that dolomitization must result in lower $\delta^{34}S_{CAS}$.

7. CONCLUSIONS

Expectedly, the $\delta^{18}O_{carbonate}$ and $\delta^{13}C_{carbonate}$ turned out to be not suitable as tool for the chemostratigraphic correlation of the stacked carbonates of study area. Unfortunately, at this state of knowledge, a similar conclusion must be drawn for $\delta^{34}S_{CAS}$. Apparently, the $\delta^{34}S_{CAS}$ seawater sulfate proxy is, like carbonates, also vulnerable to diagenetic overprinting. However, the processes that cause the overprint for $\delta^{18}O_{carbonate}$ and $\delta^{13}C_{carbonate}$ may not be identical to the processes that alter $\delta^{34}S_{CAS}$. As for the carbonates, the question becomes if careful screening of samples by methods such as microscopy, oxygen and carbon isotope analysis of carbonate, and cathode luminescence investigations can be utilized to assess if obtained $\delta^{34}S_{CAS}$ are likely overprinted or if they display primary signatures. Moreover, taking multiple samples along beds might help to obtain an estimate for the original $\delta^{34}S_{CAS}$. Following the argument that overprinting tends to cause $\delta^{34}S_{CAS}$ to be light, one would consider the heaviest $\delta^{34}S_{CAS}$ as the most accurate value. An increased sampling density would reveal if there are true trends in $\delta^{34}S_{CAS}$, or if the data simply scatter. Finally, one could target specific carbonate phases within the rocks for CAS extraction, for example by employing microdrilling. While these measures are likely to improve the fidelity of $\delta^{34}S_{CAS}$ they come at a price, namely the need for massively increased sample numbers, and additional testing. This caveat presents a major challenge to the application of $\delta^{34}S_{CAS}$ as a chemostratigraphic tool in an industry setting, where high throughput and low costs are essential.

Not all my findings are discouraging. For example, I extracted CAS from calcitic and dolomitic samples in quantities that allowed for sulfur isotope analysis from as little as 28 g of crushed sample. This is significantly less than the 150-300 g used in previous studies (Kampschulte and Strauss, 2004; Marenco et al., 2008). Furthermore, I found at least one

example that indicates that $\delta^{34}S_{CAS}$ from dolomite are not necessarily giving lighter isotope values than the $\delta^{34}S_{CAS}$ of their calcitic counterparts, which makes me hopeful that with precaution, also $\delta^{34}S_{CAS}$ from dolomite can be considered a recorder of $\delta^{34}S$ of seawater sulfate. Moreover, I made two intriguing observations. First, CAS contents of calcitic and dolomitic samples are very low compared to compilations from previous studies. Leaving the possibility of sampling artifacts aside, this finding would imply that the diagenetic events affecting my samples led to a particularly strong release of sulfate from the carbonates, or that the seawater in which the carbonates formed was relatively sulfate poor. The second finding is that the sample set from the Victorio Peak Formation appears to show a secular change in $\delta^{34}S$ of seawater sulfate, indicating that basin restriction may have occurred during the Leonardian time slice – a finding that could be compatible with low sulfate contents in the surface waters of the basin. These indicators of possible restriction are consistent with the fact that the basinal equivalent of the Victorio Peak Formation, the Bone Springs Formation, has been interpreted as corresponding to an organic-rich anoxic basin facies (Newell et al., 1953; Kirkby, 1982; Fitchen, 1992).

8. OUTLOOK / FUTURE WORK

In a review on chemostratigraphy, Weissert et al. (2008) mentions the potential of the seawater $\delta^{34}S_{sulfate}$ record as chemostratigraphic tool, referring to time slices where there are prominent fluctuations in the Cretatceous and Cenozoic sulfur isotope curve. Currently, $\delta^{34}S_{CAS}$ as a chemostratigraphic tool lacks the high temporal resolution that has been established for carbon, oxygen, and strontium (Veizer et al., 1999). The power of the most commonly used chemostratigraphic tool, $\delta^{13}C_{carbonate}$ and $\delta^{18}O_{carbonate}$ is the short residence time of carbonate in the ocean-atmosphere system, which allows to record short-time excursions, and the amazing sampling density throughout Earth's geological past and across a wide range of paleogeographic settings, a data set that has accumulated since Sam Epstein's discovery around 1951 that ancient ocean temperatures can be determined from $\delta^{18}O_{carbonate}$. The beauty of this massive data set of $\delta^{13}C_{carbonate}$ and $\delta^{18}O_{carbonate}$ is that for stratigraphic purposes, one can match up shifts between different sampling locations, often referred to 'wiggle matching'. These shifts in isotope composition can often still be detected when the carbonates have been affected by diagenesis, because the trends remain detectable even if the absolute value is shifted. Does the seawater $\delta^{34}S_{sulfate}$, as recorded as $\delta^{34}S_{CAS}$ hold the same potential?

Throughout the Phanerozoic, sulfate concentrations in the oceans shifted, but were likely never below 1mmol/l (today approximately 29 mmol/l), and sulfur fluxes in the ocean-atmosphere system remained always at least ten times smaller than the carbon fluxes. Consequently, the residence time of sulfate in the ocean is much longer than carbonate, which means that the seawater $\delta^{34}S_{sulfate}$ record only tracks major prolonged changes in sulfur fluxes, thus does not record short-time excursions. Based on this consideration, $\delta^{34}S_{CAS}$ cannot be expected to be an as powerful tool for high-resolution wiggle matching as $\delta^{13}C_{carbonate}$ and

$\delta^{18}O_{carbonate}$. Within the framework of this thesis, I took an unconventional approach by re-interpreting $\delta^{34}S_{CAS}$-chemostratigraphy as a tool for intrabasinal correlations, instead of a recorder of the global seawater $\delta^{34}S_{sulfate}$ record. Within a restricted basin, the residence time of sulfate would be much shorter, potentially giving way for a high-resolution $\delta^{34}S_{sulfate}$ record with many shifts and wiggles. In this case, what would it take to establish $\delta^{34}S_{CAS}$ as a powerful chemostratigraphic tool for intrabasinal correlation, i.e. to establish a high-resolution seawater $\delta^{34}S_{sulfate}$ record in a basin? Two components would be key to reach this goal; sampling and a data interpretation. With respect to sampling one would need to follow the success story of $\delta^{13}C_{carbonate}$ and $\delta^{18}O_{carbonate}$, which is essentially based on high sampling density. Probably, for the interval studied in the framework of this thesis, one would need to increase the sample number by a factor of ten (i.e. rather 350 samples than 35). This data set could be augmented by simultaneous analysis of $\delta^{34}S_{pyrite}$, which should show the same trends, just with an isotope offset. One could further augment the $\delta^{34}S_{sulfate}$ record by extracting barite, and where available, probably from near-shore settings, primary gypsum. Secondly, one would need to interpret that data in a fashion that acknowledges that there are samples that are distinctly more and others that are distinctly less reliable recorders of $\delta^{34}S_{sulfate}$. Quality-checks of samples by methods such as microscopy, oxygen and carbon isotope analysis of carbonate, cathode luminescence, and ion microprobe would be helpful in making such an assessment. In general, one would expect that bulk CAS samples are likely less reliable recorders of $\delta^{34}S_{sulfate}$ signatures than CAS that has been obtained from shell material that was extracted from the rock by micro-drilling. Finally, once a high-resolution data set is established, one would need to take into account that it is much more likely that $\delta^{34}S_{CAS}$ have been altered to lighter values, than to heavier values. Thus, the envelope that falls on the side of the heavy isotope compositions of a $\delta^{34}S_{CAS}$ data set might be

considered a better high-resolution seawater $\delta^{34}S_{sulfate}$ record of a basin than trendlines based on smoothing techniques such as moving averages. If this approach is further accompanied by analyses of $\delta^{18}O_{CAS}$, and the analysis of the content and isotopic composition of inorganic (i.e. pyrite and native sulfur) and organic sulfur, multi-proxy chemostratigraphic correlations could be performed. Such multi-proxy approaches are likely more robust as they are not prone to be skewed by single outliers.

It is interesting to note that dolomite can form in the small semi-closed pores or micro-niches of shell borings and micro-borings within grain dominated calcitic carbonates. These micro-niches retain connate water and become anoxic due to microbial activity. The latter mediates the precipitation of dolomite (Strohmenger et al., 2014). This raises the question, if sulfate in these micro-niches becomes isotopically heavy, and if trapped in newly formed dolomite, it also drives $\delta^{34}S_{CAS}$ heavy?

Probably the most pressing next step in future exploration of $\delta^{34}S_{CAS}$, employing some of the mentioned screening techniques, is to carefully evaluate my findings of low CAS contents of calcitic and dolomitic samples in combination with the fact that the sample set from the Victorio Peak Formation appears to show a secular change in $\delta^{34}S$ of seawater sulfate. If confirmed, these findings would yield unprecedented insight into the history of the Permian Basin.

9. FIGURES

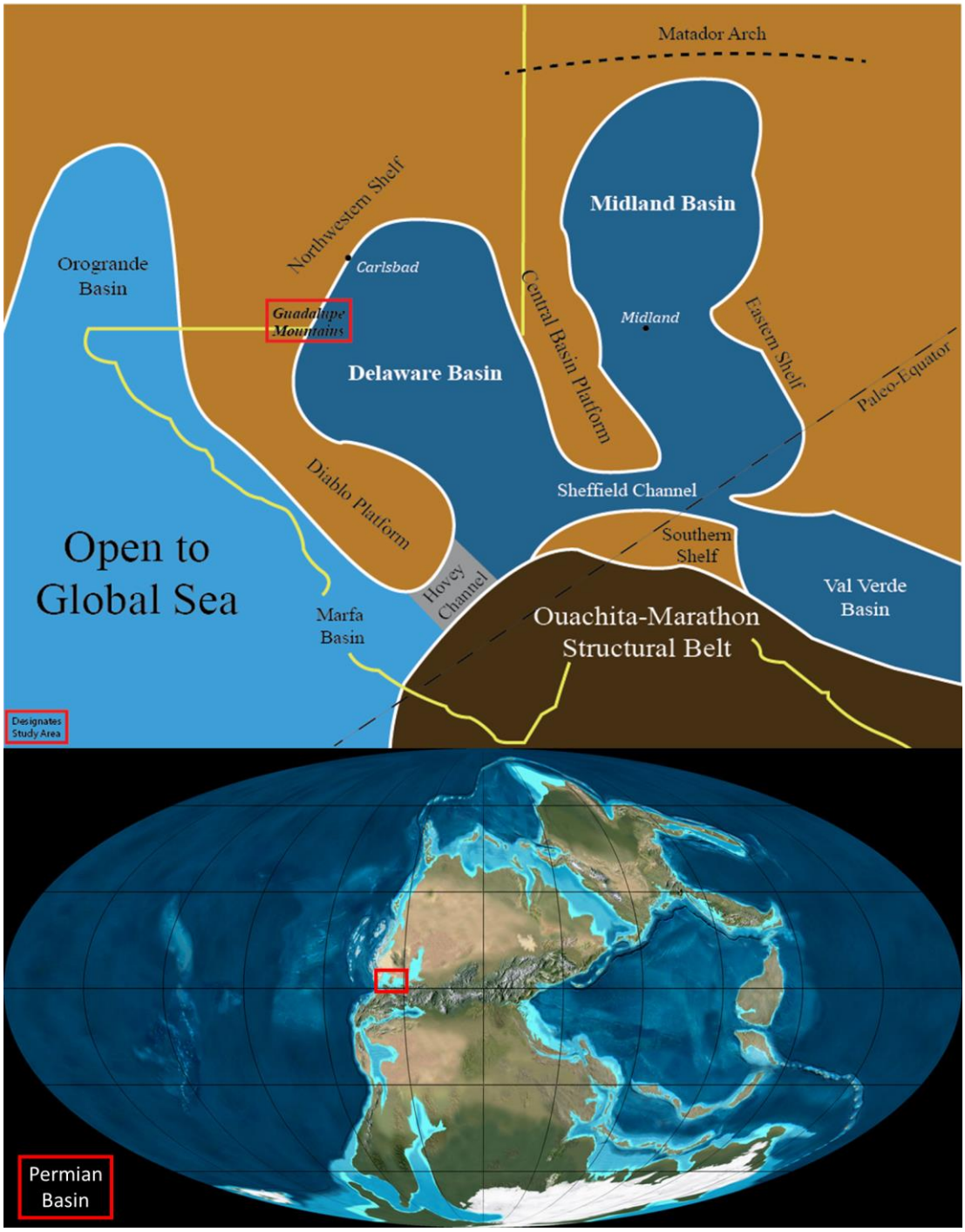

Figure 1: Paleogeographic Map of the Permian Basin during the Guadalupian Epoch.
Map shows major platform, basin elements, study area, and possible restriction along the Hovey Channel separating the Permian Basin from the Global Sea. Modified from Ward et al. (1986) and Blakey (2001).

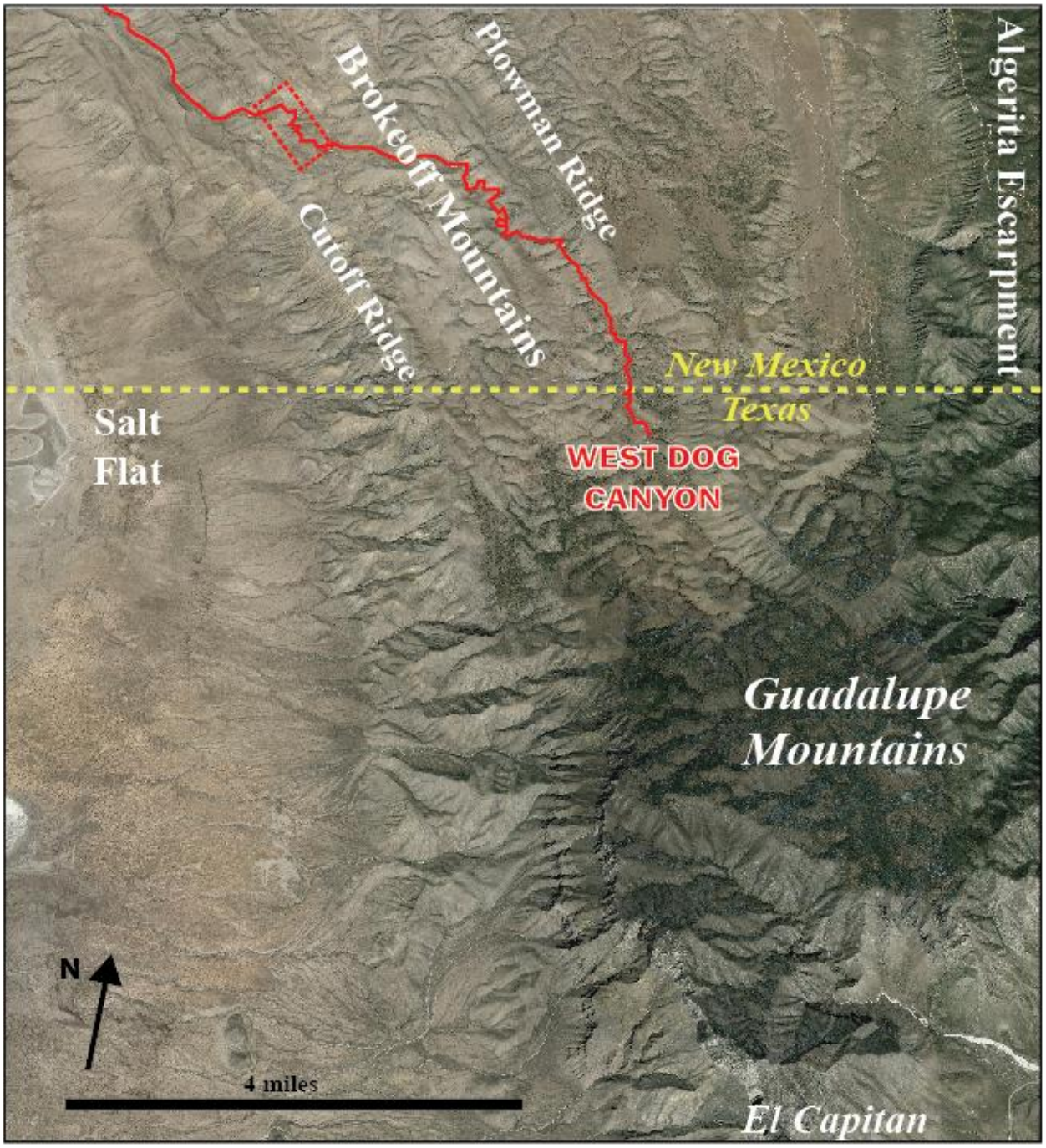

Figure 2: Google Earth image of Guadalupe Mountain region.
Highlighted on this Google Earth image, along with major physiographic features of the area. Study area within West Dog Canyon is shown with the red box.

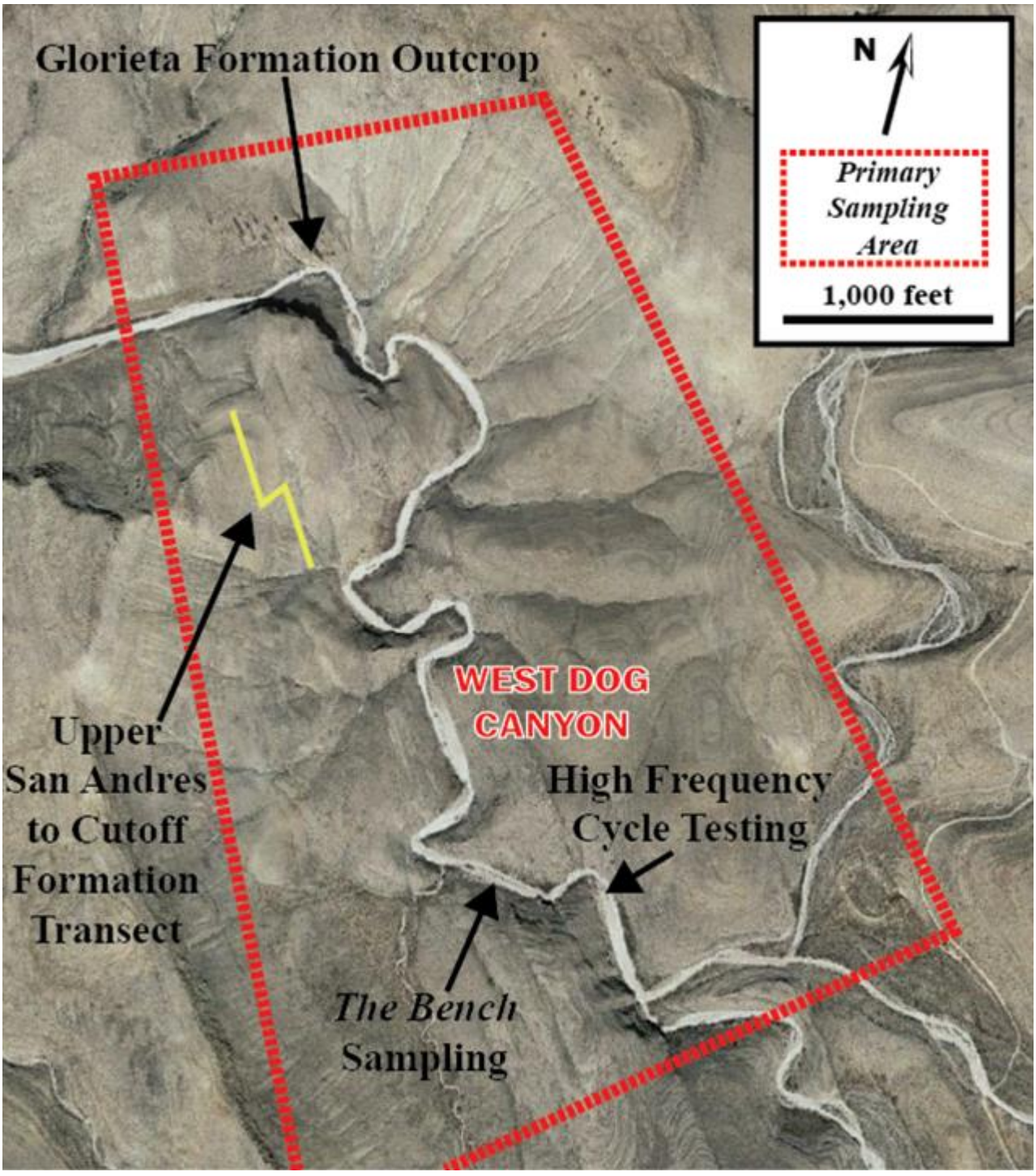

Figure 3: Google Earth image of primary study area within West Dog Canyon.
Red box shows primary sampling area. Coordinates for Glorieta Formation: 32°03'48.32" N 104°57'7.66" W; Top of Transect (Upper San Andres Formation): 32°03'27.63" N 104°57'13.08" W; Bottom of Transect (Cutoff Formation): 32°03'23.59" N 104°57'01.24" W; The Bench: 32°03'14.826" N 104°56'43.799" W; High Frequency Cycle Testing: 32°05'15.29" N 104°56'40.33" W.

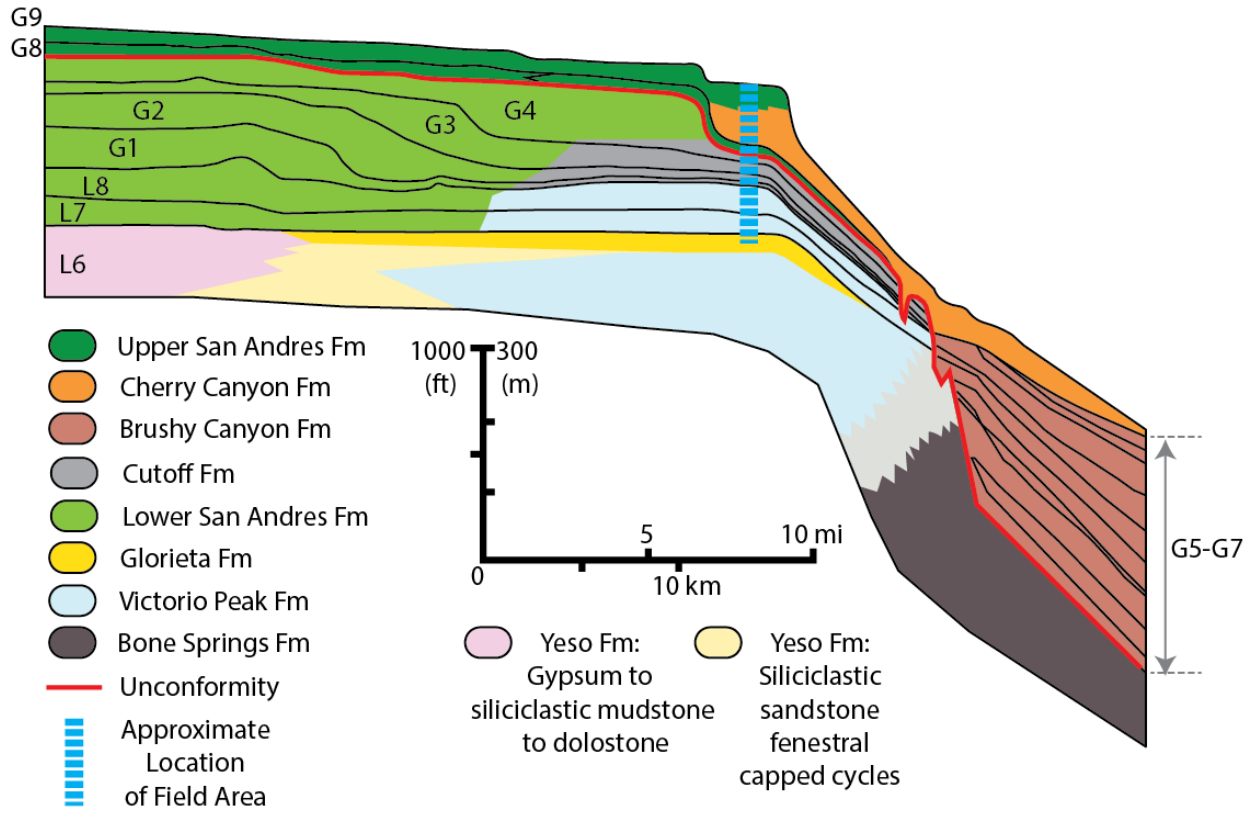

Figure 4: Lithostratigraphy of the platform complex, illustrating HFSs L6-G9.
The blue dashed line is the approximate location of the field area in the Brokeoff ~~Mountain~~mountains on the shelf/outer shelf of the platform. Modified from Kerans & Ruppel (1994) and Kerans & Kempter (2002).

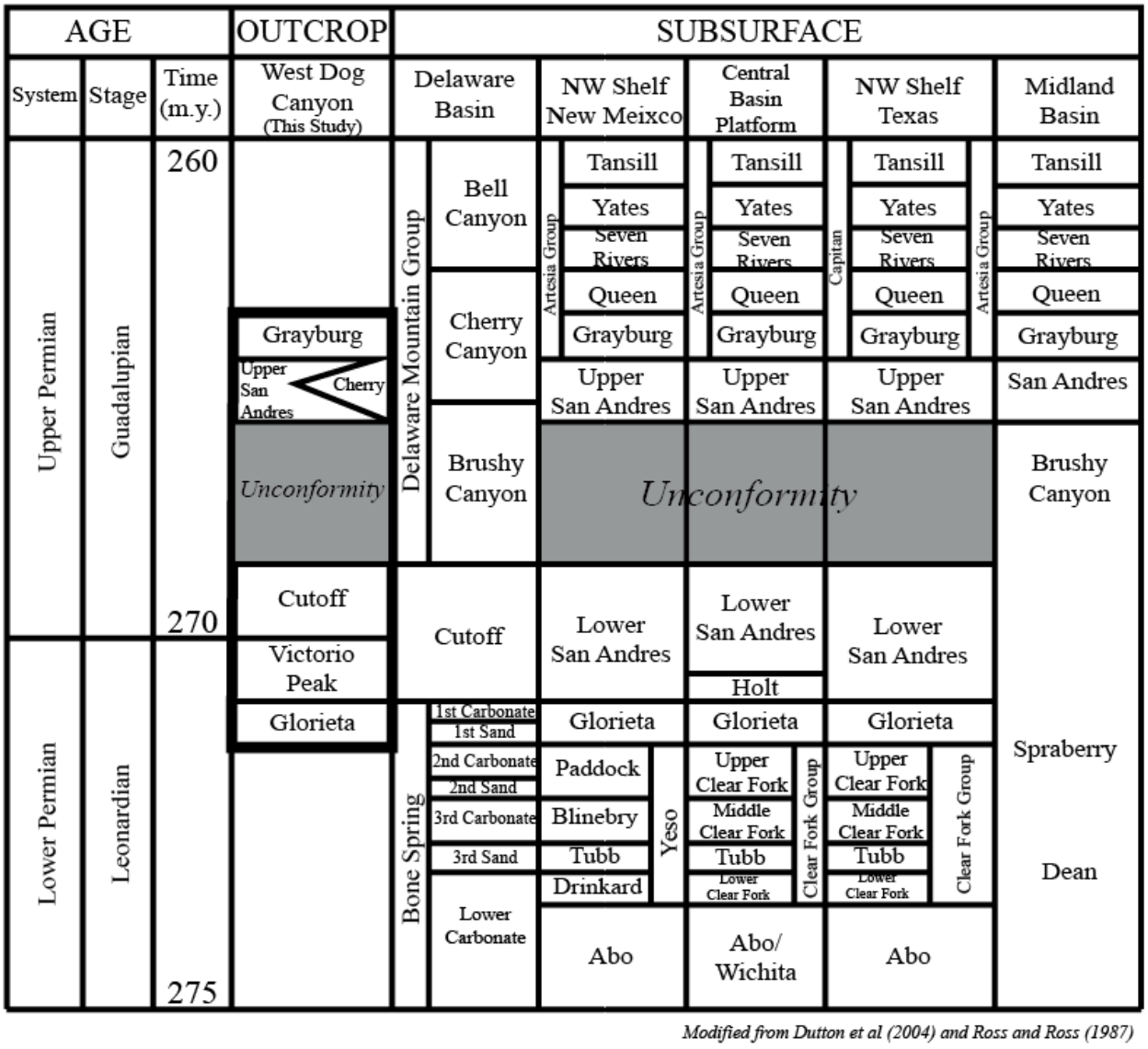

Modified from Dutton et al (2004) and Ross and Ross (1987)

Figure 5: Stratigraphic architecture of the Permian Basin.
Depicts relationship between the studied outcrops (box in bold) and the subsurface. Note: 'Cherry' is short for Cherry Canyon Formation.

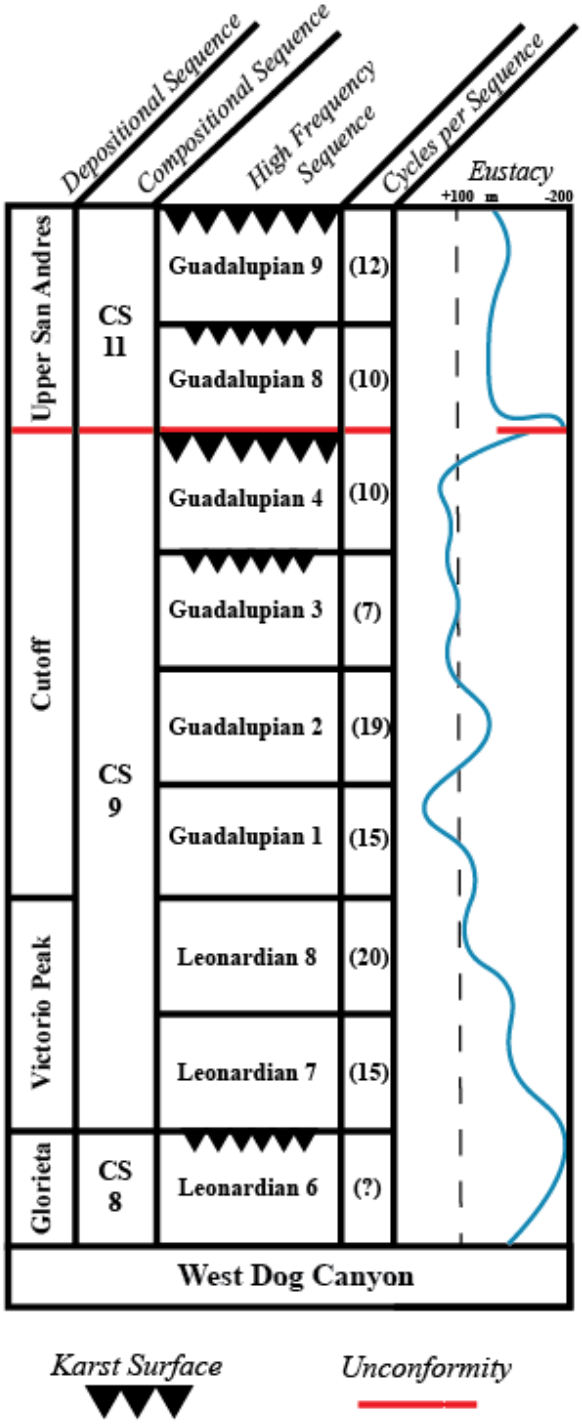

Figure 6: Stratigraphic nomenclature of the major units found within the West Dog Canyon. The red line illustrates the sedimentary bypass unconformity (corresponds to the basinal Brushy Canyon Formation) that separates the Cutoff from the Upper San Andres Formation.

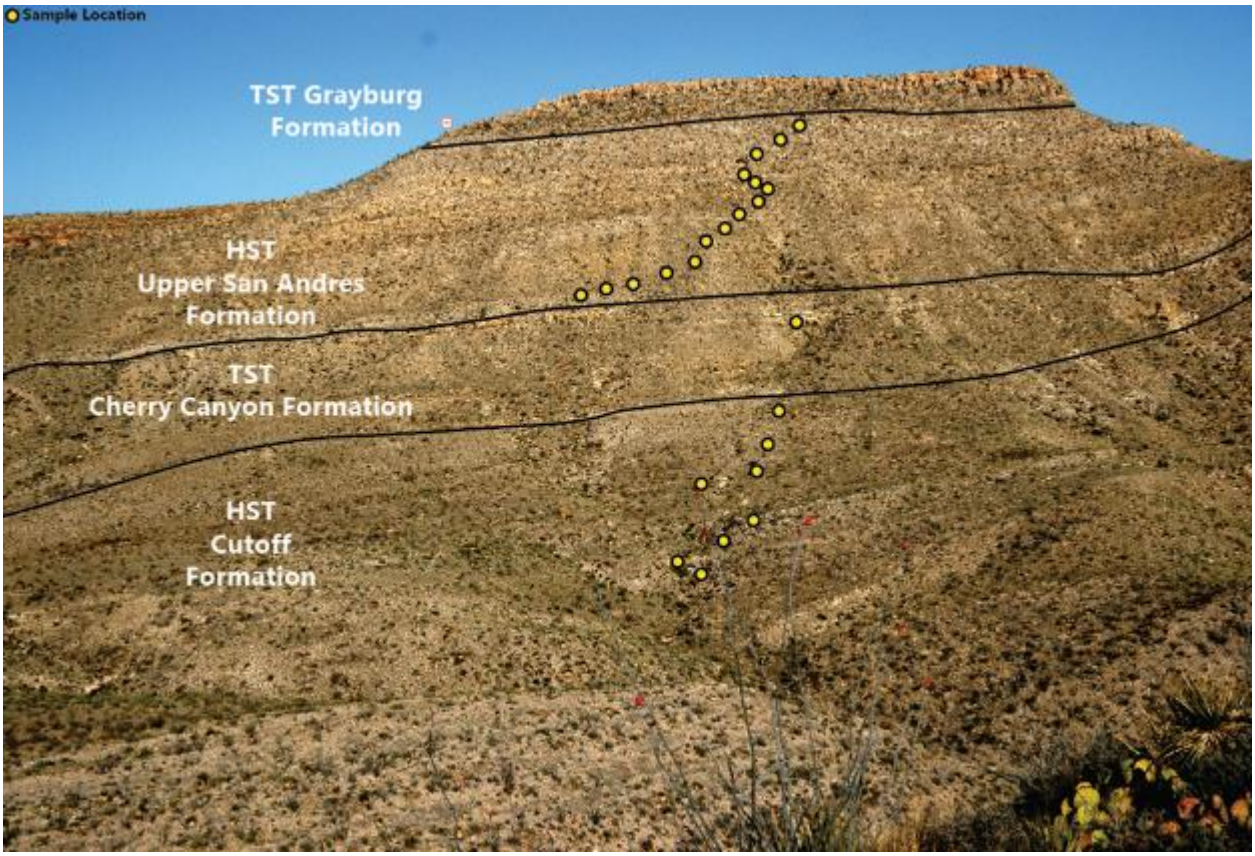

Figure 7: Transect from Cutoff Formation (base) to the Grayburg Formation (top of the hill). Samples were taken from the Cutoff Formation, the siliciclastic Cherry Canyon Formation, and the Upper San Andres Formation. At the field site, the Cherry Canyon Formation follows on top of the Cutoff Formation. In other areas, the Cherry Canyon Formation interfingers with the Upper San Andres Formations.

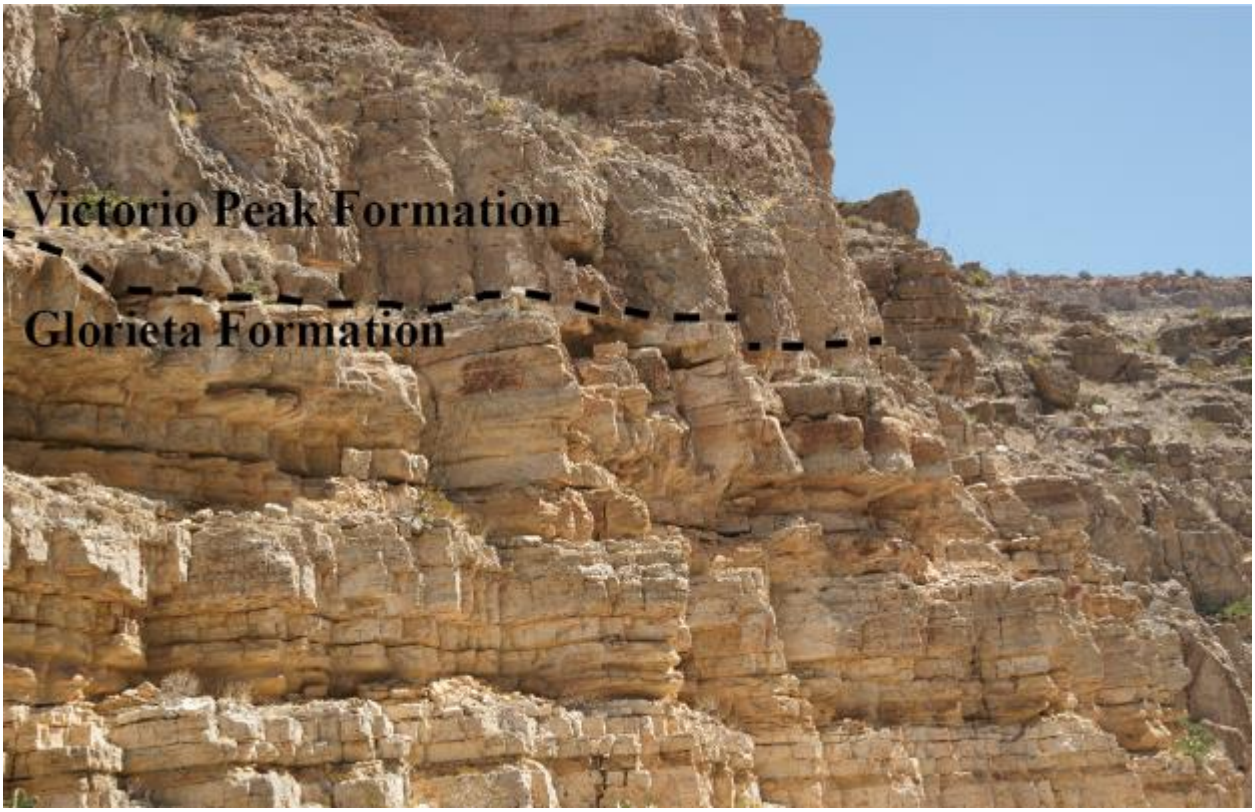

Figure 8: Contact between the Glorieta and Victorio Peak Formations.
The darker overlying Victorio Peak Formation is composed of open marine skeletal packstones. The sediments of the lighter Glorieta Formation consist of dolomitic beds formed in peritidal cycles and of fine grained siltstones with carbonate cements.

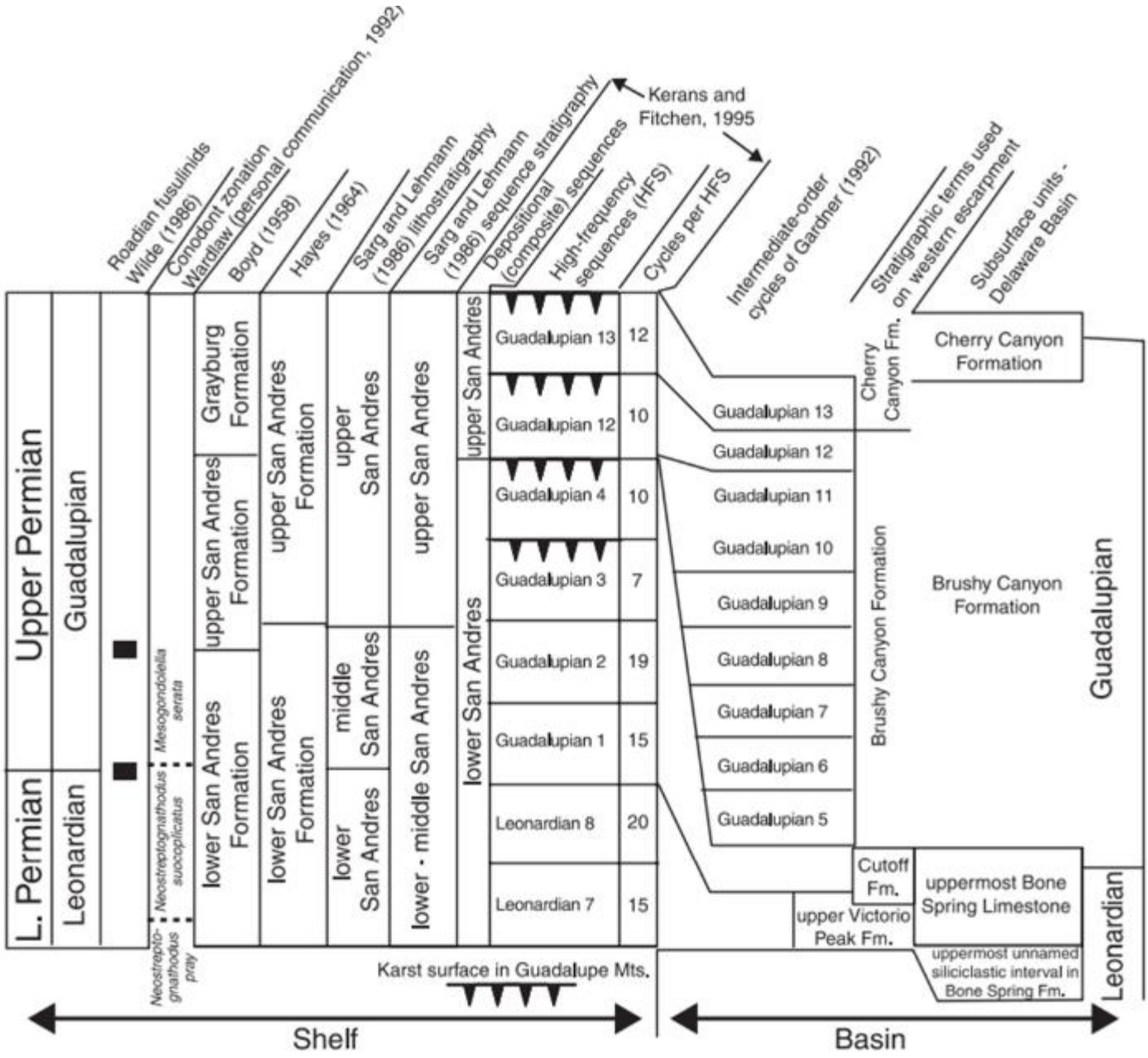

Figure 9: Past regional studies (up to 1995) and stratigraphic interpretations of the formations described in this study.
The Glorieta Formation, stratigraphically below the Victorio Peak Formation, is not depicted. Note that changes to the HFS numbering of the Upper San Andres Formation have been made to G8-G9. The Brushy Canyon Formation now corresponds to HSFs G5-G7.

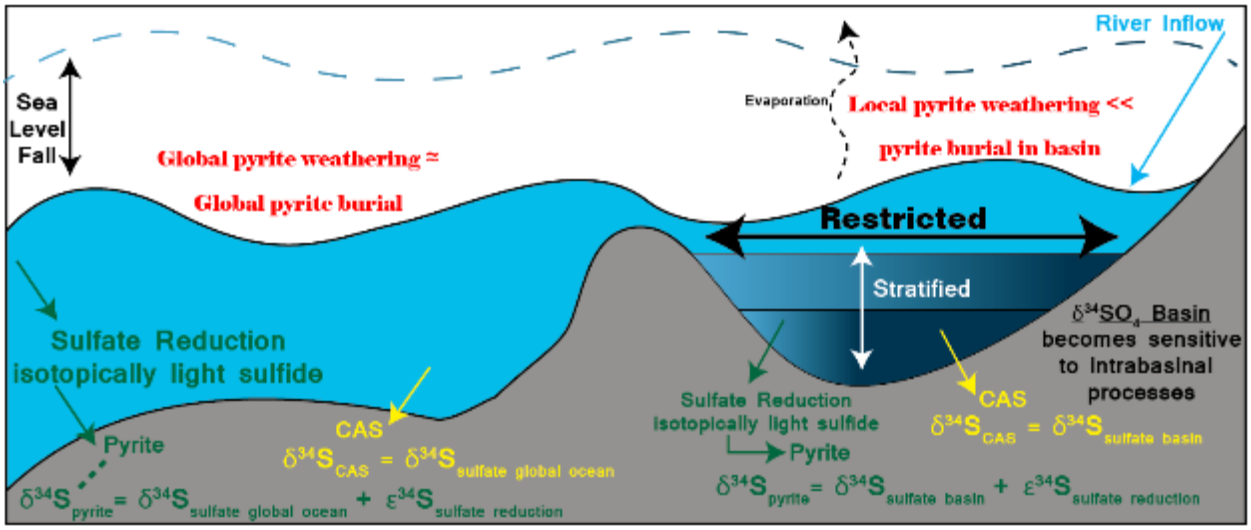

Figure 10: $\delta^{18}O_{CAS}$ & $\delta^{34}S_{CAS}$ during sea level lowstands. Due to basin restriction and subsequent stratification of the water body, a reduced amount of oxygen is available for the mineralization of organic matter. Once oxygen is fully depleted (anoxia/anoxic conditions) sulfate reducing bacteria dominate the mineralization of organic matter, by coupling its oxidation to the reduction of sulfate to sulfide (H_2S). Microbial sulfate reduction drives the $\delta^{18}O_{sulfate}$ and $\delta^{34}S_{sulfate}$ to heavier values, while producing sulfide that is depleted in ^{34}S relative to sulfate. A part of the produced isotopically light sulfide reacts with iron to form pyrite (FeS_2), whereas another part can be re-oxidized back to sulfate. While the isotope composition of sulfide is preserved in pyrite ($\delta^{34}S_{pyrite}$, typically isotopically light), the typically heavy $\delta^{18}O_{sulfate}$ and $\delta^{34}S_{sulfate}$ is captured as $\delta^{18}O_{CAS}$ and $\delta^{34}S_{CAS}$ as carbonates precipitate.

Basin Disconnected From Sea (LST)

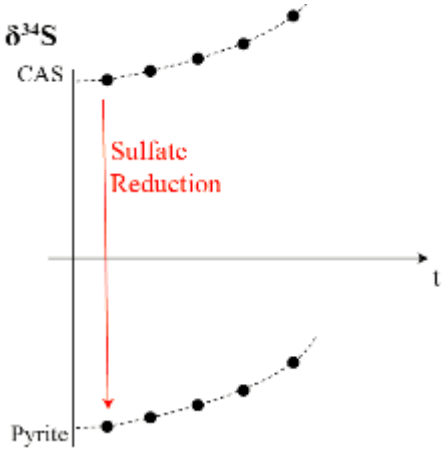

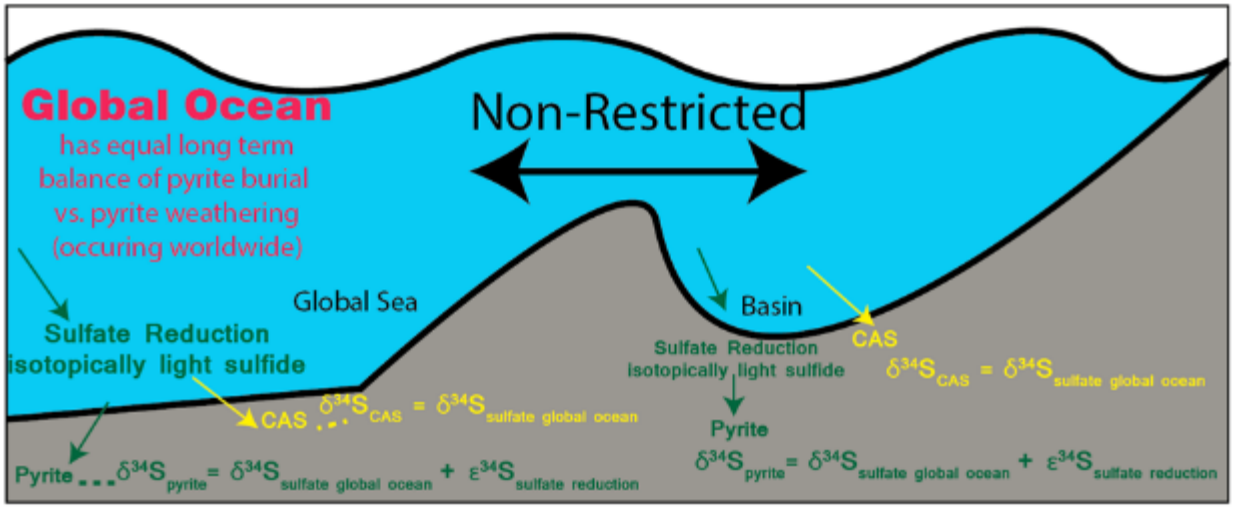

Figure 11: $\delta^{18}O_{CAS}$ & $\delta^{34}S_{CAS}$ during sea level highstands. The $\delta^{18}O_{sulfate}$ and $\delta^{34}S_{sulfate}$ in a marine basin can change from steady global marine sulfate isotope signatures during periods of relative sea level highstands, to rapidly changing signatures during basin detachment during relative sea level lowstands. During highstands, I expect the basin signature to be that of the global sea and as such observe no deviation in its $\delta^{18}O_{sulfate}$ and $\delta^{34}S_{sulfate}$.

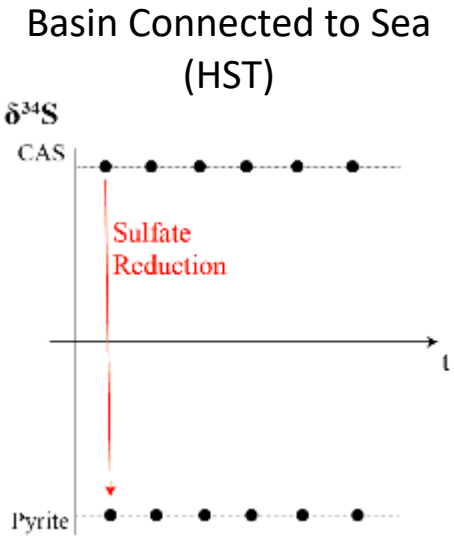

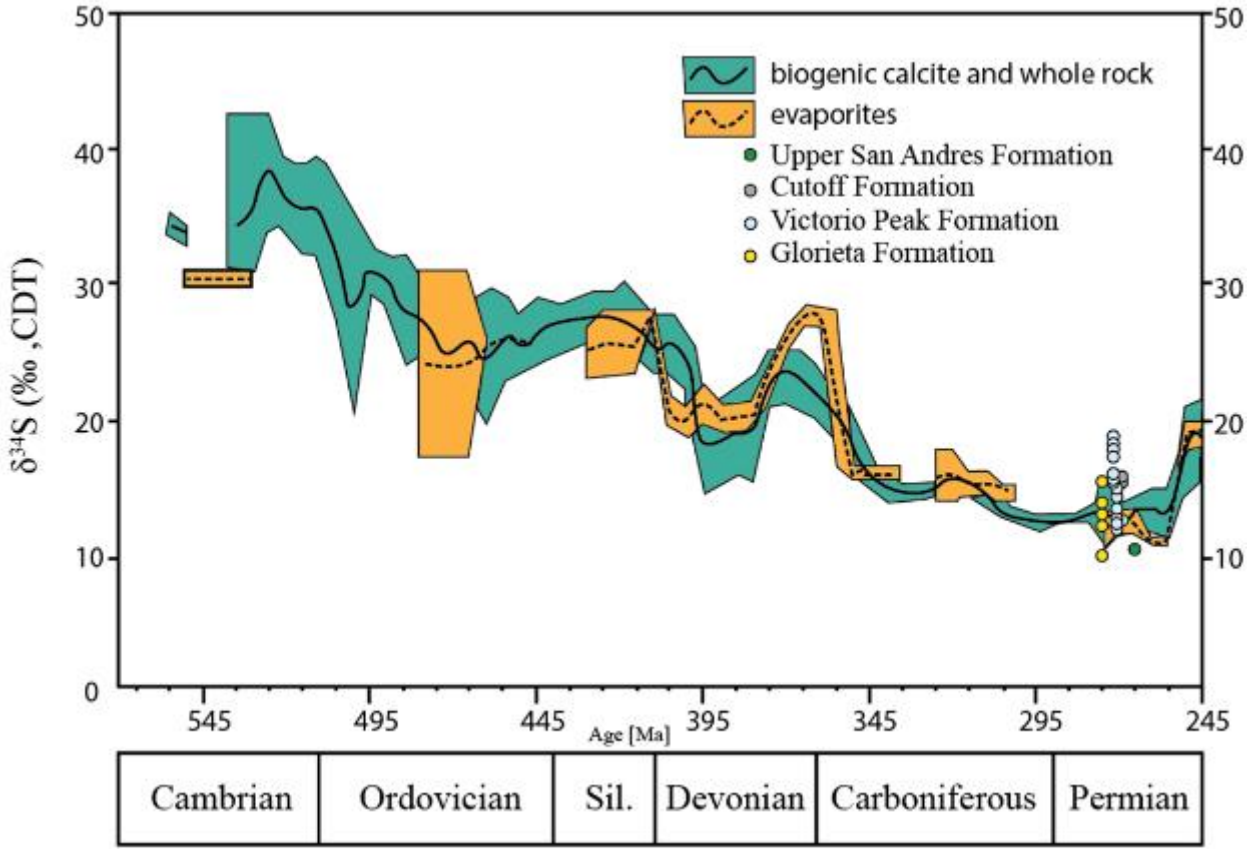

Figure 12: The sulfur isotope record for Paleozoic seawater sulfate.
Presented as a moving average (±95% confidence) with $\delta^{34}S_{CAS}$ added from this study. Modified from Kampschulte and Strauss, 2004.

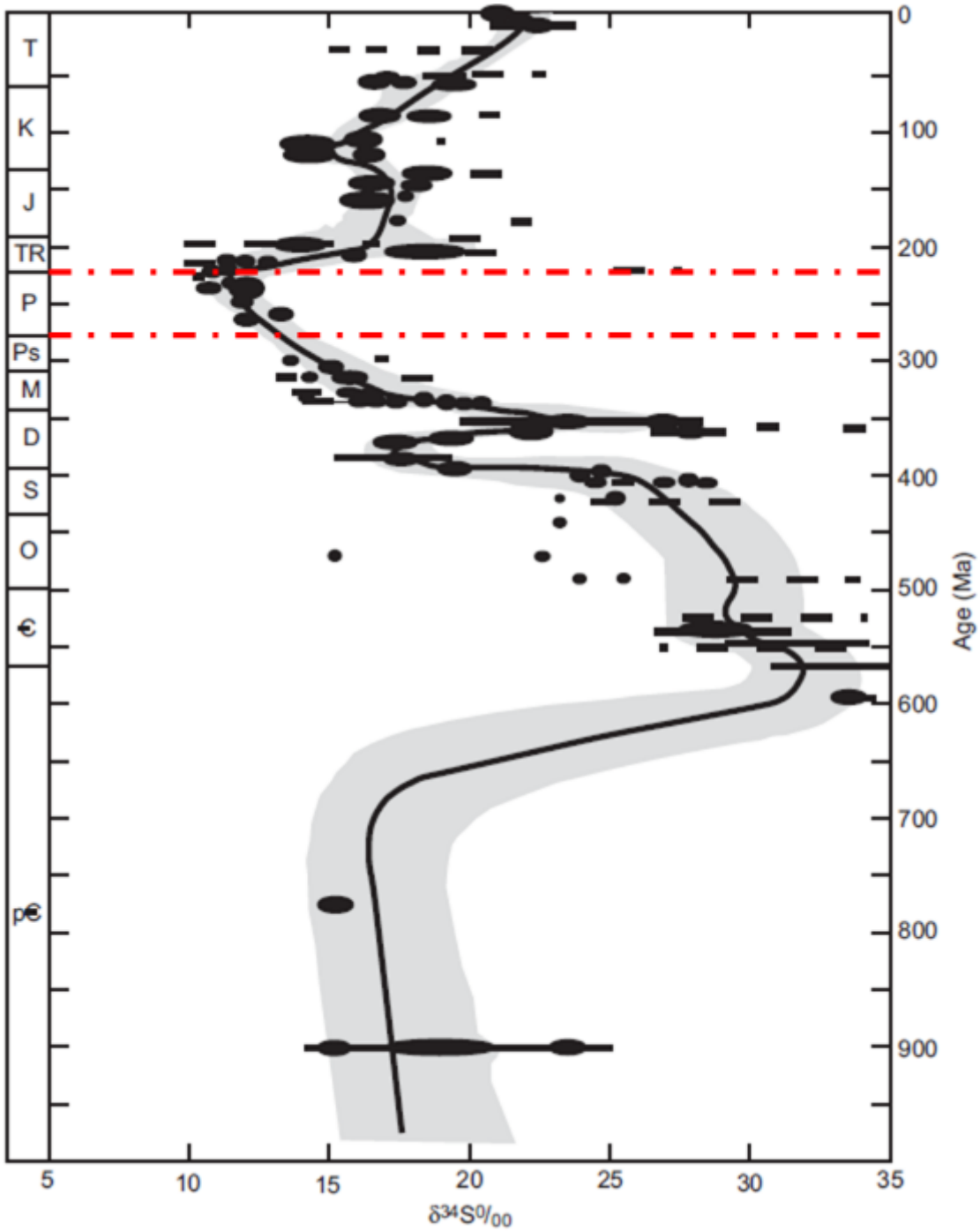

Figure 13: Global sulfur isotope curve during Phanerozoic time.
Study interval bracketed between red dot-dashed lines. During Permian Time, the curve for the global sulfur isotope composition is at its lowest value, displaying an average of +12‰, and a steady signal. Modified from Claypool et al., 1980.

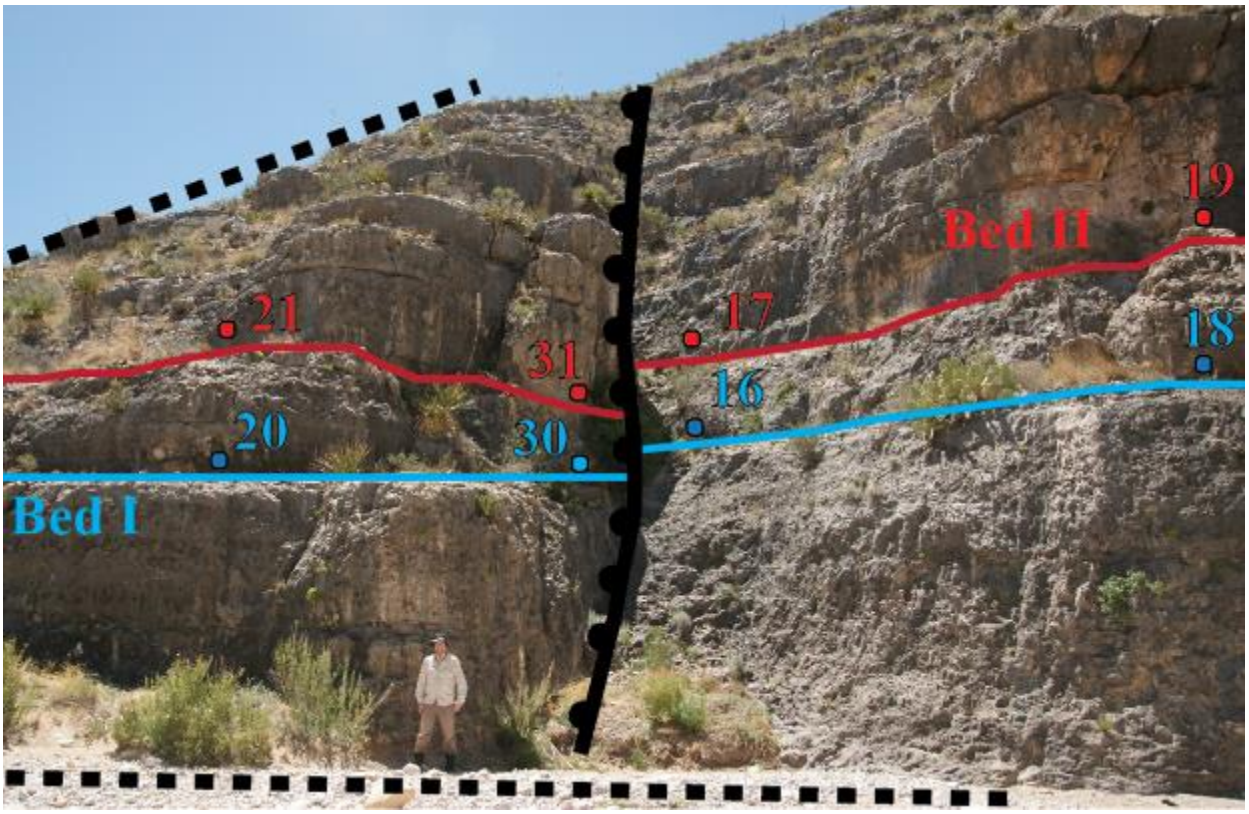

Figure 14: The Bench.
The primary sample collection point to test isotopic continuity across a normal fault. Eight samples were collected across two beds, Bed I and Bed II. Dashed lines illustrate two major faults, one to the left over the ridge and the other in the creek bed.

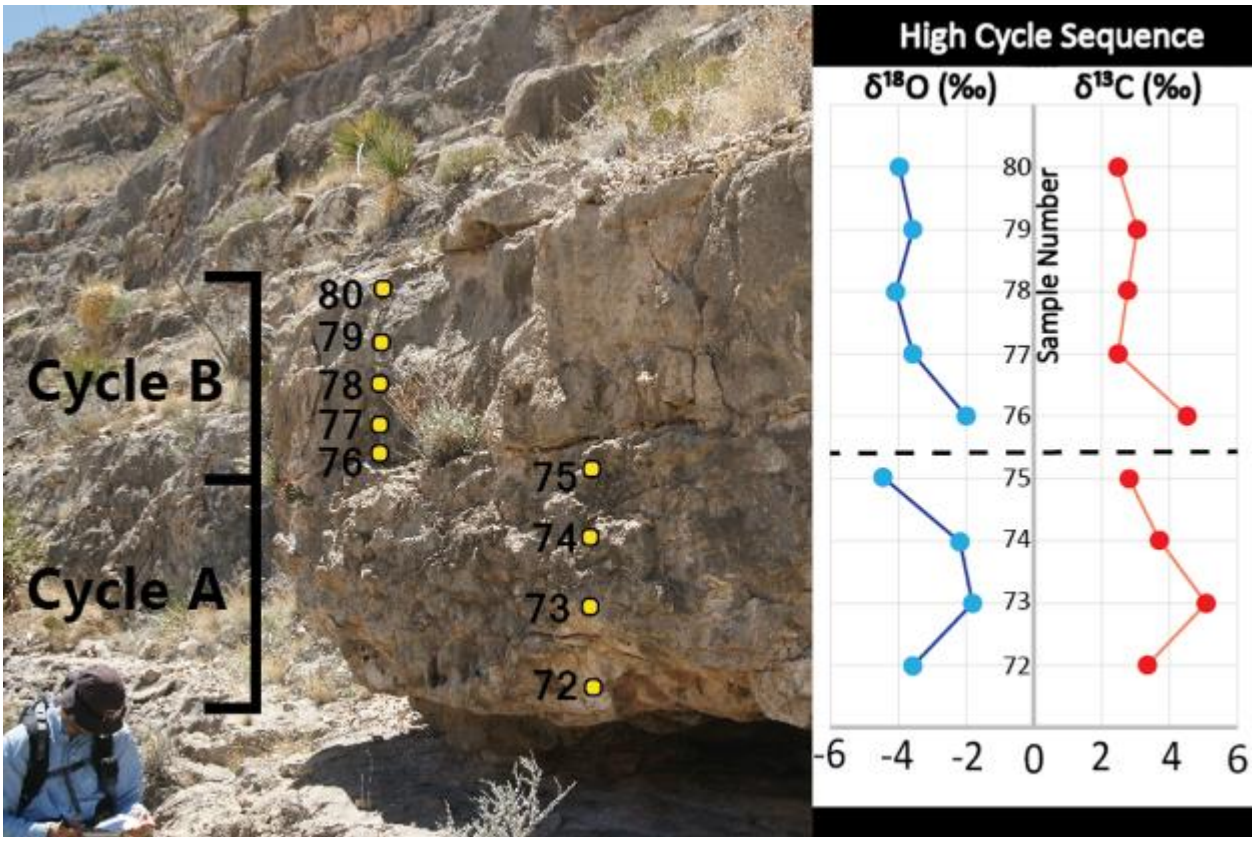

Figure 15: Carbon and oxygen isotope trends of carbonates over two high frequency cycles. This test was conducted with two transects across two cycles within the Victorio Peak Formation. In total, nine samples were collected across Cycle A & Cycle B, each cycle is 80 cm thick.

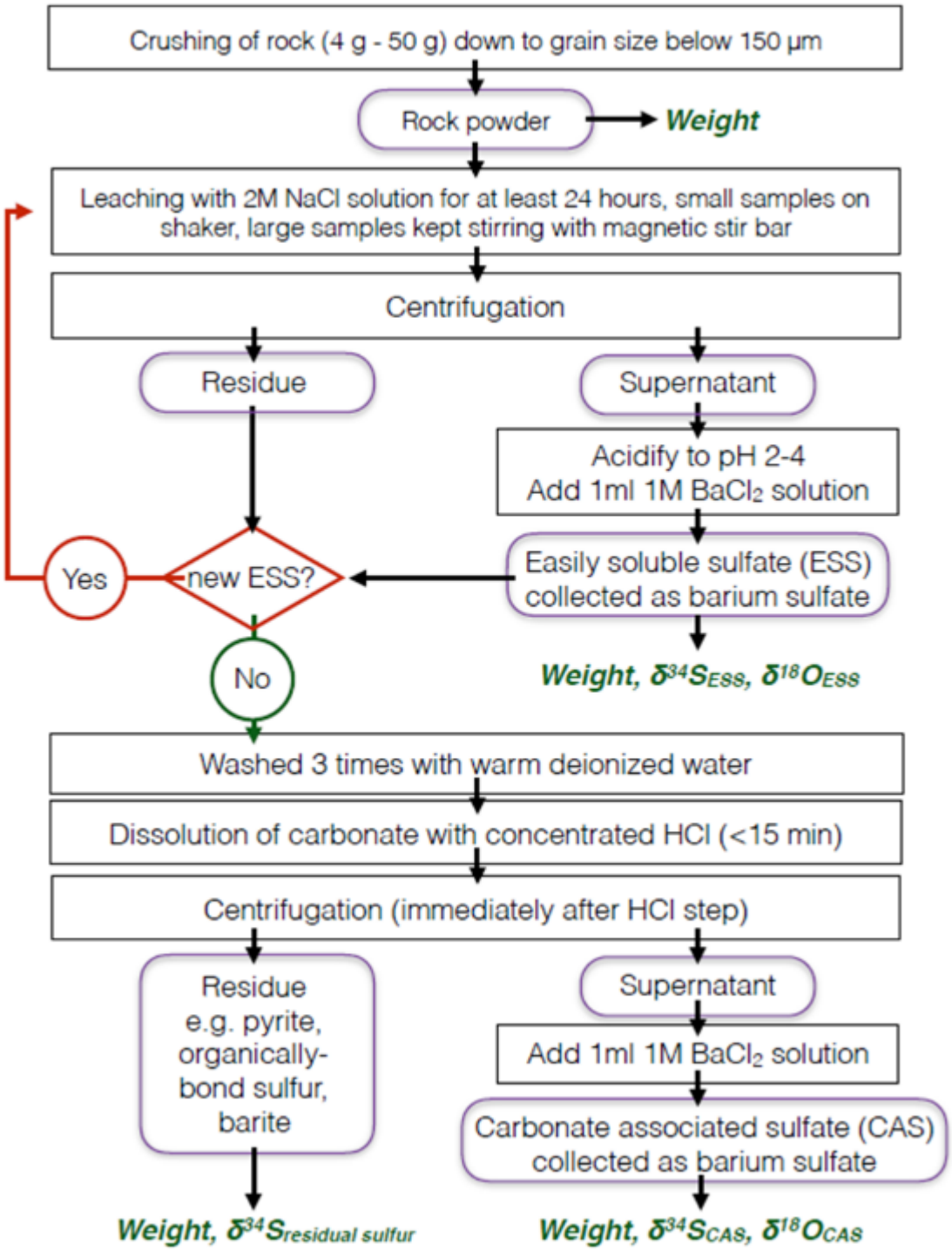

Figure 16: Schematic of the geochemical methodology for the extraction of sulfur phases.

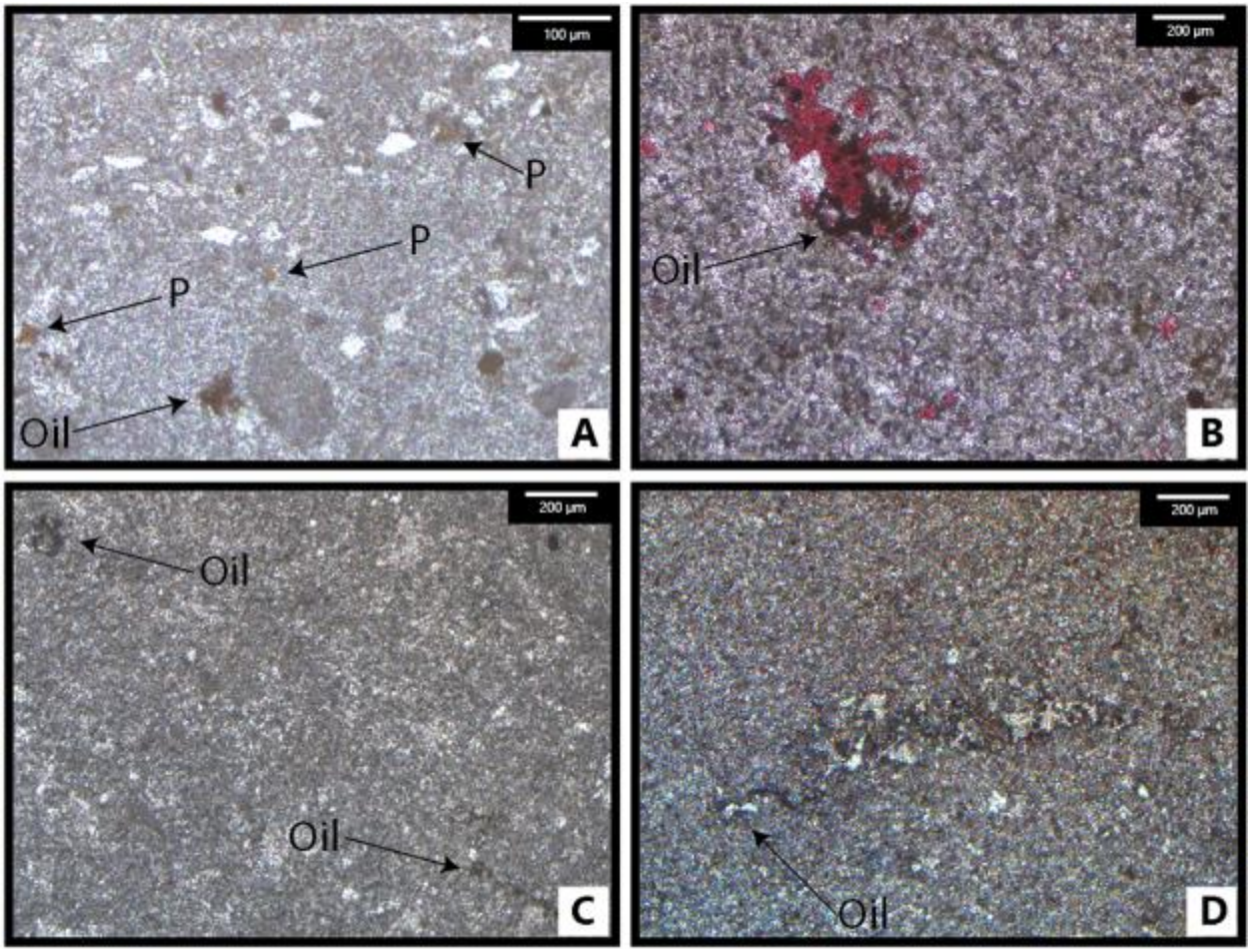

Figure 17: Dead oil and pyrite were found throughout the entire study area.
(A) Glorieta Formation: dolomicrite with pyrite (P), quartz, pellets, and oil staining (Sample #63, 10x magnification, stained red with Alizarin Red S, reflected light). (B) Victorio Peak Formation: nonfossiliferous dolomicrite with spotty calcification in red, oil found next to calcite (Sample #16, 4x magnification, stained red with Alizarin Red S, cross-polarized light). (C) Cutoff Formation: micritization of ooid grain rim (top left), dissolution and replacement of ooid nuclei allowing for dead oil to migrate through into the tight dolostone (Sample #55, 4x magnification, cross-polarized light). (D) Upper San Andres Formation: apparently, oil seeped through stylolite within dolostone (Sample #33, 4x magnification, cross-polarized light).

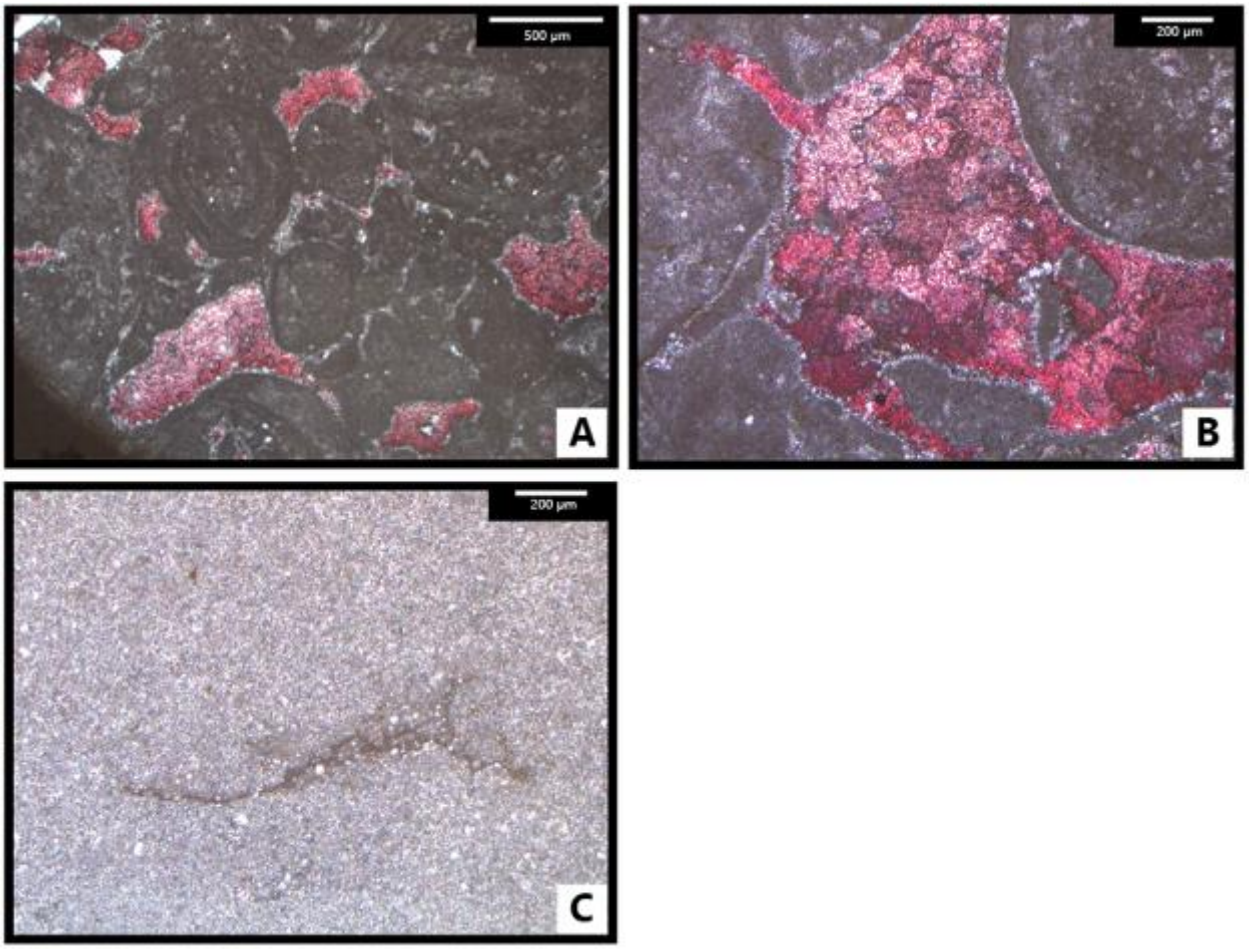

Figure 18: Photomicrographs of samples from the Glorieta Formation.
(A) Glorieta Formation: Peloids and fecal pellets within dolomicrite matrix (Sample #58, 2.5x magnification, stained red with Alizarin Red S, cross-polarized light). (B) Glorieta Formation: Blocky calcite forming within poorly compacted pore space during deeper burial cementation (Sample #58, 4x magnification, stained red with Alizarin Red S, cross-polarized light). (C) Glorieta Formation: Pressure dissolution of dolomicrite. Note the pressure twinning of calcite and faint oxidation along the stylolite seam (Sample #63, 4x magnification, polarized light).

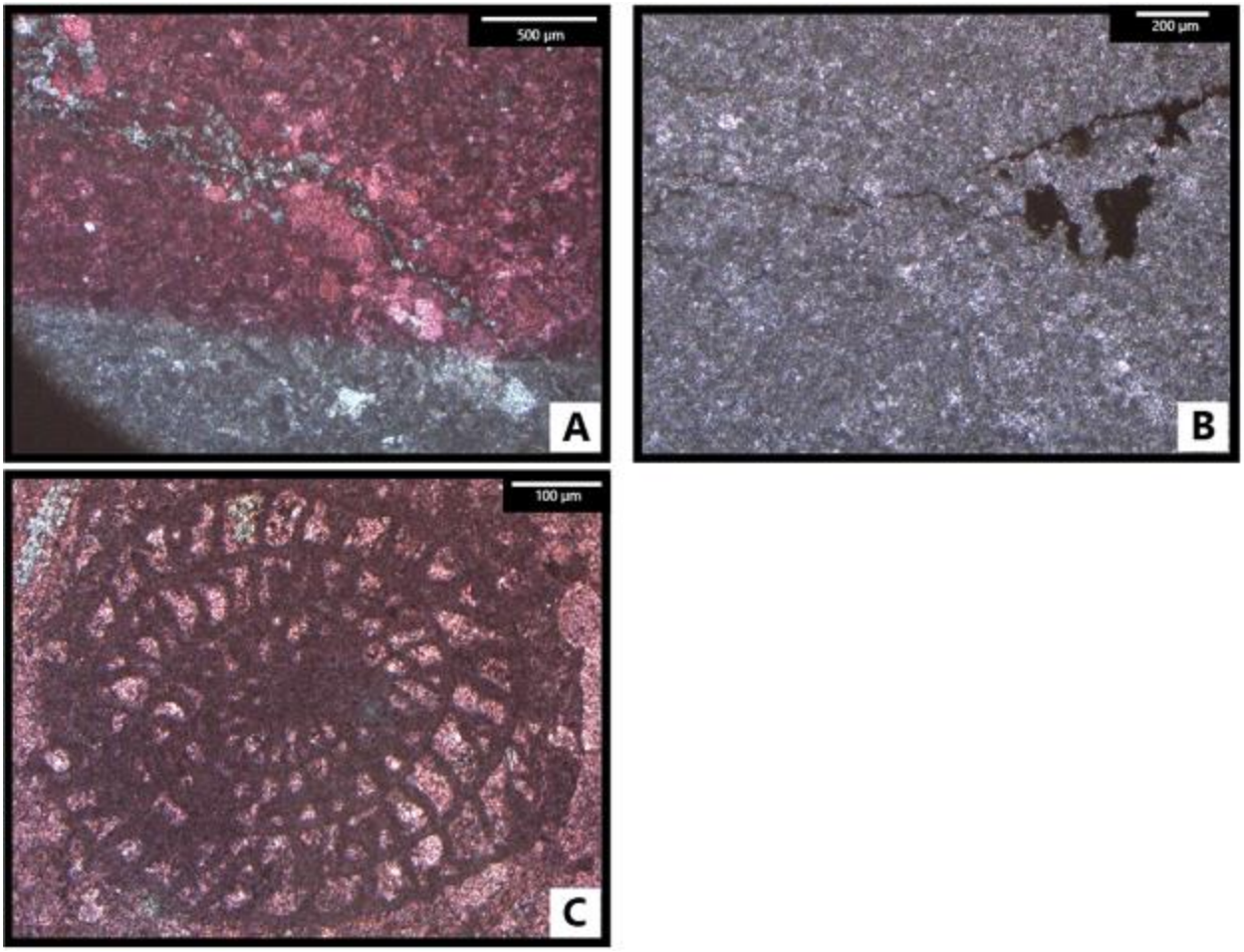

Figure 19: Photomicrographs of samples from the Victorio Peak Formation.
(A) Victorio Peak Formation: small dolomitized dissolution crack (clear) through calcite matrix (stained red) with Alizarin Red S and provides example of how Mg-rich fluid may have used stylolites as horizontal conduits for dolomitization (Sample #21, 2.5x magnification, stained red with Alizarin Red S, cross-polarized light). (B) Victorio Peak Formation: Dolostone found with dead oil along stylolite, supporting hypothesis that fluids were migrating through stylolites within the Victorio Peak Formation (Sample #5, 4x magnification, stained red with Alizarin Red S, cross-polarized light). (C) Victorio Peak Formation: well preserved fusulinids like this are the dominant fossil found throughout the formation (Sample #29, 10x magnification, stained red with Alizarin Red S, polarized light).

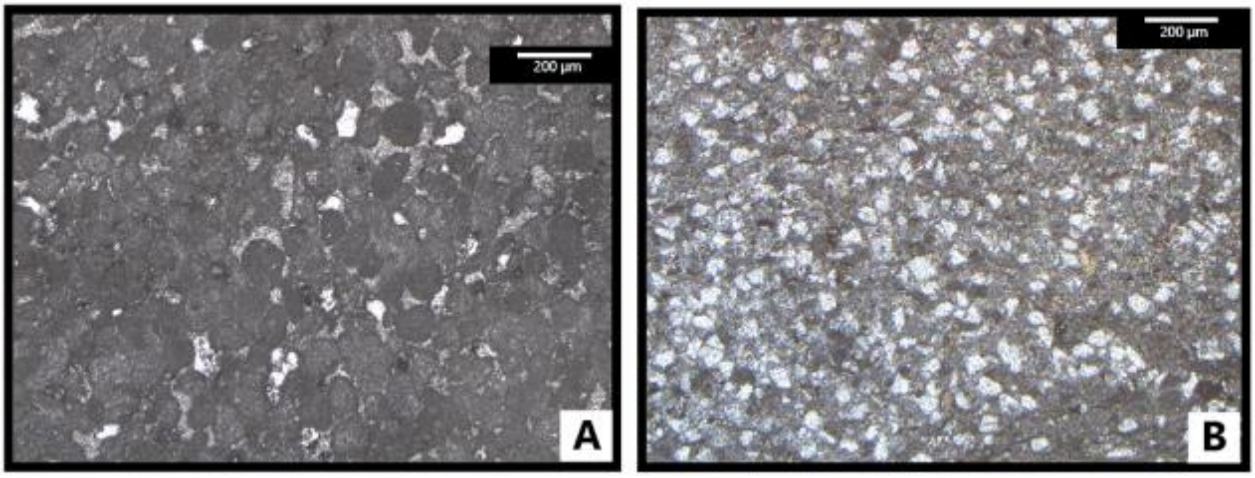

Figure 20: Photomicrographs of samples from the Cutoff (A) and San Andres Formation (B). (A) Cutoff Formation: abundant pellets within a highly dolomitized grainstone with significant contribution quartz grains. This input of quartz and the poor compaction between the grains is not typical for the entire Cutoff Formation. It is an indication that the sediments of this outcrop belong to the uppermost part of the Cutoff Formation, just prior to the establishment of the Brushy Canyon bypass, forming the HSF unconformity of G5-G7 (Sample #49, 4x magnification, polarized light). (B) Upper San Andres Formation: dolomitic intercrystalline porosity of idiotopic dolomite characterized by rhombic shaped euhedral to subhedral crystals that display a porphyrotopic texture with dolomite crystals floating in a dolomicritic matrix with fine opaque rhombohedrals of pyrite (Sample #37, 4x magnification, plain polarized light).

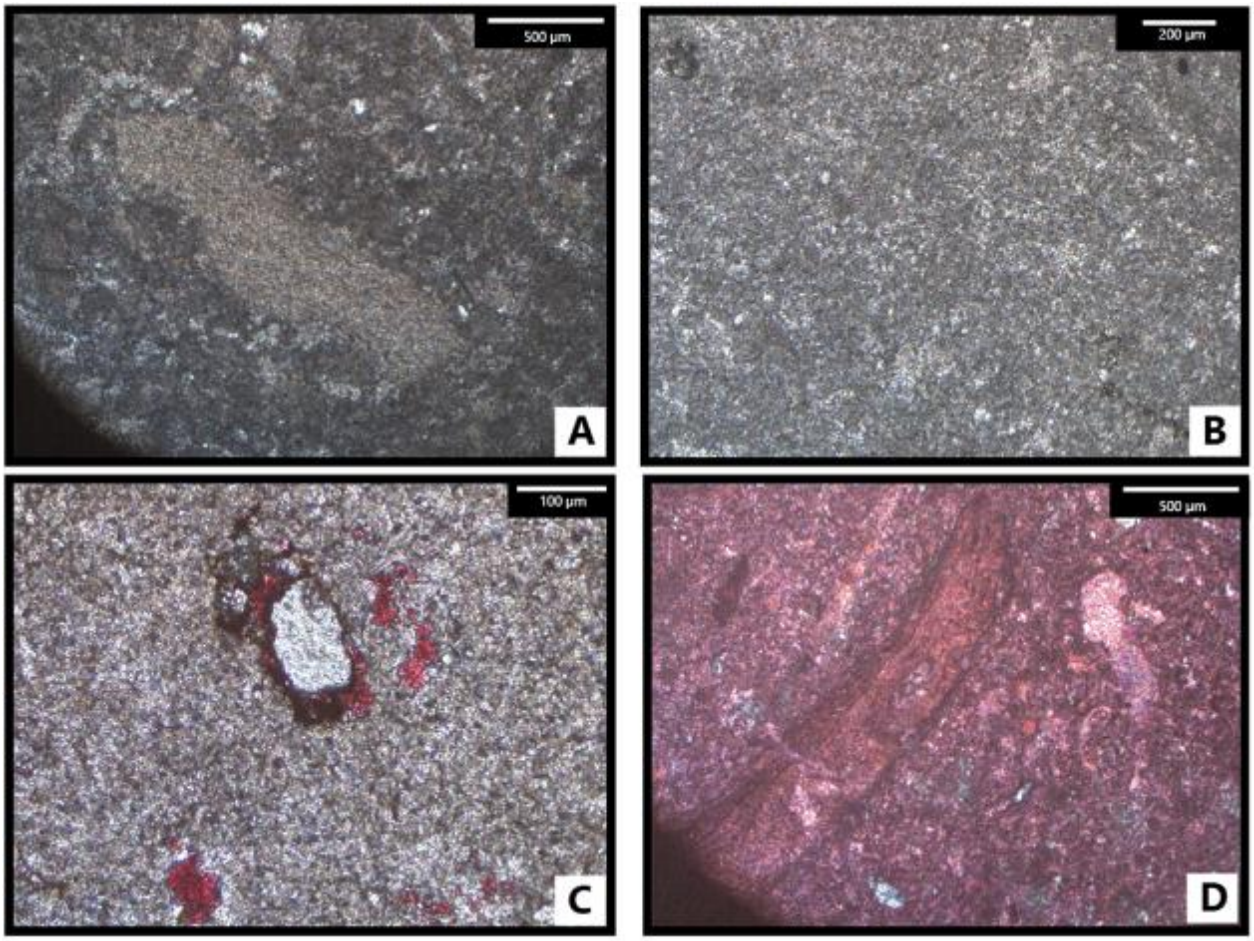

Figure 21: Photomicrographs of samples from the "Bench".
(A) Sample 18 from Bed I of The Bench contains micritic mud, is rich in pyrite, and contains brachiopod fragments as shown in the photomicrograph (Victorio Peak Formation, 2.5x magnification, polarized light). (B) Sample 30 from Bed I of The Bench displays a micritized ooid grain rim (top left). Dissolution and replacement of ooid nuclei allowed dead oil to migrate through the tight dolostone (Victorio Peak Formation, 4x magnification, cross-polarized light). (C) Sample 20 from Bed I of The Bench: dolomicrite with spotty calcification (stained red) around a dolomitic grain, oil around calcite (Victorio Peak Formation, 10x magnification, stained red with Alizarin Red S, cross-polarized light). (D) In comparison to the other Bed II samples 17, 19, and 31, sample 21 from Bed II is much more fossil rich (fragments of brachiopods, bivalves, and benthic foraminifera) and contains much coarser calcite crystals (Victorio Peak Formation, 2.5x magnification, stained red with Alizarin Red S, cross-polarized light).

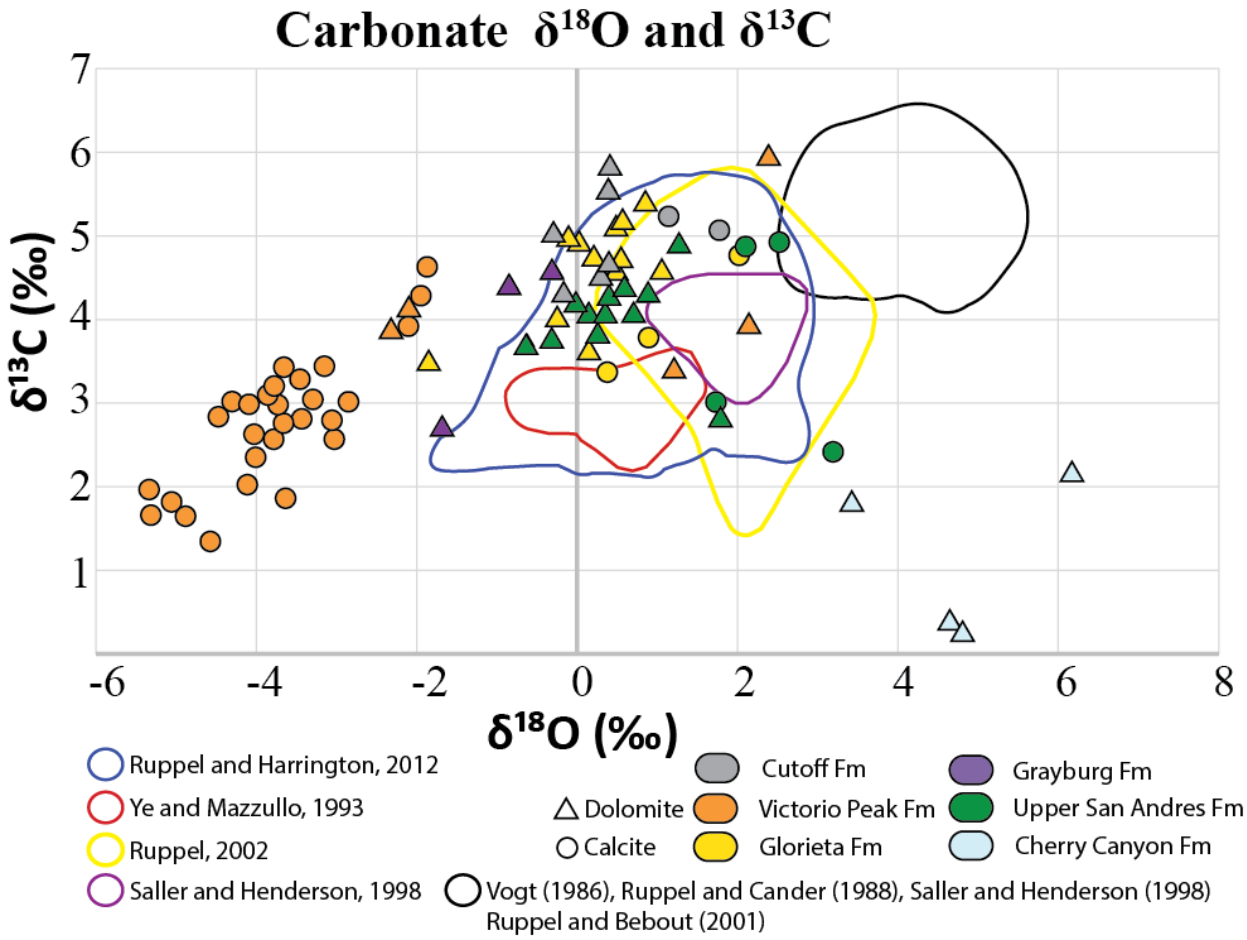

Figure 22: Carbon and oxygen isotope signatures of carbonates.

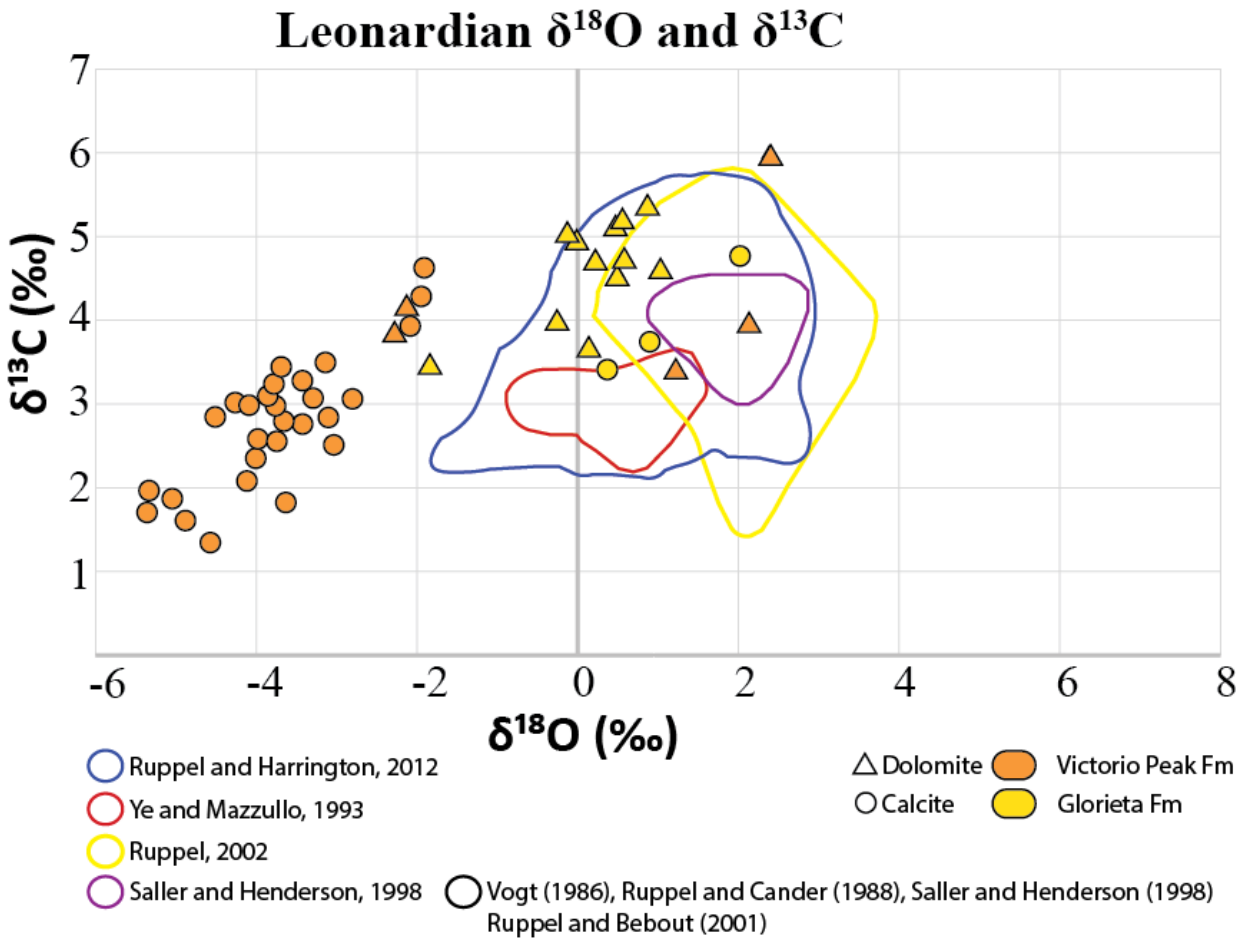

Figure 23: Carbon and oxygen isotope signatures of carbonates for the Leonardian-aged Glorieta and Victorio Peak Formations.

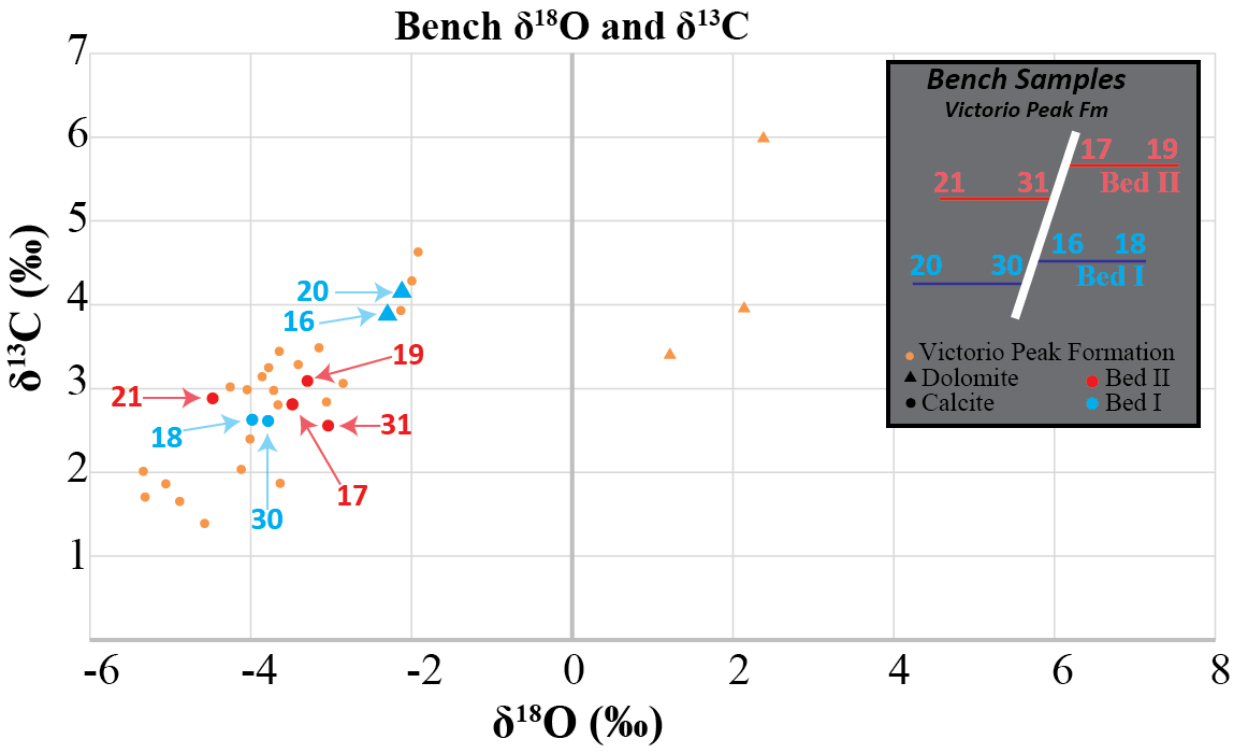

Figure 24: The Bench carbon and oxygen isotope signatures compared to other samples from the Victorio Peak Formation.

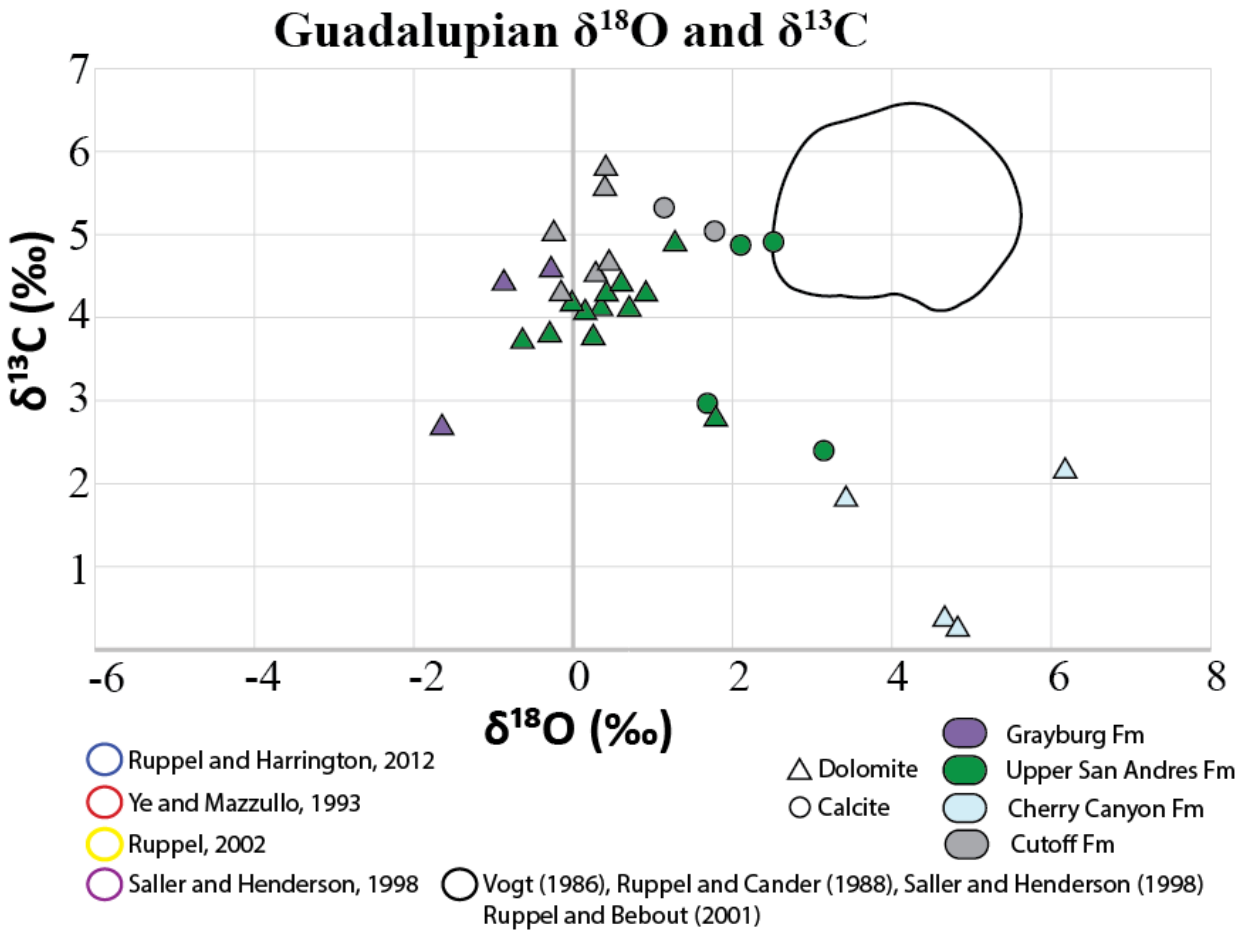

Figure 25: Carbon and oxygen isotope signatures from carbonates for the Guadalupian-aged Cutoff, Cherry Canyon, Upper San Andres, and Grayburg Formations.

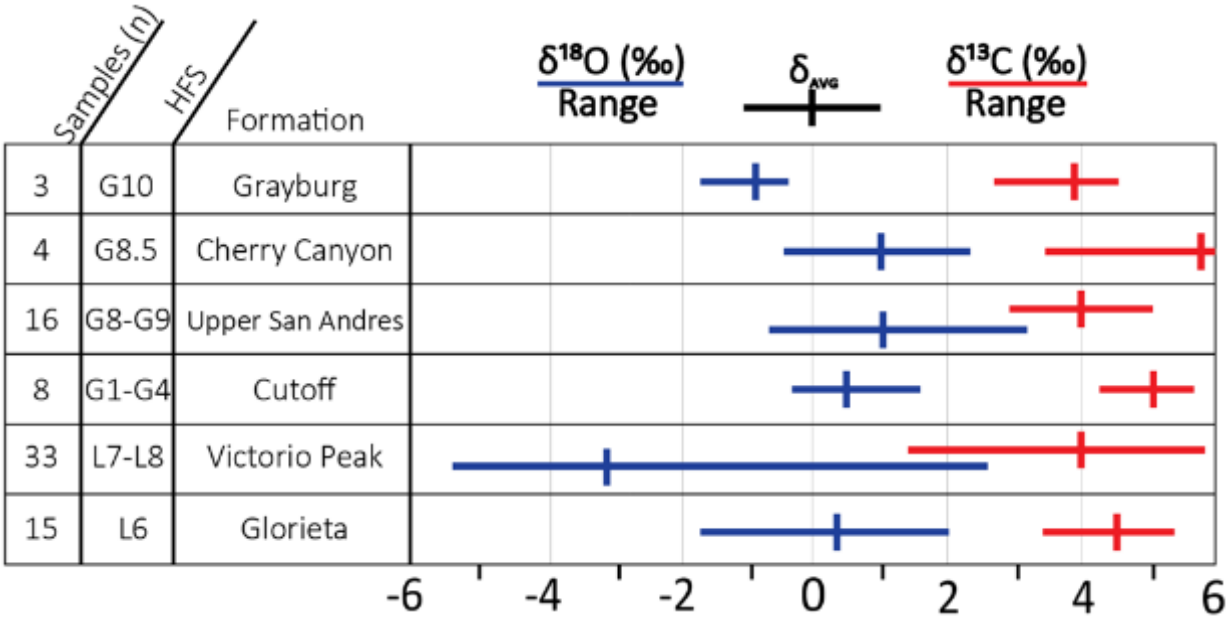

Figure 26: Range and average of $\delta^{18}O_{carbonate}$ and $\delta^{13}C_{carbonate}$ for the 79 samples analyzed.

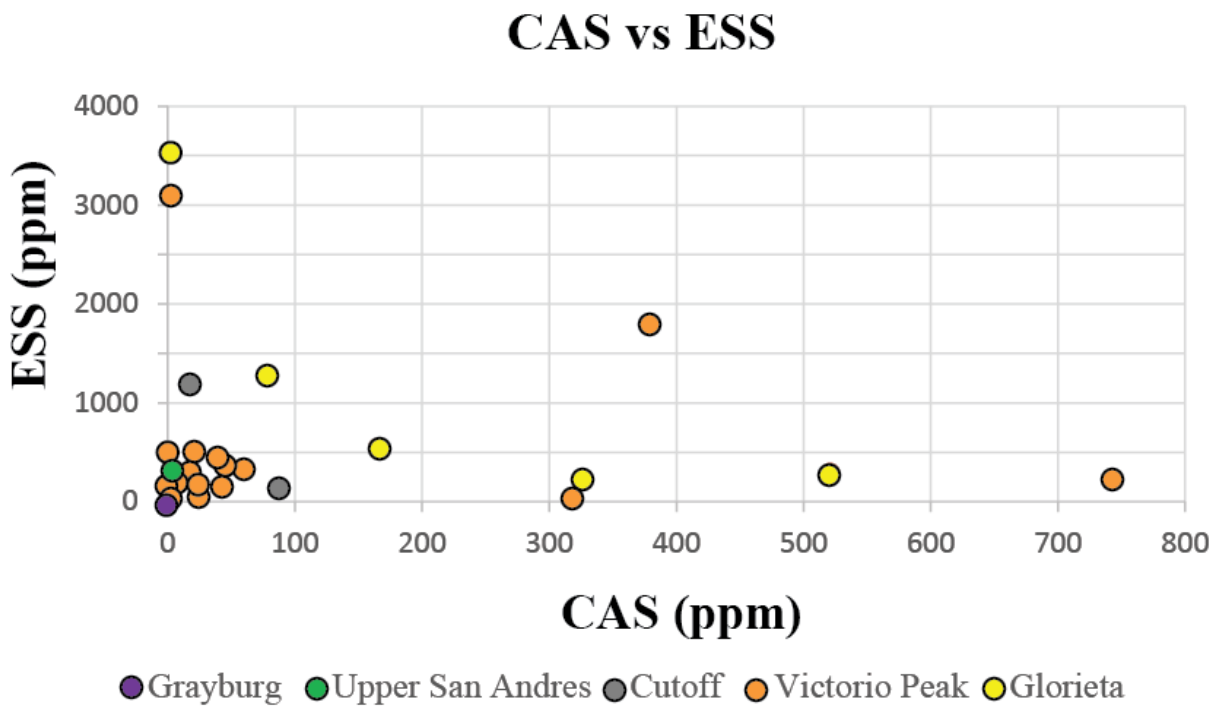

Figure 27: ESS content compared to CAS content.
There is no correlation between high ESS and high CAS content, indicating that my geochemical method properly segregates ESS from CAS.

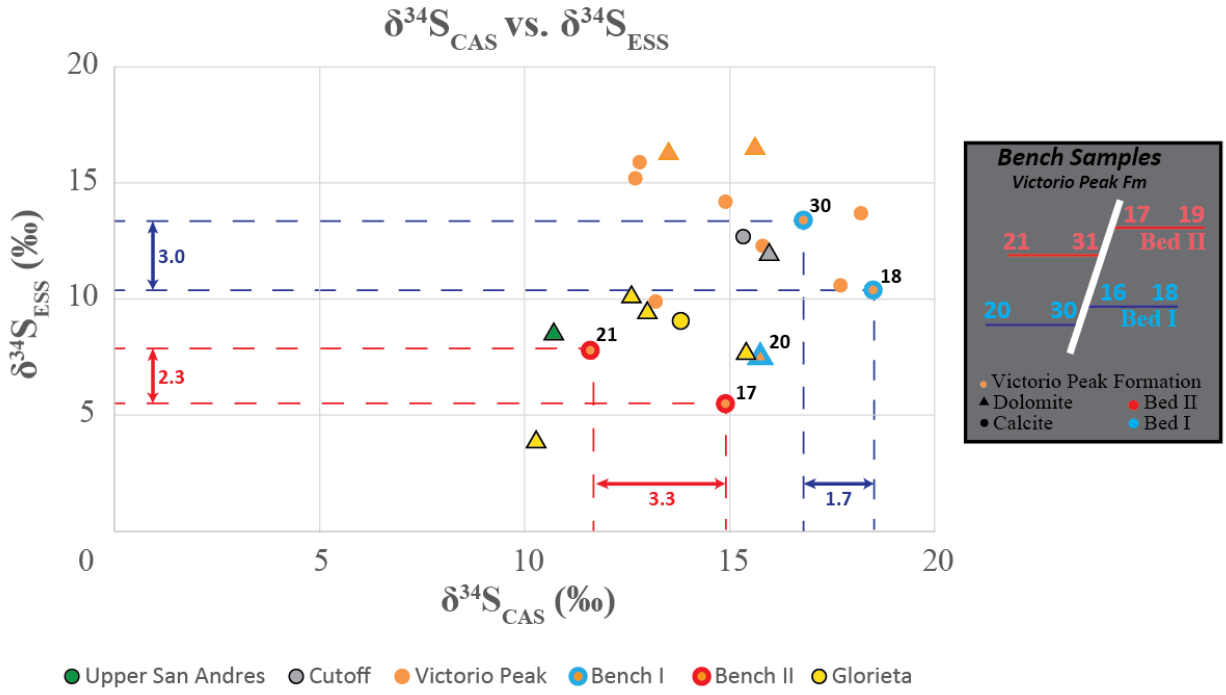

Figure 28: $\delta^{34}S_{ESS}$ as compared to $\delta^{34}S_{CAS}$.
Graph shows that there is no correlation between $\delta^{34}S_{ESS}$ and $\delta^{34}S_{CAS}$ indicating the extraction methodology was successful.

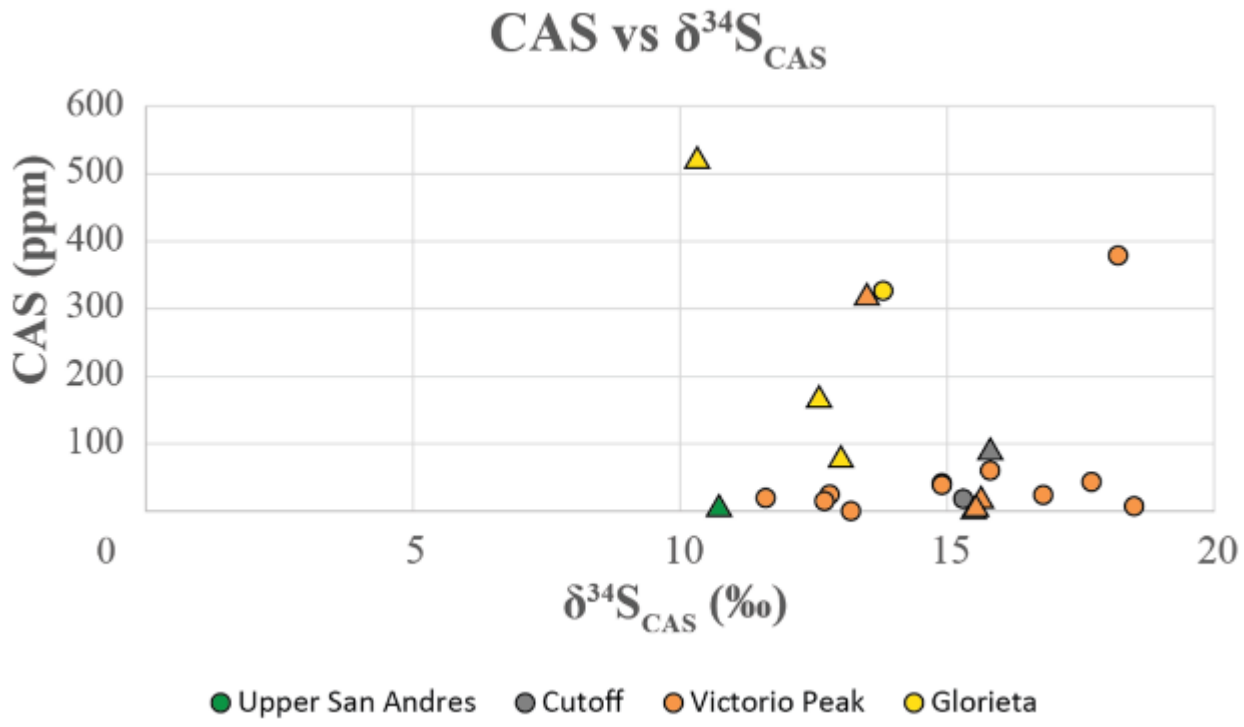

Figure 29: Comparison of CAS concentration vs. $\delta^{34}S_{CAS}$.
Contamination of CAS with sulfate from pyrite oxidation, could be the cause for the outlier with >500 ppm CAS content and a $\delta^{34}S_{CAS}$ of less than 11‰.

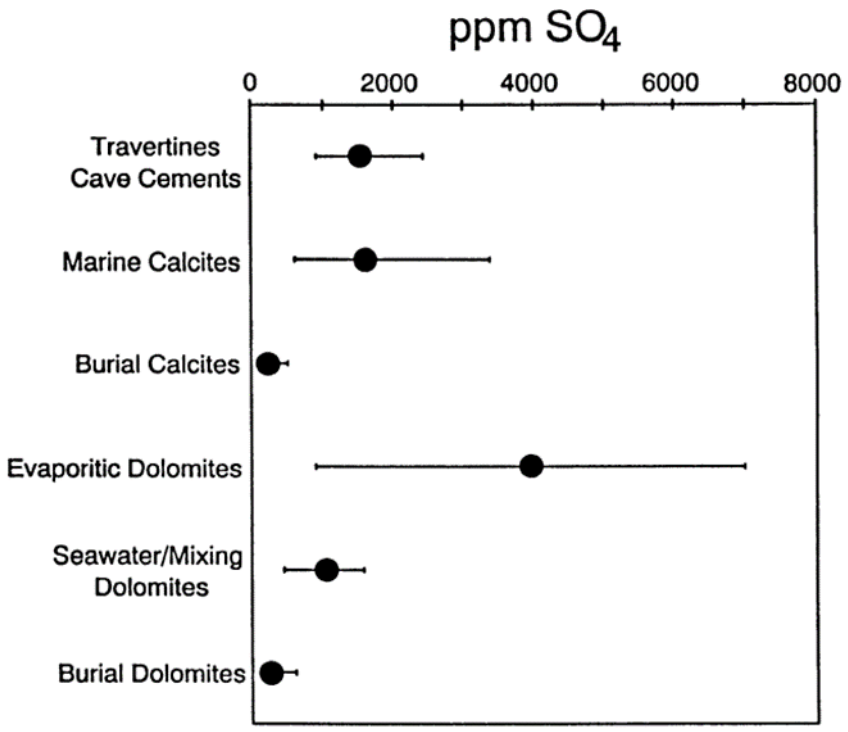

Figure 30: Range of CAS in carbonates.
Sulfate concentration ranges (horizontal bars) and average concentrations (solid circles) of well-characterized calcite and dolomite samples from Ordovician to Miocene (Staudt and Schoonen 1995).

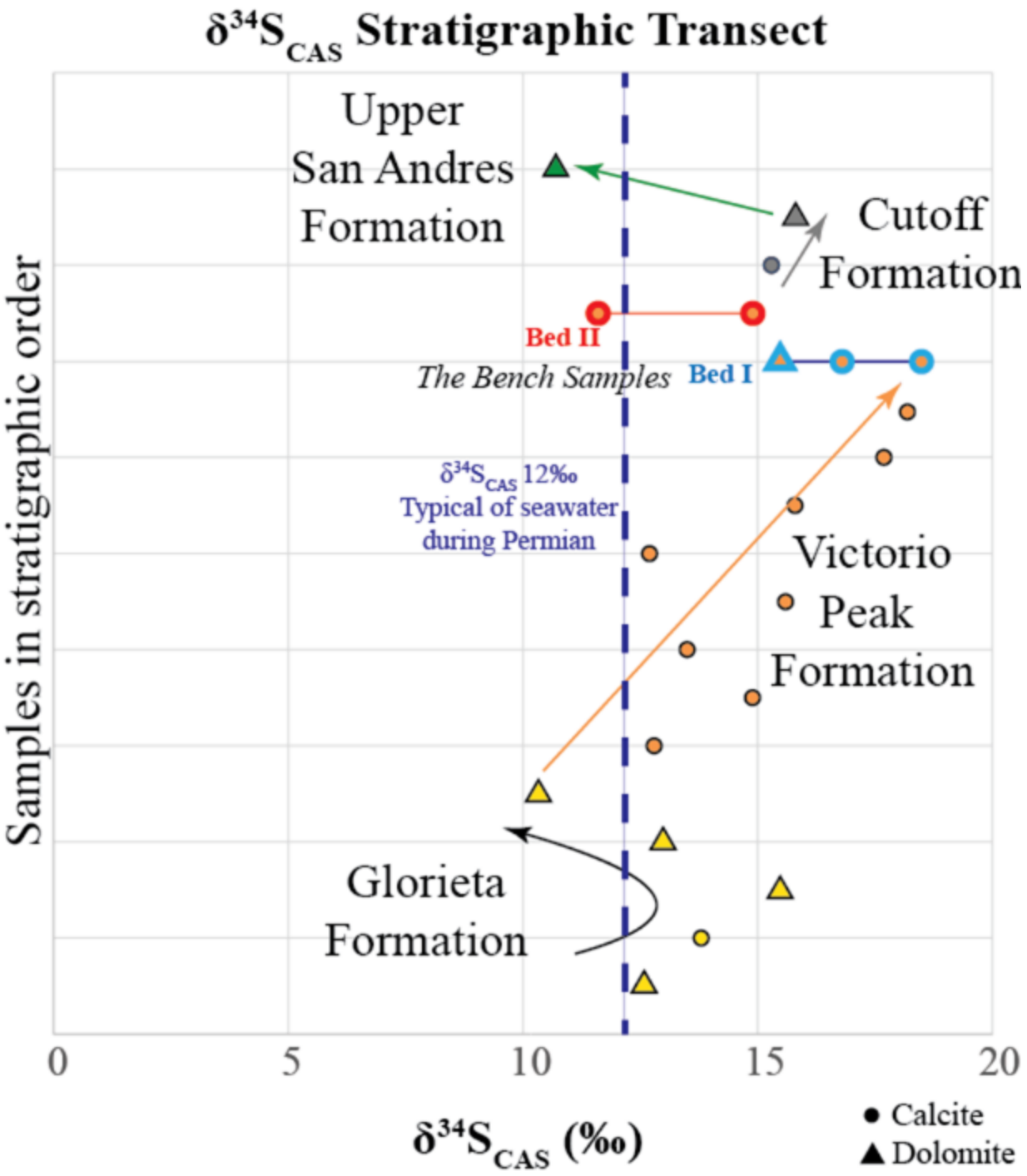

Figure 31: Trends in $\delta^{34}S_{CAS}$ when samples are arranged in stratigraphic order.
Note: stratigraphic order does not illustrate formation thickness or age (i.e. is not to scale).

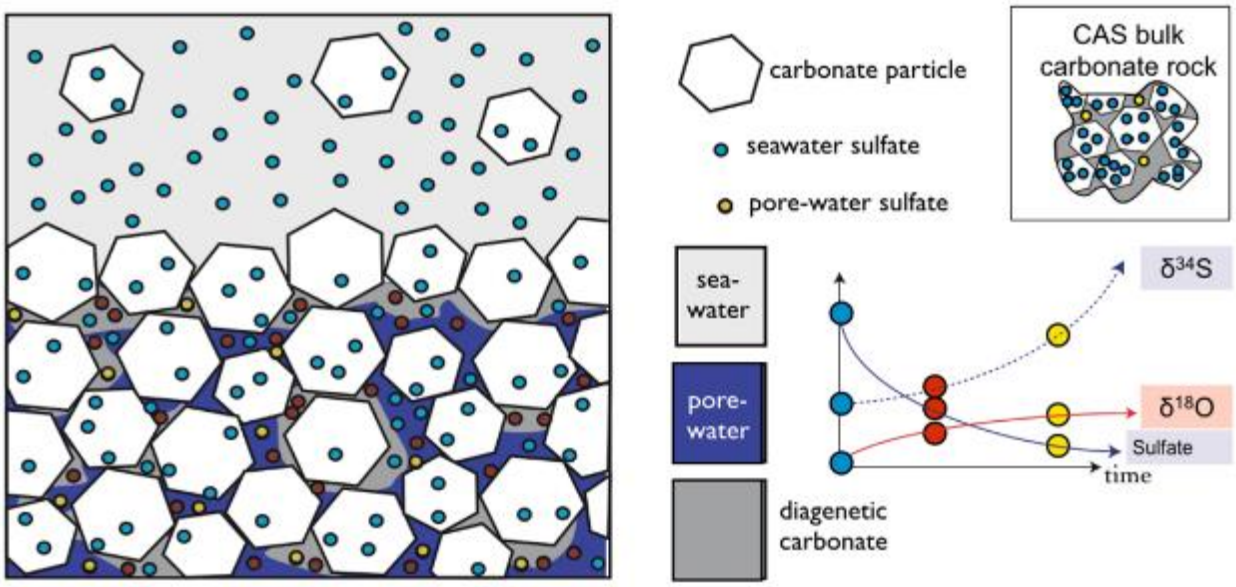

Figure 32: Visual illustration of how heavy $\delta^{34}S_{CAS}$ may be produced during carbonate precipitation with microbial sulfate reduction within marine sediments.

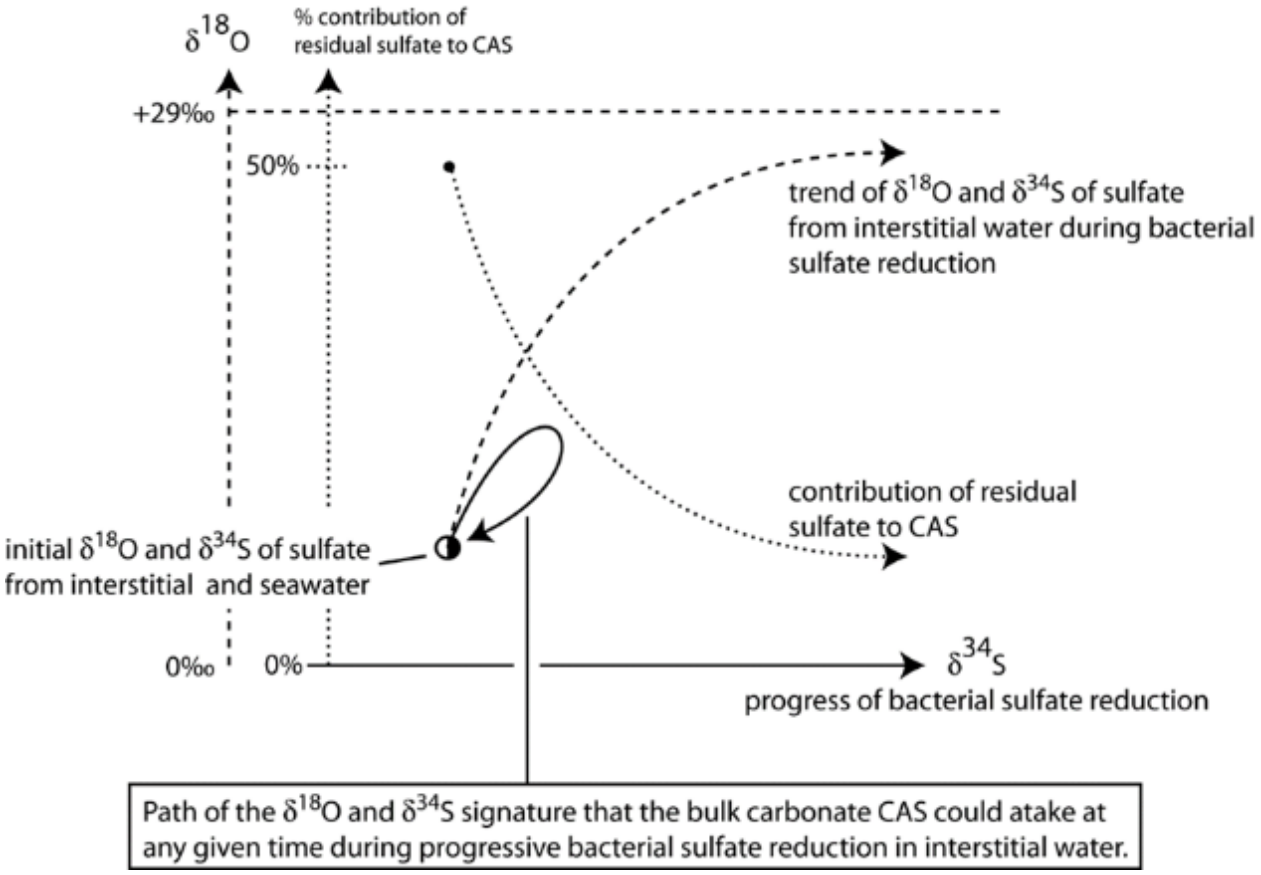

Figure 33: Illustration of potential shifts in the isotopic composition of $\delta^{34}S_{CAS}$.
For a substantial increase in the $\delta^{34}S$ of dissolved sulfate to take place, the amount of sulfate must be limited – a condition that also limits the amount of sulfate that can be incorporated in the carbonates formed during diagenesis.

REFERENCES

Adams, J.E., 1965, Stratigraphic-Tectonic Development of Delaware Basin: AAPG Bulletin, v. 49, no. 11, p. 2140–2148.

Allan, J.K., and Wiggins, W.D., 1993, Appendix I. Conventions for Reporting Isotope Data: v. 53, p. 1–2.

Amerman, R., Nelson, E.P., Gardner, M.H., and Trudgill, B., 2011, Submarine mass transport deposits of the Permian Cutoff Formation, West Texas, U.S.A.: internal architecture and controls on overlying reservoir sand deposition, *in* Mass-Transport Deposits in Deepwater Settings, SEPM, Special Publication 96, p. 235–267.

Atchley, S.C., Kozar, M.G., and Yose, L.A., 1999, A Predictive Model for Reservoir Distribution in the Permian (Leonardian) Clear Fork and Glorieta Formations, Robertson Field Area, West Texas: AAPG Bulletin, v. 83, no. 7, p. 1031–1056.

Baldermann, A., Deditius, A.P., Dietzel, M., Fichtner, V., Fischer, C., Hippler, D., Leis, A., Baldermann, C., Mavromatis, V., Stickler, C.P., and Strauss, H., 2015, The role of bacterial sulfate reduction during dolomite precipitation: Implications from Upper Jurassic platform carbonates: Chemical Geology, v. 412, p. 1–14, doi: 10.1016/j.chemgeo.2015.07.020.

Beales, F.W., 1965, Diagenesis in pelleted limestones: Dolomitization and Limestone Diagenesis, v. SEPM Special Publication 13, p. 49–70.

Berner, E.K., and Berner, R.A., 1987, The Global Water Cycle: Geochemistry and Environment: Prentice-Hall, Englewood Cliffs.

Bissell, H.J., 1972, Three-Dimensional Stylolites and Migratory Routes of Oil and Gas: ABSTRACT: AAPG Bulletin, v. 56, no. 3, p. 604–604.

Blakey, R. C., 2007, Carboniferous-Permian paleogeography of the Assembly of Pangaea: In, Wong, Th.E (Ed.): Proceedings of the XVth International Congress on Carboniferous and Permian Stratigraphy. Utrecht, 10-16 August 2003. Royal Dutch Academy of Arts and Sciences (Amsterdam) p. 443-456.

Boyd, D.W., 1958, Permian sedimentary facies, central Guadalupe Mountains, New Mexico: State Bureau of Mines and Mineral Resources, New Mexico Institute of Mining & Technology.

Chambers, L.A., and Trudinger, P.A., 1979, Thiosulfate formation and associated isotope effects during sulfite reduction by Clostridium pasteurianum: Canadian Journal of Microbiology, v. 25, no. 6, p. 719–721, doi: 10.1139/m79-104.

Claypool, G.E., Holser, W.T., Kaplan, I.R., Sakai, H., and Zak, I., 1980, The age curves of sulfur and oxygen isotopes in marine sulfate and their mutual interpretation: Chemical Geology, v. 28, p. 199–260, doi: 10.1016/0009-2541(80)90047-9.

Deffeyes, K.S., Lucia, F.J., and Weyl, P.K., 1965, Dolomitizanon of Recent and Plio-Pleistocene Sediments by Marine Evaporite Waters on Bonaire Netherlands Antilles:

Dutton, S.P., Kim, E.M., Broadhead, R.F., Raatz, W.D., Breton, C.L., Ruppel, S.C., and Kerans, C., 2005, Play analysis and leading-edge oil-reservoir development methods in the Permian basin: Increased recovery through advanced technologies: AAPG Bulletin, v. 89, no. 5, p. 553–576, doi: 10.1306/12070404093.

Fitchen, W.M., 1993, Sequence stratigraphic framework of the upper San Andres Formation and equivalent basinal strata in the Brokeoff Mountains, Otero County, New Mexico: New Mexico Geological Society 44th Annual Fall Field Conference Guidebook, p. 185–193.

Fitchen, W.M., 1992, Sequence stratigraphy of the Upper San Andres formation and Cherry Canyon Tongue (Permian, Guadalupian), Southern Brokeoff Mountains, New Mexico. [Master's of Arts]: University of Texas at Austin.

Garcia-Fresca, B., Lucia, F.J., Jr, J.M.S., and Kerans, C., 2012, Outcrop-constrained hydrogeological simulations of brine reflux and early dolomitization of the Permian San Andres Formation: AAPG Bulletin, v. 96, no. 9, p. 1757–1781, doi: 10.1306/02071210123.

Gardner, M.H., and Sonnenfeld, M.D., 1996, Stratigraphic changes in facies architecture of the Permian Brushy Canyon Formation in Guadalupe Mountains National Park, west Texas: Society of Economic Paleontologists and Mineralogists Permian Basin Section, , no. PBS SEMP, p. 17–40.

Given, R.K., and Lohmann, K.C., 1985, Derivation of the Original Isotopic Composition of Permian Marine Cements: Journal of Sedimentary Research, v. 55, no. 3.

Hill, C.A., 1999, Reevaluation of the Hovey Channel in the Delaware Basin, West Texas: AAPG Bulletin, v. 83, no. 2, p. 277–294.

Hunt, D., and Fitchen, W.M., 1999, Compaction and the Dynamics of Carbonate-Platform Development: Insights from the Permian Delaware and Midland Basins, Southeast New Mexico and West Texas, U.S.A: Society for Sedimentary Geology, v. SEPM Special Publication, No. 63, p. 75–106.

Hurd, G.S., Kerans, C., Fullmer, S., and Janson, X., 2016, Large-Scale Inflections in Slope Angle Below the Shelf Break: A First Order Control On the Stratigraphic Architecture of Carbonate Slopes: Cutoff Formation, Guadalupe Mountains National Park, West Texas, U.S.A.: Journal of Sedimentary Research, v. 86, no. 4, p. 336–362.

James, N.P., and Jones, B., 2015, Origin of Carbonate Sedimentary Rocks: John Wiley & Sons.

Kampschulte, A., and Strauss, H., 2004, The sulfur isotopic evolution of Phanerozoic seawater based on the analysis of structurally substituted sulfate in carbonates: Chemical Geology, v. 204, no. 3–4, p. 255–286, doi: 10.1016/j.chemgeo.2003.11.013.

Katz, M.E., Wright, J.D., Miller, K.G., Cramer, B.S., Fennel, K., and Falkowski, P.G., 2005, Biological overprint of the geological carbon cycle: Marine Geology, v. 217, no. 3–4, p. 323–338, doi: 10.1016/j.margeo.2004.08.005.

Kerans, C., and Fitchen, W.M., 1995, Sequence hierarchy and facies architecture of a carbonate-ramp system: San Andres Formation of Algerita Escarpment and western Guadalupe

Mountains, West Texas and New Mexico: Bureau of Economic Geology, University of Texas at Austin Vol. 235.

Kerans, C., Fitchen, W.M., Gardner, M.H., Sonnenfeld, M.D., Tinker, S.W., and Wardlaw, B.R., 1992, Styles of sequence development within uppermost Leonardian through Guadalupian strata of the Guadalupe Mountains, Texas and New Mexico: West Texas Geological Society, v. 92, no. 1.

Kerans, C., and Kempter, K., 2002, Hierarchical stratigraphic analysis of a carbonate platform, Permian of the Guadalupe Mountains: Bureau of Economic Geology, The University of Texas at Austin.

Kerans, C., Lucia, F.J., and Senger, R.K., 1994, Integrated Characterization of Carbonate Ramp Reservoirs Using Permian San Andres Formation Outcrop Analogs: AAPG Bulletin, v. 78, no. 2, p. 181–216.

Kerans, C., and Tinker, S.W., 1999, Extrinsic Stratigraphic Controls on Development of the Capitan Reef Complex:

Kerans, C., and Tinker, S.W., 1997, Sequence Stratigraphy and Characterization of Carbonate Reservoirs:

Kim, S.-T., Coplen, T.B., and Horita, J., 2015, Normalization of stable isotope data for carbonate minerals: implementation of IUPAC guideline: Geochimica et Cosmochimica Acta, v. 158, p. 14, doi: 10.1016/j.gca.2015.02.011.

King, P.B., 1948, Geology of the Southern Guadalupe Mountains, Texas: U.S. Government Printing Office.

King, P.B., Henbest, L.G., Yochelson, E.L., and Cloud, P., 1965, Geology of the Sierra Diablo Region, Texas: U.S. Geological Survey 185.

Kirkby, K.C., 1982, Deposition, erosion, and diagenesis of the upper Victoria Peak Formation (Leonardian), southern Guadalupe Mountains, West Texas [unpublished M.S. thesis]: University of Wisconsin.

Marenco, P.J., Corsetti, F.A., Kaufman, A.J., and Bottjer, D.J., 2008, Environmental and diagenetic variations in carbonate associated sulfate: An investigation of CAS in the Lower Triassic of the western USA: Geochimica et Cosmochimica Acta, v. 72, no. 6, p. 1570–1582, doi: 10.1016/j.gca.2007.10.033.

Meissner, F.F., 1972, Cyclic sedimentation in Middle Permian strata of the Permian basin, west Texas and New Mexico: in Elam, J., and Chuber, S., eds., Cyclic Sedimentation in the Permian Basin: West Texas Geological Society, p. 203–232.

Milner, S., 1976, Carbonate Petrology and Syndepositional Facies of the Lower San Andres Formation (Middle Permian), Lincoln County, New Mexico: Journal of Sedimentary Research, v. 46, no. 3.

Milner, S., 1978, Genesis, provenance, and petrography of the Glorieta Sandstone of eastern New Mexico: New Mexico Bureau of Mines and Mineral Resources 25.

Mitchum, R.M., and Wagoner, J.C., 1991, High-frequency sequences and their stacking patterns: sequence-stratigraphic evidence of high-frequency eustatic cycles: Sedimentary Geology, v. 70, p. 131–160.

Montgomery, S.L., 1998, Permian Clear Fork Group, North Robertson Unit: Integrated Reservoir Management and Characterization for Infill Drilling, Part I-Geologic Analysis: AAPG Bulletin, v. 82, no. 10, p. 1797–1814.

Newell, N.D., Rigby, J.K., Fischer, A.G., Whiteman, A.J., Hickox, J.E., and Bradley, J.S., 1953, The Permian reef complex of the Guadalupe Mountains region, Texas and New Mexico; a study in paleoecology: W.H. Freeman, San Francisco.

Ohkouchi, N., Kawamura, K., Kajiwara, Y., Wada, E., Okada, M., Kanamatsu, T., and Taira, A., 1999, Sulfur isotope records around Livello Bonarelli (northern Apennines, Italy) black shale at the Cenomanian-Turonian boundary: Geology, v. 27, no. 6, p. 535–538.

Patterson, R.J., and Kinsman, D.J.J., 1982, Formation of Diagenetic Dolomite in Coastal Sabkha Along Arabian (Persian) Gulf: AAPG Bulletin, v. 66, no. 1, p. 28–43.

Paytan, A., and Gray, E.T., 2012, Sulfur Isotope Stratigraphy, *in* The Geologic Time Scale 2012, DOI: 10.1016/B978-0-444-59425-9.00009-3, Elsevier, B.V, p. 167–179.

Pingitore, N.E., Meitzner, G., and Love, K.M., 1995, Identification of sulfate in natural carbonates by x-ray absorption spectroscopy: Geochimica et Cosmochimica Acta, v. 59, no. 12, p. 2477–2483, doi: 10.1016/0016-7037(95)00142-5.

Planavsky, N.J., Bekker, A., Hofmann, A., Owens, J.D., and Lyons, T.W., 2012, Sulfur record of rising and falling marine oxygen and sulfate levels during the Lomagundi event: Proceedings of the National Academy of Sciences of the United States of America, v. 109, no. 45, p. 18300–18305, doi: 10.1073/pnas.1120387109.

Ramondetta, P.J., Guetzow, D.D., Dauzat, R., Merritt, R., and Garza, J., 1982, Facies and Stratigraphy of the San Andres Formation, Northern and Northwestern Shelves of the Midland Basin, Texas and New Mexico: Rep. Invest., Univ. Tex. Austin, Bur. Econ. Geol.; (United States), v. 128.

Rennie, V.C.F., and Turchyn, A.V., 2014, The preservation of and in carbonate-associated sulfate during marine diagenesis: A 25 Myr test case using marine sediments: Earth and Planetary Science Letters, v. 395, p. 13–23, doi: 10.1016/j.epsl.2014.03.025.

Ruppel, S.C., 2002, Geological Controls on Reservoir Development in a Leonardian (Lower Permian) Carbonate Platform Reservoir, Monahans Field, West Texas: Bureau of Economic Geology, University of Texas at Austin 266.

Ruppel, S.C., 1998, Subregional development of reservoir porosity at a major Permian unconformity: San Andres Formation, West Texas: AAPG Annual Convention: American Association of Petroleum Geologists, v. 2, p. A566.

Ruppel, S.C., and Cander, H.S., 1988, Dolomitization of shallow-water platform carbonates by sea water-derived brines: San Andres formation (Guadalupian), West Texas: Society of Economic Paleontologists and Mineralogists, v. SEPM Special Publication, no. 43, p. 245–262.

Ruppel, S.C., and Harrington, R.R., 2012, Facies and Sequence Stratigraphy: Critical Tools for Reservoir Framework Definition, Fullerton Clear Fork Reservoir, Texas, *in* Anatomy of a Giant Carbonate Reservoir: Fullerton Clear Fork (Lower Permian) field, Permian Basin, Texas, Studies in Geology 63, American Association of Petroleum Geologists and Bureau of Economic Geology, Tulsa, Oklahoma, U.S.A., p. 5–48.

Saller, A.H., and Henderson, N., 1998, Distribution of Porosity and Permeability in Platform Dolomites: Insight from the Permian of West Texas: AAPG Bulletin, v. 82, no. 8, p. 1528–1550.

Sarg, J.F., and Lehmann, P.J., 1986, Facies and Stratigraphy of Lower-Upper San Andres Shelf Crest and Outer Shelf and Lower Grayburg Inner Shelf, *in* San Andres/Grayburg Formations, Guadalupe Mountains, New Mexico. and Texas, PBS-SEPM Pub., Midland, Texas, p. 9–36.

Sarg, J.F., Markello, J.R., and Weber, L.J., 1999, The Second-Order Cycle, Carbonate-Platform Growth, and Reservoir, Source, and Trap Prediction: SEPM Special Publication, , no. 63, p. 11–34.

Scholle, P., 2003, Introduction and Virtual Geologic Field Trip to the Permian Complex, Guadalupe and Delaware Mountains, New Mexico, West Texas: NSDL Scout Report for the Physical Sciences.

Scholle, P.A., and Ulmer-Scholle, D.S., 2003, A Color Guide to the Petrography of Carbonate Rocks: Grains, Textures, Porosity, Diagenesis, AAPG Memoir 77: AAPG.

Southwell, J., and Stoudt, E., 2001, Geologic Observations Concerning Reservoir Development in the Glorieta Formation (Permian, Leonardian) in the Robertson, Wharton and South Harris Units; Robertson and Harris Fields, Gaines County Texas: Publications-West Texas Geological Society, v. 175–176.

Staudt, W.J., and Schoonen, M.A.A., 1995, Sulfate Incorporation into Sedimentary Carbonates, *in* Geochemical Transformations of Sedimentary Sulfur, ACS Symposium Series 612, American Chemical Society, p. 332–345.

Stoudt, E.L., and Raines, M.A., 2004, Reservoir Characterization in the San Andres Formation of Vacuum Field, Lea County, New Mexico: Another Use of the San Andres Algerita Outcrop Model For Improved Reservoir Description: , p. 191–214.

Strohmenger, C.J., Sadooni, F., McKenzie, J., Bontognali, T., and Vasconcelos, C., 2014, Microbial-Mediated Dolomite from Coastal Sabkha Environments of Abu Dhabi and Qatar: Analogues to Subsurface Arid Climate Dolomitized Reservoir Rocks: Houston, TX.

Theiling, B.P., and Coleman, M., 2015, Refining the extraction methodology of carbonate associated sulfate: Evidence from synthetic and natural carbonate samples: Chemical Geology, v. 411, p. 36–48, doi: 10.1016/j.chemgeo.2015.06.018.

Todd, R.G., 1976, Oolite-Bar Progradation, San Andres Formation, Midland Basin, Texas: AAPG Bulletin, v. 60, no. 6, p. 907–925.

Treude, T., Orphan, V., Knittel, K., Gieseke, A., House, C.H., and Boetius, A., 2007, Consumption of methane and CO2 by methanotrophic microbial mats from gas seeps of the anoxic black sea (vol 73, pg 2271, 2007): APPLIED AND ENVIRONMENTAL MICROBIOLOGY, v. 73, no. 11, p. 3770, doi: 10.1128/AEM.00806-07.

Vandeginste, V., and John, C.M., 2013, Diagenetic Implications of Stylolitization In Pelagic Carbonates, Canterbury Basin, Offshore New Zealand: Journal of Sedimentary Research, v. 83, no. 3, p. 226–240, doi: 10.2110/jsr.2013.18.

Veizer, J., Ala, D., Azmy, K., Bruckschen, P., Buhl, D., Bruhn, F., Carden, G.A.F., Diener, A., Ebneth, S., Godderis, Y., Jasper, T., Korte, C., Pawellek, F., Podlaha, O.G., et al., 1999, 87Sr/86Sr, δ13C and δ18O evolution of Phanerozoic seawater: Chemical Geology, v. 161, no. 1–3, p. 59–88, doi: 10.1016/S0009-2541(99)00081-9.

Vogt, J.N., 1986, Dolomitization and anhydrite diagenesis of the San Andres (Permian) Formation, Gaines County, Texas: Master's thesis, University of Texas at Austin.

Walker, J.C.G., 1986, Global geochemical cycles of carbon, sulfur and oxygen: Marine Geology, v. 70, no. 1, p. 159–174, doi: 10.1016/0025-3227(86)90093-9.

Ward, R.F., Kendall, C.G.S.C., and Harris, P.M., 1986, Upper Permian (Guadalupian) Facies and Their Association with Hydrocarbons–Permian Basin, West Texas and New Mexico: AAPG Bulletin, v. 70, no. 3, p. 239–262.

Weissert, H., Joachimski, M., and Sarnthein, M., 2008, Chemostratigraphy: Newsletters on Stratigraphy, v. 42, no. 3, p. 145–179, doi: 10.1127/0078-0421/2008/0042-0145.

Wotte, T., Shields-Zhou, G.A., and Strauss, H., 2012, Carbonate-associated sulfate: Experimental comparisons of common extraction methods and recommendations toward a standard analytical protocol: Chemical Geology, v. 326–327, p. 132–144, doi: 10.1016/j.chemgeo.2012.07.020.

Ye, Q., and Mazzullo, S.J., 1993, Dolomitization of lower Permian platform facies, Wichita Formation, north platform, Midland basin, Texas: Carbonates and Evaporites, v. 8, no. 1, p. 55–70, doi: 10.1007/BF03175163.

Ziegenbalg, S.B., Brunner, B., Rouchy, J.M., Birgel, D., Pierre, C., Böttcher, M.E., Caruso, A., Immenhauser, A., and Peckmann, J., 2010, Formation of secondary carbonates and native sulphur in sulphate-rich Messinian strata, Sicily: Sedimentary Geology, v. 227, no. 1–4, p. 37–50, doi: 10.1016/j.sedgeo.2010.03.007.

VITA

Eric Steven Bergersen was born in Houston, Texas. Upon graduating from Stratford High School in Houston, he entered Texas A&M University. In August of 2012, he graduated with a Bachelor of Science in Environmental Geoscience and a minor in Business. During the following years, he was employed at Arcadis, an engineering and environmental consulting firm, as a geologist.

In August of 2014 he moved to El Paso to pursue his Master's of Science in Geology at University of Texas at El Paso (UTEP). During that time he maintained part-time status with Arcadis. While at UTEP he served as the team captain for the 2016 American Association of Petroleum Geologists (AAPG) Imperial Barrel Award team, where they took first place internationally out of 176 schools from 42 countries. In May of 2016 he worked as an intern geologist at Apache Corporation in their Permian Basin Exploitation and Development group.

After completing his Master's thesis, Eric plans to move Houston with his wife where he will join a Houston based oil and gas exploration and production company as an exploration geologist.

Email: bergersen828@gmail.com

This thesis was typed by the author, Eric Bergersen.